Journal of Energy Challenges and Mechanics

ISSN 2056-9386

http://www.nscj.co.uk/JECM/

Volume 3, Issue 3
October 2016

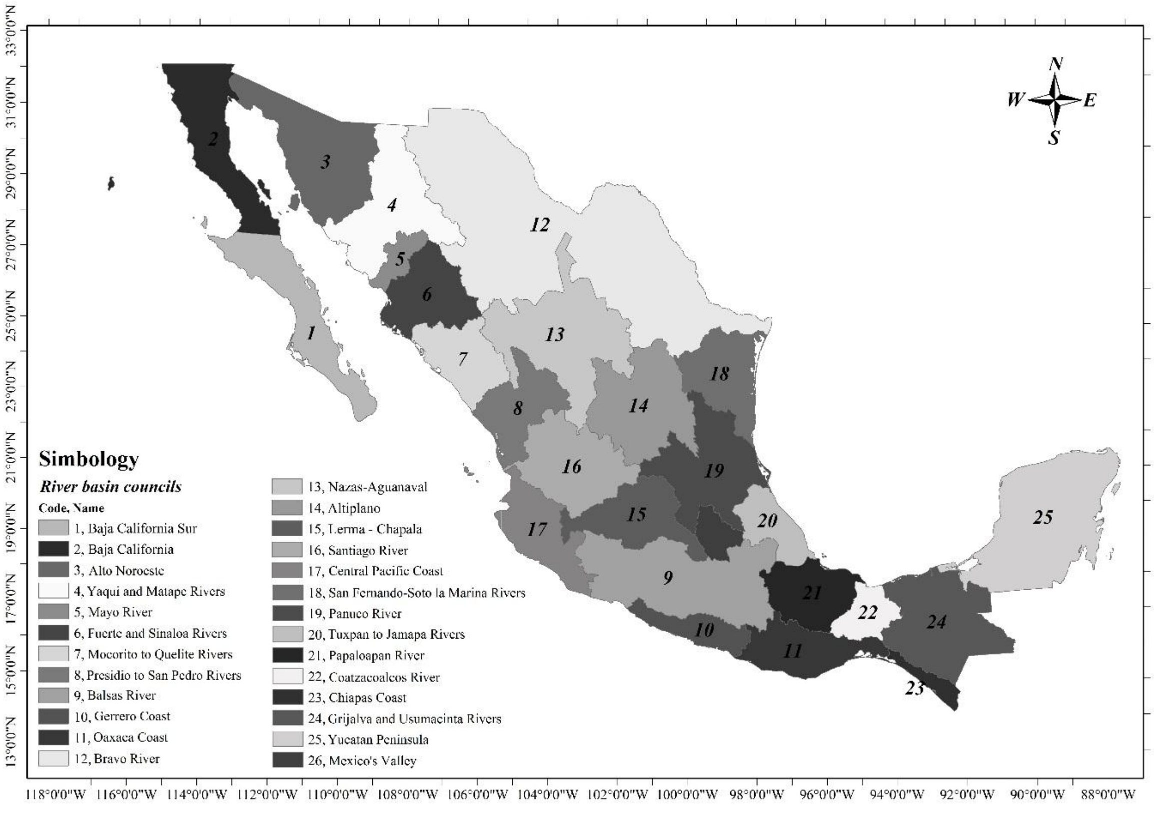

Featured article:

The National Drought Policy in Mexico

Felipe I. Arreguín Cortés[1], Mario López Pérez[1], David Korenfeld Federman[2], David Ortega-Gaucin[1]*

[1]Mexican Institute of Water Technology, Paseo Cuauhnáhuac 8532, Col. Progreso, 62550, Jiutepec, Morelos, México

[2]Independent consultor

North Sea

North Sea Conference & Journal LTD
2 Charlestown Walk, Cove Bay, AB12 3EZ, Aberdeen, Scotland, United Kingdom
http://www.nscj.co.uk/JECM/ | jecm@nscj.co.uk | +44(0)1224 875635

Journal of Energy Challenges and Mechanics
http://www.nscj.co.uk/JECM/
ISSN 2056-9386
Volume 3 (2016) issue 3

TABLE OF CONTENTS pages

©2016 North Sea

©2016 North Sea

Journal of Energy Challenges and Mechanics
http://www.nscj.co.uk/JECM/

ISSN 2056-9386
Volume 3 (2016) issue 3, article 1

Addressing the factors causing inefficiency of fossil fuel power generation in Saudi Arabia

沙特阿拉伯化石燃料发电效率低下的因素研究

Mohammad Althaqafi*, Qingping Yang

College of Engineering, Design and Physical Science, Brunel University London, UB8 3PH, UK

Mohammad.althaqafi@brunel.ac.uk

Accepted for publication on 3rd August 2016

Abstract - **The Efficiency of fossil fuel generation has improved significantly over the last decade and still has a potential for further improvement. The type of fuel and technologies have played a crucial role in this trend, but several factors can affect the efficiency with different impacts, such as equipment aging, operation, maintenance and fuel subsidies, as well as others. This paper aims to identify the main factors causing the current relatively low-efficiency level in fossil power generation in Saudi Arabia. First, generation efficiency was calculated to determine the average level according to the fuel type and technology in use. Second, the results were benchmarked against other countries to determine the actual gap. Third, actual detailed data related to the power plants' performance was collected and critically analyzed. In conclusion, we found that the average efficiency of fossil power generation in the country is below the international average. Between 2007 and 2013 the country's average was around 28% and in 2014 it was about 31%. The results show that the power plants' operation is a primary cause of the current level of efficiency. In addition, the available generation stock has a potential to reach higher than the current level.**

Keywords - **Efficiency, Electricity, Generation, Fossil Fuel.**

I. INTRODUCTION

Saudi Arabia (SA) is the largest oil producer in the world and possess around one fifth of the world's proven oil reserves [1]. The kingdom's economy relies heavily on oil exports in its annual budget. Oil represents 85% of the country's export earnings [1]. 8.6 Million barrels of oil per day were exported in 2013 out of a total production of 11.6 Million barrels per day [2]. SA is the world's twelfth energy consumer [3]. Oil consumption has doubled during the last decade and reached 3 Million barrels of oil [4], resulting in the country becoming the sixth largest oil and gas consumer in the world [5]. Recently, local consumption has reached 38% of total primary energy in the kingdom, according to the Saudi Deputy Minister of Energy [6].

Electricity generation consumes 39% [7] of local oil consumption and 43% of total produced natural gas and the rest are distributed in other sectors such as transport, industry and others. Fossil fuel is the sole source of electricity generation (47% gas and 53% oil as of 2013), 1.6 Million Barrel of Oil Equivalent (BOE) are burned every day in power plants [8]. This figure is growing on an annual basis. As a result, the share of export could be reduced by 3 Million barrels per day by 2028 [9] if the current situation continues, which will undoubtedly affect the national economy.

Electricity demand in SA is increasing on a yearly basis. In 2013, a 9.1% increase was recorded in peak demand [10]. On average, there was an annual growth of 8% during the previous decade [11], compared to 2.1% globally. This trend is projected to continue for the next few years, leading to the doubling of the current amount of primary energy by 2030, as the Department of Petroleum and Mineral Resources in SA has warned [6].

Generation efficiency has not shown a significant improvement during the last decade, whilst new power plants are built yearly to meet the demand. Official reports have not seriously considered this topic, although limited publications and some external reports mention the low efficiency in Saudi Arabia. In general, generation efficiency in Saudi Arabia is considered among the lowest countries in the world

The remainder of this paper is organised as follows. Section II provides the background of the electricity industry in SA and Section III discusses the efficiency trend and losses in the

©2016 North Sea

country in the past and exposes the main causes leading to inefficiency. Section IV describes the data collection, efficiency calculation and analysis applied in this paper. The main results and findings are presented and discussed in Section V. Finally, Section VI concludes the paper.

II THE POWER SECTOR IN SAUDI ARABIA

In Saudi Arabia, electricity is generated utilizing fossil fuels only. Heavy Fuel Oil (HFO), Light Fuel Oil (LFO), diesel and gas are the primary source of power as shown in Fig. 1 with an equal share of oil and gas [12]. Coal is not used for power generation. The Saudi Electricity Company (SEC) is the primary electricity provider in SA. It is 81% owned by the government. It owns the transmission and distribution networks and around 70% of the existing power plants. It generates 70% of the country's total demand.

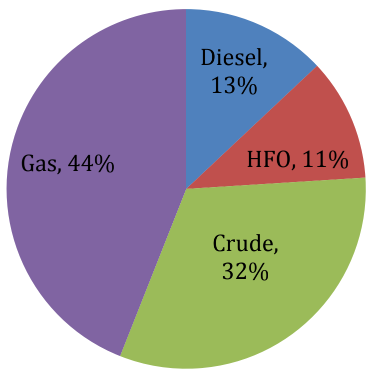

Fig. 1, Annual fuel consumption in electricity generation in SA by fuel type.

A remarkable rise in peak load recorded on an annual basis with projection to reach 75 (GW) by 2020 [12] as presented in Fig. 2. This upsurge demands massive investment in infrastructure expansion with an estimated 500 Billion Saudi Riyals for the next ten years [13]. As a result, 40% of the generation capacity is less than six years old and only 4% have operated for more than 35 years [12], as shown in Fig. 3.

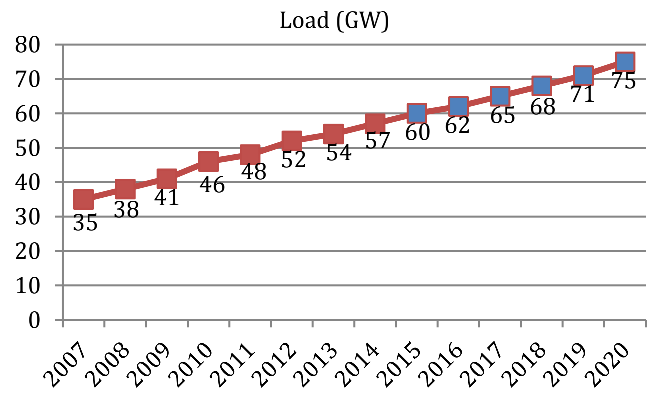

Fig. 2, Actual and projected load in SA.

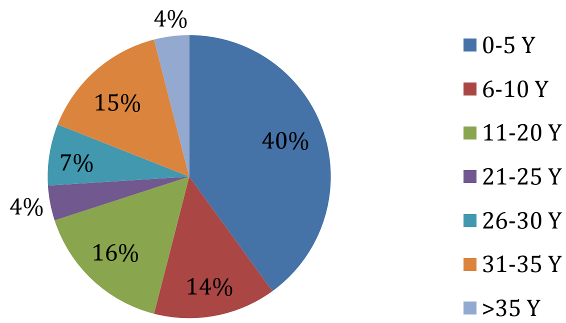

Fig. 3, Age of generation units in SA based on capacity.

2.1 FOSSIL FUEL POWER PLANTS CHARACTERISTICS

There are three main types of technologies used in the kingdom: gas turbines (GT), steam turbines (ST) and combined cycle turbines (CC). Diesel turbines are less than 1% of total generation stock, therefore, they are not considered here. Gas turbine has some advantages over others. First, the cost of investment is less than CC and ST. Second, it does not require long hours to start up which means quick response to demand. Nevertheless, it does not operate with high efficiency (30%-35%) [11]. Steam turbine can operate at higher efficiency (35%-40%). However, it is not suitable to respond to peak load quickly. It requires more hours to warm up. Combined cycle is the most efficient available technology, and it can reach 50% or more, but its investment cost is very high. In Saudi Arabia, gas turbines represent half of the generation stock (47%), followed by 40% steam turbines, 12% combined cycles and 1% diesel generators [12], as shown in Fig. 4.

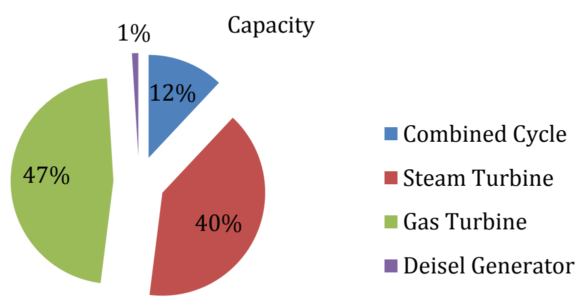

Fig. 4, Generation units by technology type.

Operation optimisation requires demand be satisfied by operating units with the lowest cost. However, the selection of power plants takes into consideration the load type (base, peak) and chooses the optimum technology to operate. Usually, power plants are ranked according to their operation cost. This order is called "merit order" [11] and is used in operation. For instance, when the demand increases, a new unit with higher cost is introduced. Nevertheless, merit order can change in some circumstances, such as maintenance schedules.

2.2 Fuel Subsidies

Electricity providers receive significant discount on petroleum fuel prices [16], as shown in TABLE 1. This is considered to be the compensation to avoid financial losses, since the tariff is determined by the government. Subsidies were literally introduced as a tool to promote equality in society and support low income households. Nevertheless, it has been proved those high income households are utilising subsidies more than the targeted segment [14]. On the supply side, it does not encourage service providers to invest in more efficient technologies and prevents them from competitive pressure [15]. In addition, it does not generate real data about the actual cost of production; as a result, operation decisions can be affected negatively.

TABLE 1 COMPARISON OF FOSSIL-FUELPRICES PAID BY ELECTRICITY PROVIDERS IN SA WITH INTERNATIONAL PRICES.

Fuel Type	Price (US $ / million BTU)	
	Local	International
HFO	0.43	15.43
Gas	0.75	9.04
Diesel	0.67	21.67
LFO	0.73	19.26

III. Historic Trend in Energy Efficiency

Globally, generation efficiency has shown significant improvement during the last decades. For instance, a study by Graus [17] aims to build a benchmark indicator for fossil fuel generation efficiency. The study was based on 14 countries[1] that consume two thirds of global fossil fuel power production. The results shows fossil fuel generation efficiency is around 35% in 2003. India has the lowest with 30% and the United Kingdom recorded the highest efficiency of 40%. However, based on the type of fuel, the efficiency of power plants that utilise gas varies from 35% in Australia up to 47% in India. In addition, the efficiency of coal fired power plants ranges from 41% in Japan to 29% in India. Finally, oil fired power plants range from 28% in India to 42% in Japan. Fig. 5 shows the weighted average efficiency of countries covered by Graus's study based on fuel type from 1990 to 2003. Natural gas efficiency jumped from 34% to 40% while oil and coal remained at the same level, around 36% and 34% respectively.

In the European Union countries (EU)[2] 55% of power is generated from fossil fuel as of 2005 [18]. Coal contributes the largest share with 30%, followed by gas 20% and oil 4%. Between the years 1990 and 2005, the efficiency of gas fired power plants improved from 30% to 45% and coal from 33% to 39%.

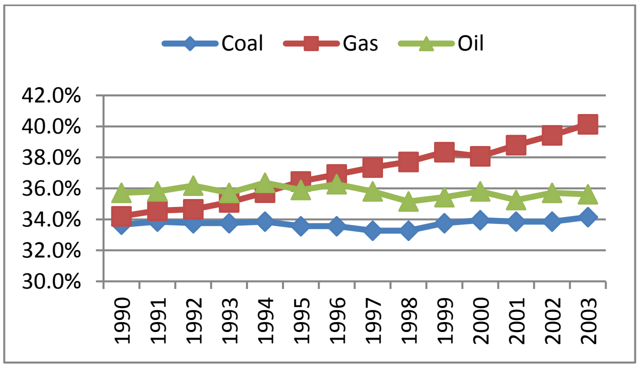

Fig. 5, Average efficiency of selected countries based on fuel type

Fig. 6 shows 3 years average efficiency of EU countries for different fuel types [18]. A three-year average efficiency shows fossil fuel fluctuates between 51% in Luxembourg and 28% in Bulgaria. Spain is the top efficient producer using gas with 50%, while Bulgaria has the least efficiency of 27%. Coal fired power plants range from 27% in Slovak Republic to 42% in Denmark. The top efficient generation utilising oil is 43% in Italy, while Czech Republic has the lowest at 21%. On average, EU countries achieved 39% for fossil power generation in 2005 [19].

---

[1] Australia, China, Denmark, Finland, France, Germany, India, Japan, Norway, South Korea, Sweden, United Kingdom and Ireland, and United States.

[2] Germany, United Kingdom, France, Italy, Spain, Sweden, Poland, Netherlands, Belgium, Czech Republic, Finland, Austria, Greece, Romania, Portugal, Bulgaria, Denmark, Hungary, Slovak Republic, Ireland, Slovenia, Lithuania, Estonia, Latvia, Cyprus, Luxembourg, Malta.

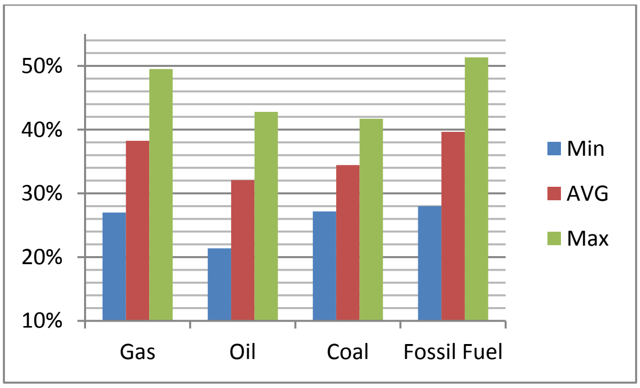

Fig. 6, Average efficiency in EU countries (2003-2005)

In 2005, coal accounted for the largest share of electricity production in the world with 40%, followed by natural gas 20% and only 7% from oil. On average, the efficiency in 2005 of fossil fuel generation was 31%, with 31% for coal, 30% for natural gas and 31.6% for oil [19]. According to Graus, it is predicted, to reach 50% on average by 2050.

3.1 Efficiency Analysis in Saudi Arabia

SA relies completely on oil and gas and does not utilise coal, which is the least efficient fossil fuel resource. But many studies either discuss the optimum energy mix and the utilisation of renewable resources [20] or focus on efficiency efforts on the demand side [21], with less attention paid to improving fossil fuel generation efficiency and limited research found on this topic. This can be related to the lack of published information of average efficiency by the governing body and the efficiency based on fuel used in power plants. The only available data was published in SEC reports from 2011 to 2013 with an average efficiency of 32%, as shown in TABLE 2. This information represents SEC power plants which accounts for 70% of the total production.

In general, SA is considered to be among the countries that have the lowest generation efficiency [22]. The generation efficiency was recorded as 30% in 2009 and 2010 [23]. Another study claimed that nominal power plants efficiency in the kingdom is far below the world average generation efficiency by comparing Saudi Arabia with the United Kingdom, which are 29.5% and 38.6% respectively [24]. From 1990 to 2010, SA average generation efficiency has improved by 0.15 percent point per year (26%-29%) compared to 41%-46% in the EU countries [10]. On the other hand, reports published by ABB [25] have shown that SA generation efficiency increased from 27% to 32% between (1990-2011), as can be seen in Fig. 7.

TABLE 2 HEAT RATE IN SA (2010-2013)

	SEC HR (BTU/kwh)[3]	SEC efficiency (C)[4]	SA efficiency (ABB)[5]
1990	N/A	N/A	27.5%
2000	N/A	N/A	29.1%
2009	N/A	N/A	31%
2010	10,920	31.25%	31%
2011	10,585	32.23%	32%
2012	10,452	32.64%	N/A
2013	10,375	32.89%	N/A

It has been suggested to increase the share of CC units to improve the efficiency since it has the lowest heat rate compared to other fossil fuel generation technologies [24]. ABB reports linked the limited improvement of efficiency in Saudi Arabia to the increasing share of natural gas in generation and CC units [25]. However, CC power plants have increased significantly between 2012 and 2013 without achieving remarkable improvement. The share of CC turbines jumped from 5.4% to 13.8%, while heat rate decreased by only 0.7% [26]. In addition, the share of production of SEC has decreased with the intervention of private firms, which are supposed to be new power plants, yet no significant improvement in efficiency has been observed.

A reduction in heat rate leads to a significant saving of fuel consumed in power plants. For example, 106 million Saudi Riyal (SR) ($28.3M)[6] was saved in 2011 by reducing the average heat rate in SEC power plants by only 0.001% [27]. Moreover, in 2014, the SEC reported a 1% reduction in heat rate results in saving 12 MBOE [28]. However, both reports have not revealed the main reasons for these improvements.

[3] [26], [27], [42]

[4] Equivalent efficiency= $\frac{3412}{\text{HR}}$

[5] [25]

[6] 1 US$ = 3.75 SR

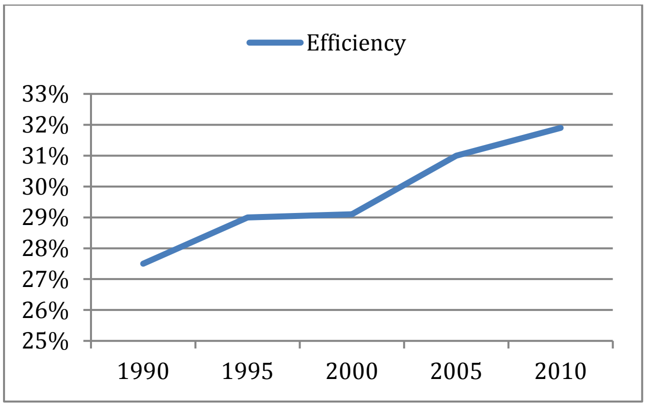

Fig. 7, Generation efficiency in SA (1990-2011)

3.2 Internal consumption and losses

The Type of fuel used in the power plant has an impact on the amount of auxiliary consumption. The largest consumption often appears in coal power plants which consume 6-8% of its gross production. On the other hand, gas based power plants have the lowest auxiliary consumption of around 2-3% and oil power plants usually 4-6% [29]. Globally, around 5% of total power production in 2007 was consumed as an auxiliary consumption. For instance, China power plants consume around 8% of their gross production as one of the highest figure in the world, followed by Russia and India with about 7% in both country [30]. On the other hand, SA power plants consume only 3% of their total production as shown in Fig. 8 [16] [17]. These figures could be linked to the fuel mix being used in producing electricity.

The world average transmission and distribution losses from 2006 to 2012 are around 8.3% [37], as shown in Fig. 9. Losses vary between countries: India has the highest loss of 20.68% and Korea the lowest at 3.54%. On the other hand, Saudi Arabia fluctuates between 8 and 10% in the last decade with an average of 8.8%. Network losses in the kingdom are among the world average range [12][25].

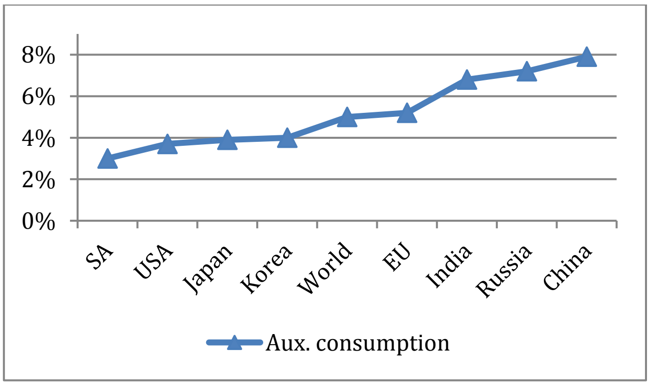

Fig. 8, Auxiliary consumption in power plants as a percentage of total production in 2007.

Electricity consumed within the power plants and power losses in networks including transmission and distribution in Saudi Arabia are within the international average.

3.3 Factors influencing efficiency.

Design efficiency or the so called name plate efficiency is the ideal efficiency. However, practically during operation, it is usually lower and known as operational efficiency. This can be linked to several factors such as operation practices, maintenance, fuel quality, cooling methods, size of power plant, environment and pollution control, as shown in Fig. 9 [31]. These factors have been classified into controllable and uncontrollable [32]. Operation and maintenance are considered to be controllable factors while the rest are uncontrollable, such as age deterioration, weather conditions etc. (500-1000 BTU/kWh) per power plant can be recovered by paying attention to controllable factors. Specifically, load hours is considered as the most significant factor affecting efficiency [31]. On average, maintenance can have a negative impact on efficiency by 0.5% but in some cases poor maintenance can reduce efficiency up to 5% [31].

Partial load operation and frequent shut down and start up consume more fuel and lead to lower operational efficiency [33] [34] [35]. Losses in efficiency are sensitive to the capacity utilization of plants. For instance, 5%-7% less than design efficiency is a result of the power plant operating at 30% of its capacity, while increasing operational capacity to 85% can reduce the losses to only 1-2% [31]. On average, 3-4% is estimated for half load operation [18]. This drop can vary according to technology. The efficiency of CC units operating at half load is 45%, instead of 52% efficiency if operated at full load [36].

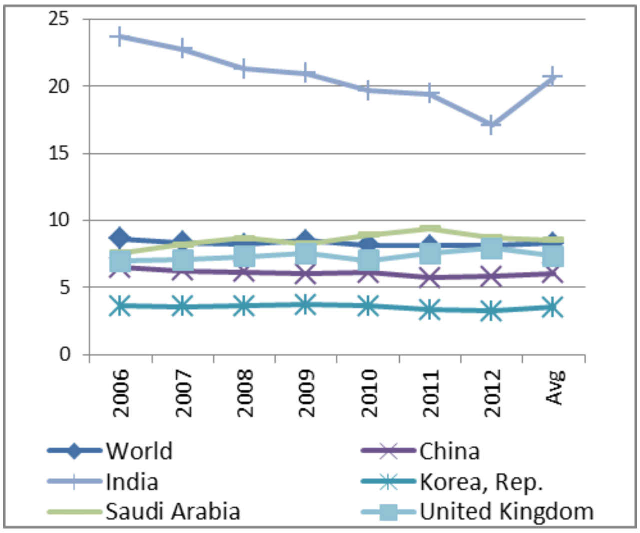

Fig. 9, Transmission and Distribution loses (%) 2006-2012

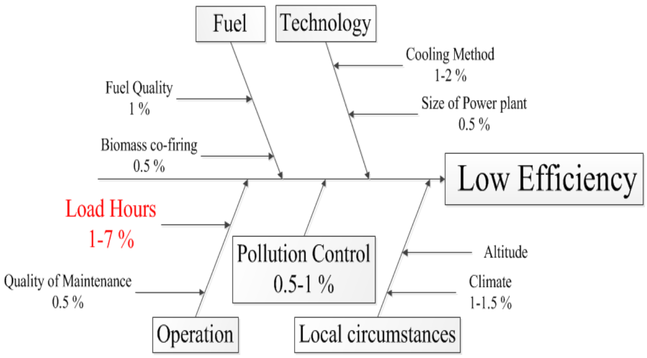

Fig. 9, Factors influencing efficiency

IV. Calculation and Analysis

This section provides a summary of the calculation and analysis performed in this study and the data used. First, the data for efficiency calculation was collected from different sources and checked. Second, efficiency is calculated utilizing the same method applied in several researches [17]. Finally, an in-depth analysis carried out to identify the causes leading to the current level of efficiency in Saudi Arabia.

4.1 Data Collection

Data of fuel used in power plants and electricity generation were taken from Electricity and cogeneration regulatory Authority in Saudi Arabia reports for the last ten years [38] and International Energy Authority website [39]. Input energy is based on gross calorific value (GCV)[7]. Output electricity is based on gross production [8]. This means auxiliary consumption, transmission and distribution losses are not considered.

In addition, detailed data of SEC's power plants was only collected from the ECRA, including the power plants' name, technology type, nominal capacity heat rate and gross generation as in 2011.

Calculating Efficiency

Efficiency is defined as "the ratio of the useful outputs energy to the input energy" [40]. The equation used for efficiency calculation is shown in Eq. (1):

$$E = \frac{P}{I} \qquad (1)$$

[7] Gross calorific value (GCV) or higher heating value (HHV) provides lower efficiency than if net calorific value (NCV) or lower heating value (LHV) is used. The variance is about 7% for oil (3 percent point) and 10% for natural gas (5-6 percent point) [43].

[8] Gross production= Net production + AUX consumption + T&D losses

Where E is the efficiency, P is the generated electricity and I is the fuel used in power plants. The efficiency is based on Higher Heating Value (HHV). This is recommended by the energy efficiency experts network, since it provides a clear picture of inefficiency [41]. Alternatively, heat rate (HR) is used to measure the amount of BTU required for generating single kWh. Nevertheless HR is an efficiency measure as presented in Eq. (2):

$$E = \frac{3412}{HR} \qquad (2)$$

4.3 Data Analysis

The generation efficiency in Saudi Arabia was calculated for the last few years. This result was benchmarked with the UK to determine the gap. The collected data of power plants from ECRA was further analyzed in detail to determine the main causes leading to the current level of efficiency, as presented in the next section.

V. Results and Discussions

The results show that the generation efficiency in Saudi Arabia is below 30% from 2007 to 2012 with no significant change. Noticeable development was achieved in 2014 by reaching 31% Fig. 10. This change is not linked to any reason in official reports, but it can be related to the new units added to the generation assets with a total capacity of 7 GW.

The amount of fuel used in electricity production was shared equally between oil and gas and remained the same during the last decade with limited change every year. The type of generation units has changed slightly as shown in Table 3. CC units have doubled from 6% to 12% during the last 6 years, GT power plants shares has decreased from 52% to 47% and ST remained the same on average.

The average age of generation units in Saudi Arabia is 14 years old, similar to the UK fossil fuel power plants which are generating at an efficiency above 45% on average as shown in Fig 12. By comparing the efficiency of the same fuel type in both countries, we found gas fueled units in SA are far below those in the UK.

SA has a potential to achieve a higher efficiency than the current level according to the existing generation stock and type of fuel in use. By considering the average efficiency of the available resources, the average could be 37%-38%.

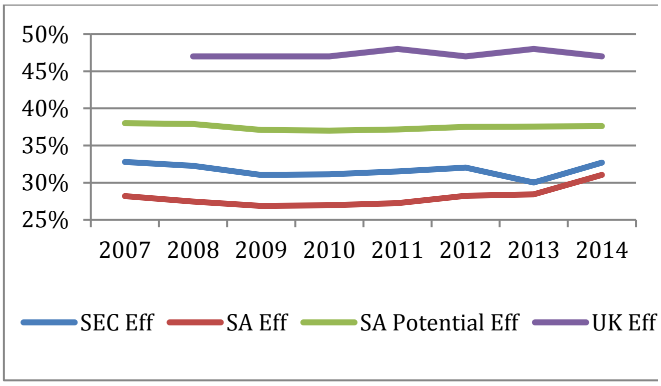

Fig. 10, Efficiency trend in SA and UK

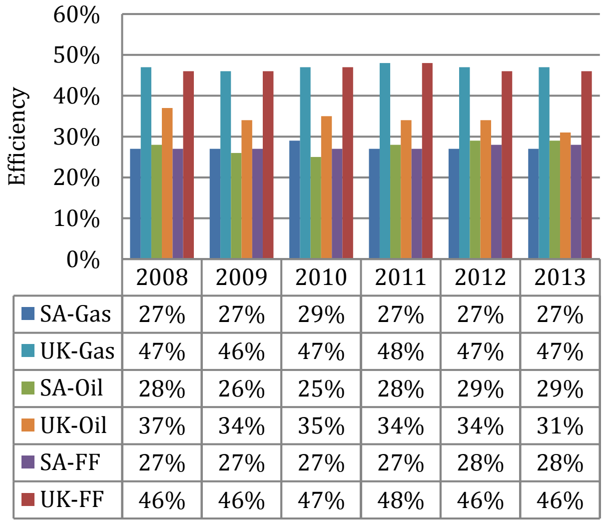

Fig. 11, Generation efficiency in SA & UK based on fuel type

TABLE 3 GENERATION UNITS' TYPE IN SABASED ON NOMINAL CAPACITY

	2009	2010	2011	2012	2013	2014	AVG
GT	52%	53%	52%	50%	50%	47%	51%
ST	41%	40%	40%	39%	36%	40%	40%
CC	6%	6%	6.1%	9.9%	12%	12%	9%
Potential Efficiency	36%	36%	36%	37%	37%	37%	37%

On the other hand, SEC generates 70% of total electricity transmitted through the networks. Its power plants' efficiency fluctuates between 32% and 31% between 2007 and 2014 higher than the country average. In terms of type of fuel consumed, oil is used more than gas with 60% against 40% respectively.

The analysis shows power plants that operate at high efficiency are being operated less than other units with lower efficiency, as shown in Fig 13. In addition, the existing most efficient technology, CC power plants, are showing an extremely low efficiency in operation compared to its design efficiency. On average, steam turbine power plants are the most utilized type by 67%, higher than combined cycle units which are used by only 52% during the year, followed by 41% for GTs. As a result, Gas turbines generate 44% of the total electricity produced by SEC. STs contribute 43% of the total production, while CCs generate only 13%.

Generation assets are not operating as efficiently as they could be and efficiency improvement is not considered as the primary objective in operation. This is related to the analysis of data showing the priority and high utilization of the least efficient units over other efficient ones.

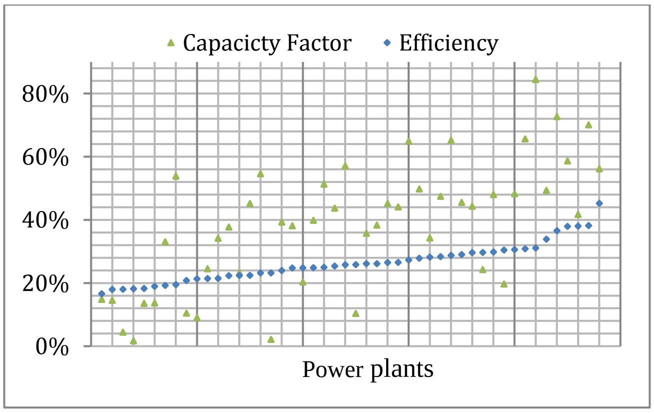

Fig. 12, Capacity factor vs. efficiency per power plant

VI. Conclusion

In this paper, the generation efficiency in Saudi Arabia's electricity sector was calculated and investigated for the years 2007 to 2014. A detailed analysis was carried out to identify the reasons affecting the efficiency.

Electricity generation efficiency in Saudi Arabia is far below the international average level. Recent research suggested that the increase in the share of high efficient units for improvement, which means further investment. This analysis shows that the existing generation technologies and type of fuel used could be utilized better to achieve a higher level of efficiency. Moreover, the operation of power plants represents a major cause of the current situation. In future, operation models will be developed and simulated to improve the electricity generation efficiency in Saudi Arabia.

REFERENCES

[1] OPEC, “Saudi Arabia facts and figures,” 2016. [Online]. Available: http://www.opec.org/opec_web/en/about_us/169.htm. [Accessed: 01-Feb-2016].

[2] EIA, “Saudi Arabia estimated petroleum net export (1980-2013),” 2013. [Online]. Available: http://www.eia.gov/countries/country-data.cfm?fips=sa#pet. [Accessed: 01-Jan-2015].

[3] L. El-katiri and B. Fattouh, “A Brief Political Economy of Energy Subsidies in the Middle East and North Africa,” *Oxford Inst. Energ Study*, no. February, 2015.

[4] S. Khan, “Energy fficiency: the first renewable,” Oxford, 2014.

[5] H. Chaoul, “Saudi Arabia Budget 2013,” Jeddah, 2013.

[6] Aleqtisadiah, “ الاستهلاك المحلي للطاقة يشكل 38 %من إنتاج المملكة, 2016”. [Online]. Available: https://www.aleqt.com/2016/02/08/article_1028401.html. [Accessed: 08-Feb-2016].

[7] M. Alowaidh, “Technology-Based Improvement for KSA Energy Intensity,” 2010.

[8] ECRA, “Annual Statistical Booklet for Electricity and Sea Water Desalination Induastries,” RIYADH, 2013.

[9] B. Alhoweish and C. Orujov, “Promoting an effective energy effi ciency programme in Saudi Arabia : challenges and Introduction : economic challenges in Saudi Arabia,” 2015, p. 100.

[10] M. Groissböck and M. J. Pickl, “An analysis of the power market in Saudi Arabia: Retrospective cost and environmental optimization,” *Appl. Energy*, vol. 165, pp. 548–558, 2016.

[11] A. Farnoosh, F. Lantz, and J. Percebois, “Electricity generation analyses in an oil-exporting country transition to non-fossil fuel based power units in Saudi Arabia,” *Energy*, vol. 69, pp. 299–308, 2014.

[12] ECRA, “Annual Statistical Booklet for Electricity and Sea Water Desalination Induastries,” 2014.

[13] Alekhbariya, “ المملكة بحاجة لتنفيذ مشاريع بقيمة 500 مليار تفادياً لأحمال الذروة, 2016”. [Online]. Available: http://www.alekhbariya.net/ar/node/5732#. [Accessed: 09-Feb-2016].

[14] R. Bacon, “Devising an energy pricing strategy for GCC countries,” Oxford, 2014.

[15] B. Fattouh and L. El-Katiri, “Energy subsidies in the Middle East and North Africa,” *Energy Strateg. Rev.*, vol. 2, no. 1, pp. 108–115, Jun. 2013.

[16] ECRA, “Activities & Achievements of the Authority,” RIYADH, 2014.

[17] W. Graus, “Power of Efficiency International comparisons of energy efficiency and CO2 emissions of fossil-based power generation,” 2010.

[18] W. Graus and E. Worrell, “Trend in efficiency and capacity of fossil power generation in the EU,” *Energy Policy*, vol. 37, no. 6, pp. 2147–2160, Jun. 2009.

[19] W. Graus, E. Blomen, and E. Worrell, “Global energy efficiency improvement in the long term: A demand- and supply-side perspective,” *Energy Effic.*, vol. 4, no. 3, pp. 435–463, 2011.

[20] A. Baras, W. Bamhair, Y. Alkhoshi, M. Alodan, S. Arabia, and U. States, “OPPORTUNITIES AND CHALLENGES OF SOLAR ENERGY IN SAUDI ARABIA,” in *American Solar Energy Society Conference*, 2012, pp. 1–6.

[21] G. Lahn and P. Stevens, “Burning Oil to Keep Cool Burning Oil to Keep Cool,” 2011.

[22] B. Fattouh, “Summer Again : The Swing in Oil Demand in Saudi,” no. July, pp. 1–8, 2013.

[23] B. Fattouh and L. El-katiri, “Energy Subsidies in the Arab World,” Oxford, 2012.

[24] Y. Alyousef and M. Abu-ebid, “Energy Efficiency Initiatives for Saudi Arabia on Supply and Demand Sides,” 2012.

[25] ABB, “Saudi Arabia Energy efficiency report,” 2013.

[26] SEC, “SEC ANNUAL REPORT,” RIYADH, 2013.

[27] SEC, “SEC ANNUAL REPORT,” RIYADH, 2011.

[28] SEC, “SEC Annual Reoprt,” RIYADH, 2014.

[29] W. H. J. Graus, M. Voogt, and E. Worrell, “International comparison of energy efficiency of fossil power generation,” *Energy Policy*, vol. 35, no. 7, pp. 3936–3951, Jul. 2007.

[30] IEA, “FOSSIL FUEL-FIRED POWER GENERATION Case Studies of Recently Constructed Coal- and Gas-Fired Power Plants,” 2007.

[31] W. Graus, M. Roglieri, P. Jaworski, and L. Alberio, “EFFICIENCY AND CAPTURE-READINESS OF NEW FOSSIL POWER PLANTS IN THE EU,” Utrecht, 2008.

[32] D. Bellman, B. Blankenship, C. Imhoff, J. DiPietro, B. Rederstorff, and X. Zheng, “ELECTRIC GENERATION EFFICIENCY,” 2007.

[33] K. Markiewicz, N. L. Rose, and C. Wolfram, “DO MARKETS REDUCE COSTS? ASSESSING THE IMPACT OF REGULATORY RESTRUCTURING ON U.S. ELECTRIC GENERATION EFFICIENCY,” 2004.

[34] H. S. (Ron) Chan, M. L. Cropper, and K. Malik, “Why Are Power Plants in India Less Efficient than Power Plants in the United States?,” *Am. Econ. Rev.*, vol. 104, no. 5, pp. 586–590, 2014.

[35] IEA, “‘Power Generation from Coal: Measuring and Reporting Efficiency Performance and CO2 Emissions,’” 2010.

[36] IEA-ETSAP, “Gas-Fired Power,” 2010.

[37] The World Bank, “Electric Power Transmission and Distribution Losses,” 2014. [Online]. Available: http://search.worldbank.org/all?qterm=transmission+and+distribution+losses&language=EN&op=&_Top/date=2014. [Accessed: 15-Dec-2015].

[38] ECRA, “Annual Statistical Booklet for Electricity and Sea Water Desalination Induastries,” RIYADH, 2012.

[39] IEA, “Saudi Arabia: Electricity and Heat,” 2013. [Online]. Available: http://www.iea.org/statistics/statisticssearch/report/?c

ountry=SAUDIARABI&product=electricityandheat&year=2013. [Accessed: 20-May-2014].
[40] D. Harvey, *Energy Efficiency and the Demand for Energy Services*. LONDON: Cromwell Press Group, 2011.
[41] G. J. M. Phylipsen, K. Blok, and E. Worrell, “International comparisons of energy efficiency-Methodologies for the manufacturing industry,” *Energy Policy*, vol. 25, no. 7–9, pp. 715–725, 1997.
[42] SEC, “SEC ANNUAL REPORT,” RIYADH, 2012.
[43] W. Graus, “International Comparison of Fossil Power Efficiency and CO2 Intensity,” 2009.

Journal of Energy Challenges and Mechanics
http://www.nscj.co.uk/JECM/
ISSN 2056-9386
Volume 3 (2016) issue 3, article 2

Monitoring of the ecological security in the north-western region of the Republic of Sakha, Russian Federation

俄罗斯联邦萨哈共和国西北地区的生态安全监测

Albina A. Goldman, Elena V. Sleptsova, Raissa P. Ivanova

Mirny Polytechnic Institute (branch) of Ammosov North-Eastern Federal University (NEFU), Mirny, Tikhonova street 5, build.1, Russian Federation

mptisvfu@mail.ru, raissa1@yandex.ru, lena-mirny@yandex.ru

Accepted for publication on 3rd September 2016

Abstract – **The paper is devoted to the environmental impact of industrial sector in Western Yakutia and the role of the Mirny Polytechnic Institute (branch) of the Ammosov North-Eastern Federal University in training specialists for oil and gas and diamond mining industries and the research carried out at the educational and scientific laboratory of complex analysis of anthropogenic disturbances of the Institute on compliance with the requirements.**

Key words – **environment, industry, oil and gas, diamond mining, ecological monitoring, East Siberia.**

I. Introduction

The Mirny Polytechnic Institute (branch) of the Ammosov North-Eastern Federal University is located in the industrial centre of Western Yakutia, Mirny city, the heart of the diamond mining province of Russia and the centre of the oil and gas industry of the Republic.

Western Yakutia is adjacent to the Arctic territory with a harsh climate and permafrost, which complicates mining operations, and slows recovery of ecosystems, exacerbating the anthropogenic impact on the environment. The Arctic environment is known to be fragile, climate conditions are harsh and the operational season is short. Success in this remote area will depend on appropriate selection of existing technologies and development of novel, more efficient ones [1].

The core of Yakutian diamond, oil and gas complex is in its western part, as the majority of positive reserves of diamonds and hydrocarbon crude are located in western and south-western parts of the republic. The largest diamond, oil and gas fields are situated in Western Yakutia.

II. Industrial sectors of the region

The area of disturbed lands in Mirny district ranks second in the Republic after the Neryungrinsky district (about 9 thousand hectares).

The history of diamond mining in Yakutia dates back to 1954, when prospectors discovered the first diamond pipe, Zarnitsa (‘Summer Lightning’). In 1957 the Soviet government established Yakutalmaz Group of enterprises, and diamond mining operations commenced. Two years later the USSR sold the first parcel of Yakutian diamonds on the world market. In 1963 the USSR entered into its first contracts with De Beers to sell its diamond production.

The history of ALROSA started in January 1957 as Yakutalmaz Group of enterprises. The Soviet diamond mining industry developed on the basis of the Mir open-pit mine and adjacent diamond placers. In those years its main open-pit mines, processing plants and related energy generating facilities were commissioned.

In February 1987 the USSR Ministry of Non-Ferrous Metals reorganized Yakutalmaz Group of production enterprises into Yakutalmaz Research and Production Association. The subsequent reorganization of Yakutalmaz and a number of stately-owned enterprises into a single joint stock company called Almazy Rossii-Sakha (Diamonds of

©2016 North Sea

Russia and Sakha) – ALROSA took place in 1992. ALROSA changed its legal entity form to public corporation.

Nowadays, ALROSA is the only diamond mining company which incorporates all the stages of diamond mining and beneficiation. In 2010 and 2011 it accounted for nearly one third of the global rough diamond production by volume, outperforming legendary De Beers. ALROSA is among the top ten of Russia's most efficient enterprises. The main operations of the company create 31,026 jobs [2].

Oil and gas extraction is a comparatively new industrial sector for Mirny district.

Russia possesses nearly a quarter of the world's proven natural gas reserves and produces around 18% of world output, second only to the US (BP, 2010 and IEA, 2012). Historically, the bulk of Russia's gas production came from the West Siberian area, which provided some 85% of the country's production in the 1990s and early 2000s. Today, the region's three major fields – Urengoyskoe, Yamburgskoe and Medvezhje – are in steady decline [3]. Many analysts suggest that future of Russia's oil and gas sector will be connected with the Arctic region [4; 5; 6].

The Sakha Republic of the Russian Federation the vast territory of which is located in the Arctic and sub-Arctic regions possesses 34 deposits of natural gas (2716 billion cubic metres) and crude oil (546 billion tons). Inferred resources of the Republic are estimated at 12 trillion cubic metres of gas and 546 million tons of oil. At the moment, only 20% of the inferred resources of the Republic have been exploited [7].

Gas prospecting in Yakutia has reached 2.3 billion cubic metres, and oil development 300 billion tons. In the two neighbouring regions of the Republic – Lensk and Mirny – the largest oil, gas and condensate fields are located: Chayandinskoye, Talakanskoye, Srednebotuobinskoye and Taas-Yuriakhskoye. These fields are included in the federal oil and gas transportation project "Power of Siberia".

All in all, 21 license holders are operating in 60 license blocks on the territory of Yakutia. The most prominent of them are GAZPROM, ROSNEFT, SURGUTNEFTEGAZ, SAKHATRANSNEFTEGAZ, Yakut Fuel Energy Co., TAASYURIAKH NEFTEGAZODOBYCHA, IRELYAKHNEFT, GAZPROMNEFT ANGARA, IRKUTSK Oil Company, and others.

The crucial year in the development of the oil and gas industry was 2004, when one of the most prominent Russian oil and gas companies SURGUTNEFTEGAZ OJSC became a license holder in Yakutia. The entrance of this company resulted in the rapid growth of the oil and gas industry. The lion's share of this volume belongs to the Talakanskoye field. Severo-Talakanskoye, Vostochno-Alinskoye, Peleduyskoye and Yuzhno-Talakanskoye fields were discovered by SURGUTNEFTEGAZ OJSC in the Sakha Republic during the period of 2007-2011 [8]. Talakanskoye, Alinskoye, Severo-Talakanskoye and Vostochno-Alinskoye fields were joined to the East Siberia – Pacific Ocean pipeline system and put into operation and maintenance. In Talakanskoye field, a pilot operation of a bitumen plant is being held at the moment.

Chayandinskoye oil and gas condensate field is located in the Lensk district of Sakha (Yakutia) Republic in the Far East region of Russia. The onshore field, also known as the Chayanda field, is being developed by GAZPROM. The onshore oil and gas field development forms a key part of the $38bn project to build the Yakutia gas production centre along with the Yakutia-Khabarovsk-Vladivostok pipeline. The integrated project is expected to create 15,000 construction jobs. The first oil production from the Chayandinskoye field is expected in 2015 and gas production is expected to start in late-2018. The field development cost is estimated to be $13.66bn. [9].

TAASYURIAKH plans to produce up to 1 million tonnes a year (20,000 barrels per day) from its East Siberian Srednebotuobinskoye field and aims to increase its output to 6.15 million tonnes (120,000 bpd) by 2016. The field with reserves of almost 1 billion barrels is connected to the East Siberia – Pacific Ocean by a 160 km pipeline [10].

The foundation of the Yakutian oil and gas production centre will increase local employment. Over 3,000 local petroleum engineers will be in demand to serve this sector [11].

The Mirny Polytechnic Institute (branch) of the Ammosov North-Eastern Federal University was founded in 1994 by the decision of Mikhail E. Nikolaev, the first President of the Sakha Republic who proclaimed this education policy to be the priority in the development of the Republic for the decades hence. It was intended to provide the ALROSA Company with needed specialists [12].

To meet the needs for specialists in oil and gas sector, the government of the Republic has opened the Petroleum Engineering Department in the Mirny Polytechnic Institute (branch) of Yakut State University (today's NEFU) in 2008.

At present the institute has prepared 2504 specialists, including 1438 mining engineers (976 of them employed by ALROSA) and 151 petroleum engineers. The majority are employed in ALROSA and leading oil and gas enterprises: GAZPROM, SURGUTNEFTEGAZ, LUKOIL, SAKHALINENERGY, SAKHATRANSNEFTEGAZ, LENSKGAZ, ALROSA GAS, IRELYAKHNEFT, BAKER HUGHES.

III. ECOLOGICAL PROBLEMS OF THE REGION

As investigators write, diamond mining development, accompanied by infrastructure and industrial development, caused significant negative environmental and social impacts in the diamond province, including:

- contamination of the river Vilyuy by dispersion of ground waters from kimberlite pipes and disposal of waste water from the processing operations;
- Twelve ‘peaceful’ underground nuclear explosions were carried out in Yakutia during 1967–1988; all but one were detonated on the territory of the present diamond province and one of them was directly linked to the diamond mining developments;
- creation of the Vilyuy hydroelectric power station and accompanying water reservoir contaminated the river with phenol and caused a reduction in the fish population in the river Vilyuy;
- deterioration of health amongst the population of the Vilyuy region linked to pollution of the river Vilyuy by heavy metals [13].

Here is the list of possible negative impacts on the environment of hydrocarbons extraction:

- deforestation on the sites for drilling wells, access roads and oil and gas pipelines;
- air pollution resulting from gas flaring and the operation of the equipment and transport;
- pollution of surface and ground water by discharge wastewater, technical liquids and petroleum products, and the depletion of water resources from excessive water consumption;
- pollution and destruction of soil and vegetation as a result of exposure equipment, and drilling waste disposal;
- the declines of wildlife populations because of disturbance of their habitats, migration routes and direct elimination;
- degradation of terrestrial ecosystems due to permafrost processes in open areas, and frequent fires caused by violation of fire safety rules;
- the degradation of terrestrial ecosystems due to changes in the hydrological regime and permafrost processes, and frequent fires caused by violation of fire safety rules.

In 1992, the Government of Yakutia initiated a programme for rehabilitation of the river Vilyuy basin (covering Kobyai, Mirny, Nyurba, Suntar Verkhnevilyuysk and Vilyuysk districts) via establishing the ‘Viluy’ Fund [13]. Several important political and economic changes in Yakutia and Russia as a whole affected the further development of this environmental programme.

Now it is widely recognized that for the management of social and environmental issues to be truly effective, moves towards sustainable development should involve constructive input from each of the three main groups of participants – industry, government and civil society [14; 15].

The public ecological Committee ‘Viluy’ drew the attention of the Government of the Republic and Russia to the environmental problem in the Vilyuy region and stimulated ALROSA to invest heavily in environmental protection measures.

To prevent or minimize disruptions to the areas where ALROSA operates the following principles aimed at reducing environmental risk are included:

- Compliance with national and international environmental legislation;
- Mitigation of negative impact on the environment by adopting management and technology solutions that take environmentally important aspects of the operations fully into account;
- Constant improvement of the environmental management system;
- Introduction of advanced technologies to achieve a higher level of environmental safety in all operating areas;
- Improved environmental awareness of the staff and their full involvement in efforts to reduce environmental risks;
- Providing open and accessible environmental performance information to the stakeholders [16].

ALROSA has now launched a new programme of environmental measures with activities mapped out from the present till 2018. They cover:

- Improvement of nature conservation management - including environmental auditing, environmental monitoring, the development and adoption of corporate standards of environmental management, and certification under ISO 14001:2004 and ISO 14001:2007 Environmental Management System’;
- Scientific and technical support of environmental activities;
- Exploration, development and deployment of innovative technologies in waste management;
- Increased openness and promoting public awareness of environmental performance.

The Company’s total environmental expenditure amounted to about RUB 5.96 billion in 2014 [16].

Over the last decade on the territory of the "diamond province", via the joint efforts of the Government of Republic, ALROSA, with the participation of the public, a lot of work aimed at reducing the negative impact of mining on the environment is being realized. As a result, the environmental situation has stabilized to a certain extent, the main problems and ways of their solution are identified.

Oil and gas extraction is a new industrial sector which also causes ecological problems to be considered and solved.

According to the Russian legislation companies should provide effective measures for the treatment and disposal of waste production and collection of oil (accompanying) gas and saline water at all stages of oil and gas production, reclamation of disturbed and contaminated land, reducing the negative impact on the environment and compensation for environmental damage caused during construction and operation of these facilities [17]. Construction and exploitation of objects of oil and gas production, processing, transportation, storage and realization of oil, gas and products of their processing are allowed at presence of projects of restoration of contaminated land in areas of temporal and (or) permanent land use, a positive conclusion of state examination of project documentation [18].

The land code requires land owners and land users to implement the reclamation of disturbed lands, restoration of their fertility and other useful properties of land and timely involvement in the economic turnover; the removal, use and preservation of fertile soil layer in the work connected with the violation of land [19]. The choice of remediation techniques should correspond to the climatic conditions, agrochemical and agrophysical properties of rocks, sanitation, and plan for the future development of disturbed land in the area [20].

In conditions of the North reclamation of disturbed lands is problematic. The main problems in reclamation are cryogenic processes, extending the areas of the violations, the lack of fertile soil for earthing due to the small capacity of the humus horizon of soils, and the problem of finding seeds and plants for biological recultivation. Most of the applied methods of reclamation in Yakutia do not take into account the specifics of the Northern territories and prefer cheap and simple technologies for remediation of soil with low-environmental efficiency, developed for the southern regions of Russia. Industrial companies use only the technical stage, levelling of the site and applying some of the soil in reclamation of the disturbed lands. As a biological stage of reclamation sowing seeds of herbaceous plants or natural regeneration are applied. Naturally, the implementation of such reclamation activities may not radically improve the environmental situation. The landscape will keep almost forever technogenic character. As a result, significant changes in water and thermal regimes and topography can also cause the degradation of adjacent undisturbed landscapes.

The problem is that there is almost no system for monitoring the compliance of restoration works of the users with the obligations. At the moment, in fact, the only form of control over the observance of norms and rules in the field of environmental protection is the industrial ecological control (IEC). This means that the companies independently plan and produce environmental monitoring, record the information and report to state regulators.

We may name a number of objective reasons why IEC is still not an effective instrument of solving ecological problems.

Firstly, the large-scale transfer of monitoring data from local level to regional and national is missing. The main part of the observation results conducted at the local level, remains on the shelves of customers and are not added to regional or national data Bank for environmental monitoring, while the state network of observation is deficient from the point of view of spatial coverage, number of points, controlled variables and control methods.

Secondly, industrial environmental control and monitoring at a considerable number of ecologically dangerous objects is not conducted or is limited to the minimum necessary scope of work, not related to the overall observing system.

Thirdly, the possibility IEC is limited by project budget, fixing the cost of the construction and operation of controlled objects.

This results in extreme distrust of the local population to reports of environmental authorities and nature users and thus to hardening of social tension. The main reason is inadequate awareness of the population about the state of the environment and insufficient objectivity and completeness of the results of industrial environmental control and monitoring.

The credentials of the controlling authorities of the Ministry of nature protection of the Republic do not apply to oil and gas companies because they relate to Federal facilities. There is also the problem of the complexity of monitoring because of location of oil and gas facilities in remote places in the forest. So the state control is conducted seldom. The state network of observation is deficient from the point of view of spatial coverage, number of points, controlled variables and control methods.

IV. Ecological Monitoring System in Mirny Polytechnic Institute

At the moment, there are few investigations of the consequences of anthropogenic impacts on Northern ecosystems, there are no evidence-based recommendations for the development and restoration of lands in Yakutia.

On the basis of the educational and scientific laboratory of complex analysis of anthropogenic disturbances of our Institute the students under the supervision of the Candidate of science in Biology Elena V. Sleptsova have organized an expedition and held an investigation of hard metals concentrations in the rivers adjacent to the oil and gas provinces. The samples of water, riverside soil and bottom silt were collected during August – September 2015 from the rivers Irelyakh, Chuonalyr, Ulakhan Botuobuya, Taas-Yuriakh and Ochuguy Botuobuya. Ulakhan Botuobuya and Taas-Yuriakh are located on the territory of Srednebotuobinskoye field next to Taas-Yuriakh settlement. For comparative analysis samples from the rivers Irelyakh, Chuonalyr and Ochuguy Botuobuya in the vicinity of Mirny town were taken. The analysis was carried out by means of the atomic absorption spectrometer ContrAA 700 according to the Measurement procedure-539-03 and Measurement procedure-80-2008.

Quantitative chemical analysis of heavy metals in the rivers in the area of Srednebotuobinskoe field showed the exceedance of Iron, Aluminum and Cadmium, which applies to 2 hazard class.

The exceedance of maximum permissible concentration (MPC) [21] of Aluminium for drinking and household, cultural and social water consumption was registered in the Taas-Yuriakh (1,5 times) and the Irelyakh (2 times) rivers; of Iron – in the Taas-Yuriakh (1,3 times) and the Ochuguy Botuobuya (1,5 times) rivers; of Cadmium – in the Ulakhan Botuobuya river (2 times) (See Table 1).

TABLE 1, HEAVY METALS CONCENTRATIONS IN NATURAL WATER, μG/L

	Irelyakh	Chuonalyr	Ulakhan Botuobuya	Taas-Yuriakh	Ochuguy Botuobuya	MPC [21]
Manganese	33	51	6,4	31	5,4	100
Copper	<1	<1	<1	<1	18,8	1000
Cadmium	<0,1	<0,1	**2,25**	0,27	<0,1	1
Aluminium	**412**	104	75	**293**	47,1	200
Iron	182	122	75	**390**	**451**	300
Zinc	71	<1	<1	77	<1	1000
Cobalt	<1	<1	<1	<1	<1	100
Chrome	<1	<1	<1	<1	<1	50
Nickel	9	<1	<1	<1	<1	20
Lead	<1	<1	<1	<1	<1	10

The danger of the exceedance of MPC in riverside soil [22] lies in the fact that it is capable of interfering with the biochemical processes of living organisms. The exceedance of MPC of active forms of Copper is marked in the Irelyakh, Chuonalyr, Ulakhan Botuobuya and Taas-Yuriakh rivers; of Zinc in the Irelyakh and Chuonalyr rivers (from 13 to 52 mg/kg); of Chrome in the Chuonalyr river (from 2,4 to 7,8 mg/kg); of Nickel in the Irelyakh, Chuonalyr, Ulakhan Botuobuya and Taas-Yuriakh rivers (from 1,4 to 24 mg/kg) (See Table 2).

TABLE 2, ACTIVE FORMS OF HEAVY METALS CONCENTRATIONS IN RIVERSIDE SOIL, MG/KG

	Irelyakh	Chuonalyr	Ulakhan Botuobuya	Taas-Yuriakh	Ochuguy Botuobuya	MPC [22]
Manganese	**236**	**533**	**185**	**212**	125	140
Copper	**29,9**	**36,9**	**5,4**	**4,45**	1,34	3
Zinc	**52**	**32**	15	17	13	23
Cobalt	4,1	2,8	3,8	2,6	1,5	5
Chrome	5,2	**7,8**	4,7	5,8	2,4	6
Nickel	**24**	**23**	**9,2**	**5,8**	1,4	4
Lead	8,1	1,3	0,97	1,3	0,71	32

The pollution of river water, riverside soil may lead to the contamination of bottom silt which may cause secondary contamination of water. The analysis of heavy metals concentrations in bottom silt displays the exceedance of MPC [22] of Manganese in the Chuonalyr and Ochuguy Botuobuya rivers. The exceedance of Copper is registered in all the rivers; of Zinc in Irelyakh and Chuonalyr; of Chrome in Irelyakh; of Nickel in Irelyakh, Chuonalyr and Ulakhan Botuobuya (See Table 3).

TABLE 3, ACTIVE FORMS OF HEAVY METALS CONCENTRATIONS IN BOTTOM SILT, MG/KG

	Irelyakh	Chuonalyr	Ulakhan Botuobuya	Taas-Yuriakh	Ochuguy Botuobuya	MPC [22]
Manganese	132	**263**	129	72	**153**	140
Copper	**28,5**	**19,9**	**4,25**	**41,34**	**33,8**	3
Zinc	**53**	**34**	9,1	18	12	23
Cobalt	3,1	4,3	3,1	1,6	1,2	5
Chrome	**7,8**	3,6	4,2	2,8	1,7	6
Nickel	**40**	**8,7**	**7,7**	2,5	0,41	4
Lead	8,4	0,55	0,8	0,1	0,33	32

The data show that the rivers, riverside soil and bottom silt in the oil and gas province are contaminated by heavy metals.

For the purpose of optimization of water pollution control we suggest the foundation of ecological observation station and regular monitoring.

We are planning further comprehensive studies with the aim of obtaining a coherent picture of the impact of oil and gas complex on environment on the territory of Western Yakutia. Effective assessment of the ecological state of Northern ecosystems is needed to predict and analyze the impact of developing industries of mining in Western Yakutia. The research results will allow to develop recommendations for the most appropriate and cost-effective ways of mining and remediation techniques in permafrost condition.

The Institute's educational and scientific laboratory of complex analysis of anthropogenic disturbances pursues the following goals:

- creation of conditions for environmental monitoring in Western Yakutia;
- investigations by specialists of MPTI in the field of ecology involving students in research activities;
- improvement of environmental education of MPTI students.

In December 2015 the laboratory was included in the register of accredited organizations, which allows controlling the objects in conformity with the necessary requirements and ensures the accuracy of the results. In future we plan to expand the scope of accreditation.

V. CONCLUSION

The institute has close ties with industrial enterprises operating in Mirny district: ALROSA, GAZPROM, ROSNEFT, SURGUTNEFTEGAZ, TAASYURIAKH NEFTEGAZODOBYCHA, IRELYAKHNEFT and others.

Organization of public ecological monitoring system in the West of Yakutia with the involvement of research and material resources of the Mirny Polytechnic Institute (branch) of Ammosov North-Eastern Federal University will give an objective integrated assessment of the impact of the oil and gas industry on the environment on the territory of Western Yakutia, which should encourage subsoil users to apply more effective measures to reduce the impact on the natural environment and increasing payments for environmental damage.

Since 2012 the institute takes part in public hearings of industrial enterprises where companies present the feasibility study of their mining projects in which they are expected to follow environmental and rehabilitation codes. One of the latest public hearings took place on March 25, 2016 in the centre of Evenkiysky National district – Olenyok, where the ALROSA Company presented the project of launching mining operations in Verkhnemunskoye deposit of the region. The meeting was attended by the local population and authorities, the representatives of the Ministry of Ecology and other public officials. The hearings resulted in signing an agreement on mining operations by ALROSA.

In April 2016 all these companies reported their activities during 2015 in Mirny administration in the presence of the indigenous population inhabiting the district.

May 24, 2016 the public hearings devoted to the ecological issues took place at the site of the TAASYURIAKH NEFTEGAZODOBYCHA with the participation of the members of the Government of the Sakha republic, administration of Mirny district and local population.

As the result of the debates during these meetings the companies were demanded to meet the requirements of the people in order to establish adequate communication between industry, local authorities and local population.

REFERENCES

1. Bishop A., Bremmer Ch., Laake A., Strobbia C., Parno P., Utskot G. Petroleum Potential of The Arctic: Challenges and Solutions. Oilfield Review Winter 2010/2011: 22, no. 4. pp. 36-49.
2. Goldman A. A., Vishnevskaya M. V., Glazun M. A., Ivanova R. P. English for Diamond Miners. Moscow : Flinta : Nauka, 2014. 492 p.
3. Lunden L. P., Fjaertoft D., Overland I., Prachakova A. Gazprom vs. other Russian gas producers: The evolution of the Russian gas sector. Energy Policy. Volume 61, October 2013, pp. 663–670.
4. Aalto P., Modernization of the Russian Energy Sector: Constraints on Utilizing Arctic Offshore Oil Resources. Europe-Asia Studies. Vol. 68, Issue 1, 2016, pp. 38-63.
5. Gautier D., Bird K., Charpentier R., and others. Assessment of Undiscovered Oil and Gas in the Arctic. Science. 29 May 2009: Vol. 324, Issue 5931, pp. 1175-1179.
6. Spencer A. M., Embry A. F., Gautier D. L., Stoupakova A. V., Sorensen K. Arctic Petroleum Geology. Geological Society Memoir. N 35. 2011. London: Geological Society of London. 818 pp.
7. The Republic of Sakha (2015, May 30). About the Republic. Official Site of The Republic of Sakha [Online]. Available: http://www.sakha.gov.ru/
8. Surgutneftegaz Launched Severo-Talakanskoye Oil Field (2011, December 28). Moscow's XIII International Energy Forum "Russian Fuel and Energy Complex in the XXI Century" [Online]. Available: http://www.mief-tek.com/564.php
9. Chayandinskoye Field, Yakutia, Russia (2015, October 13) News, views and contacts from the global Hydrocarbons industry [Online]. Available: http://www.hydrocarbons-technology.com/projects/chayandinskoye-field-yakutia-russia/
10. Eastern Siberia: Oil and Gas (2015, October 14) Capable Translations [Online]. Available: http://www.capabletranslations.com/
11. Goldman A.A. Petroleum Engineering Education in NEFU, Yakutia // Journal of Siberian Federal University. 2015. No. 8. pp. 1551-1559.
12. Goldman A.A. Buduscheje sozdajotsa v nastojaschem (Mirny Polytechnic Institute: Future is created in the present). Gornyi Zhurnal = Mining Journal. 2014. No. 1. pp. 6-9.
13. Yakovleva N., Alabaster T. Tri-sector partnership for community development in mining: a case study of the SAPI Foundation and Target Fund in the Republic of Sakha (Yakutia) // Resources Policy. Volume 29, Issues 3–4, September–December 2003, pp. 83–98.
14. Acquah P.C., 1994. Government environmental regulations and implementation in the mining sector. Natural Resources Forum 18 (3), 193–206.
15. Davy A., 1999. Social responsibility and governments. Mining Environmental Management 7 (1), pp. 16–17.
16. About us. Alrosa (2015, June 22). *Alrosa* [Online]. Available: http://eng.alrosa.ru/

17. Federal Environmental Law d.d. 10 January 2002 (R.E. 29 December 2015).
18. Federal Law Concerning Ecological Examinations d.d. 23 November 1995 (R.E. 29 December 2015).
19. Land Code of the Russian Federation d.d. 25 October 2001 # 136-FL.
20. Order of the Ministry of Natural Resources and Environment of the Russian Federation and the Committee of the Russian Federation for Land Resources and Land Management d.d. 22 December 1995 # 525/67 On approval of fundamentals of soil reclamation and topsoil management.
21. Maximum Permissible Concentration (MPC) of chemical substances in water for drinking and household, cultural and social water consumption: Hygienic Regulations. HR 2.1.5.1315-03. – Moscow, Russian Register of potentially dangerous chemical and biological substances, Ministry of Health of Russian Federation. 2003. 154 p.
22. Maximum Permissible Concentration (MPC) of chemical substances in soil: Hygienic Regulations. HR 2.1.7.2041-06. – Moscow, Federal Sanitary and Epidemiological Center of Federal Service for Consumer Rights Protection and Human Welfare. 2006. 15p.

Journal of Energy Challenges and Mechanics

http://www.nscj.co.uk/JECM/

ISSN 2056-9386
Volume 3 (2016) issue 3, article 3

Optimized reactive power management across different voltage levels on the example of medium-voltage grids

中壓電網示例中跨不同電壓電平之優化無功功率管理

Steffen Garske[1]*, Marcel Sarstedt[1], Lutz Hofmann[1], Jorge Velasquez[2], Sebastian Lehnhoff[2]

[1]*Institute of Electric Power Systems, Electric Power Engineering Section, Leibniz Universität Hannover, 30167 Hanover, Germany*
[2]*OFFIS – Institute for Information Technology, 26121 Oldenburg, Germany*

garske@ifes.uni-hannover.de

Accepted for publication on 3rd September 2016

Abstract - **The secure supply of ancillary services in the future electrical energy supply system is an important question of both distribution and transmission system. Decentralized generation units provide an increasing share of the electrical power generation. Thus, these units are an important factor within the overall grid state. The latest grid code requirements for generation units, depending on voltage level and nominal power, include the ability of reactive power provision, in the distribution grid mainly for voltage band optimization. This required reactive power provision and in addition, the current grid expansion as well as the grid integration of new consumers, e.g. electric mobility, leads to ongoing changes within the reactive power exchange between all voltage levels. In future grid states an optimized reactive power exchange will be needed for a secure grid operation. In this paper, the results of the interdisciplinary research project "iQ" for optimized reactive power management of medium-voltage grids regarding the high-voltage level are described as well as the outlook for further research questions in the field of reactive power exchange across all voltage levels.**

Keywords - **power system management; reactive power control; distributed power generation; wind power generation, smart grids**

I. INTRODUCTION

The provision of reactive power is an important ancillary service for as well the transmission system as the distribution system of the electric power grid. Because the transmission of reactive power over long distances leads to massive voltage drops, it has to be solved as a local problem and the reactive power demand of all grid components and consumers has to be provided for all points in time within varying grid states. Traditionally the synchronous generators of conventional power plants provided with different field ratios in addition to static VAR compensators or flexible alternating current transmission systems (FACTS) the reactive power demand in the transmission system. To optimize the compliance with the tolerable voltage bands in the transmission system a three-level concept comparable to the control power reserve has been established [1]. First the transformer tap-changers are set automatically to secure predefined voltage set-points. Secondly the set-points of the voltage regulators of the synchronous generators are optimized or reactive power compensators are switched on. Afterwards optimal power flow (OPF) methods are used to monitor and optimize all control variables.

The reactive power demand of distribution grids has been depending on the active power demand of the loads. Low load states in (medium-voltage) grids with high shares of cables lead to reactive power provision[I] for the higher voltage levels, peak load states to a high reactive power demand (see Fig. 1) [2]. Within the ongoing transformation of the energy supply system the share of distributed generation (DG) units mainly using renewable energy sources (RES) is increasing. The primary energy sources of the DG are thereby fluctuating with time. Because the DG units are mainly connected in the distribution grid and hence to the low-voltage (LV), medium-voltage (MV) or high-voltage (HV) grid, the load flow direction between all voltage levels as well as the amount of reactive power exchange is changing. Furthermore the correlation between active and reactive power is getting more and more unpredictable and independent of the current load situation, but more dependent on the current feed-in of the distributed generation and ratio of DG and loading. This leads on the one

[I] In this paper current and voltage are assumed the same direction in a passive load ("*Verbraucherzählpfeilsystem*")

©2016 North Sea

hand to points in time where distribution grids start to provide reactive power to the ultra-high-voltage (UHV) level and on the other hand to increasing reactive power demand in all voltage levels.

In future grid states with high shares of DG synchronous generators of conventional power plants may no longer be evenly distributed in the transmission system and active in all points in time. Hence the future reactive power supply in the highest system level will presumably have to be reassigned and the reactive power exchange within all voltage levels rearranged (see Fig. 1).

A classic characteristic load state is a low load state without active or reactive power supply of DG units. In this grid state power lines with high nominal voltages with low loading provide reactive power (blue arrows in Fig. 1) because of their capacitive characteristics and the load state below the natural operational. The low reactive power demand (red arrows in Fig. 1) of normally high demanding loads, as e.g. industrial loads, could in this case be supplied by the capacitances of power lines and the synchronous generators, which in some cases could also operate underexcited (see Fig. 1). Within such load cases in some extent the MV level especially in rural regions could provide reactive power to the HV level.

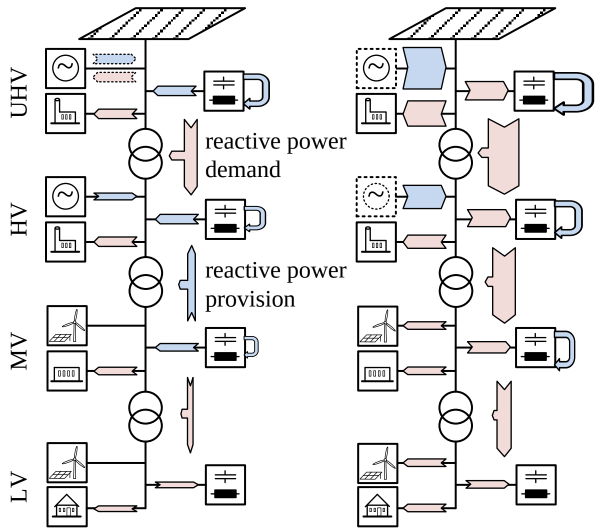

Fig. 1, Change of reactive power demand and exchange within all voltage levels

One future problematic grid state could be a high load state with active and reactive power supply of DG units with e.g. a fixed inductive power factor cos(φ) to handle the problem of voltage increase at high feed-in of active power [3], [4]. In load cases like this the reactive power exchange throughout all voltage levels would be clearly different. All power lines (including the cables) would demand reactive power because the inductive share exceeds the capacitive characteristic because of the load state above the natural operation. Also the loads and transformers demand reactive power. The demand of the DG units is dependent on their active power supply, thus fluctuating with time. Without a high-level coordination and a possible loss of the synchronous generators in the UHV level the reactive power supply within all voltage levels could be demanding, because first a high demand and second a high exchange of reactive power has to be supplied and controlled.

Several solutions for this problem are discussed. Under reserve of the future grid expansion plans, the integration of high-voltage direct current (HVDC) power lines with the according voltage source converters (VSC) could provide additional reactive power sources in the transmission system. This could lead to more control variables in a hybrid grid operation with high-voltage alternating current (HVAC) and HVDC systems [5]. Also classic solutions with expansion of static VAR compensators or other FACTS are a possible solution with well-known modeling and simulation approaches [6], [7]. Because one driver of the reactive power exchange variations are the DG in the distribution system, an optimized reactive power management with the use of DG units and an optimized reactive power exchange within all voltage levels is also a common solution [2], [8], [9].

II. Reactive Power Management of Distribution and Transmission Grids

As a consequence of the high generation of DG in the lower voltage levels, voltage band problems can occur if the power supply is not handled correctly [10]. Therefor the grid codes and requirements for generation units in the medium or low-voltage grids demand detailed outlined reactive power provision of generation units. This has been progressively increased with the growing share of DG in the energy supply system. The grid codes are specified depending on nominal voltage and power of the generation units [3], [4]. In this way voltage band problems and the need of grid expansion can be minimized. In addition with the beginning of the year 2016 the European Commission in cooperation with the European Network of Transmission System Operators (ENTSO-E) published comparable binding grid codes for all voltage levels [11]. The national grid codes will be complemented with the new requirements and define open issues.

One challenge within the analyses and standardization of distribution grids is the high diversity of these grids, especially in the lower voltage levels. The relevant grid parameters as e.g. load density, length of lines, share of cables and saturation with DG vary extensively between e.g. rural and urban grids as well as between different regions. Hence every distribution grid is considered to be very individual. The German forum network technology / network operation (VDE FNN) has published a guideline for the evaluation of the reactive power ability of distribution grids [8]. These guidelines are considered in the scenario definition (see 3.2) and stationary simulations of this study (see 3.3).

The reactive power provision is one important aspect in the evaluation of the possibilities as well as the boundaries of a future energy supply system mainly based on DG using RES. Because this is an integrated matter of both system levels (transmission and distribution system) a coherent

 ©2016 North Sea

overall system model is needed to analyze the interactions across all voltage levels [12], [13], [14]. The research project *Smart Nord* developed several interdisciplinary methods and approaches for research questions in the fields of decentralized coordination procedures, integrated markets, micro grids, capability and environment as well as the power grid and European market [12]. One aspect in the working package 4.1 was the development of a voltage level comprehensive system model (see Fig. 2) to evaluate the integration of DG units in addition to an existing grid and market model of the ENTSO-E transmission system [13], [15], [16]. This model was used to analyze both stationary as well as dynamic processes [17].

The project *Smart Nord* covered the analyses of active power supply of DG within all voltage levels, frequency stability analyses with control power reserve of DG units and voltage band optimization in the transmission system [17]. Within the analyses of stationary processes the reactive power provision was briefly simulated with synthetic high-voltage grids and several scenarios [18] for adapted versions of a medium-voltage benchmark grid [19]. The research question covered the pan European integrated grid and market simulation, thus an effective large-scale approach was used.

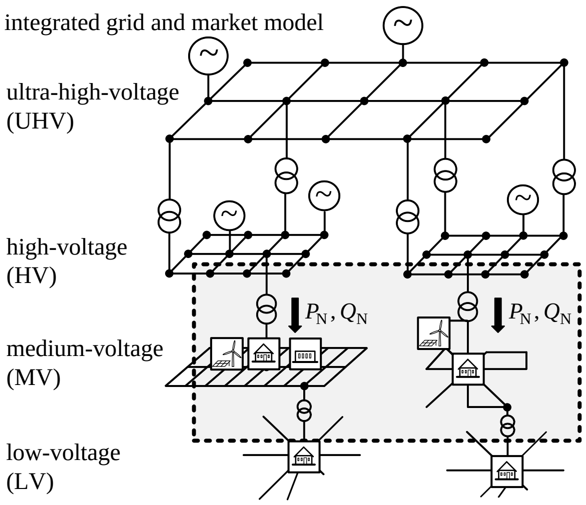

Fig. 2, Adapted cohesive grid and load model [18]

Considering the high divergence of medium-voltage grids and the increasing interconnection of the transmission and distribution system, a more detailed approach for analyses of an optimized reactive power exchange between different voltage levels was needed. Thus within the follow-up project to *Smart Nord* the research project “iQ” – intelligent reactive power management – stationary analyses of several medium-voltage grids in different scenarios have been realized to identify the reactive power ability of characteristic distribution grids [20]. In this way possible reactive power provision concepts between medium and high-voltage grids could be elaborated. The cohesive grid and load model was reduced to the MV and HV level and the total aggregated grid power consumption (P_N, Q_N) at the high-voltage side of the main transformer of the single MV grids including all loads, generation units and losses are used as main resulting variables (see Fig. 2 and Fig. 4 to Fig. 7).

III. Research Project iQ

The interdisciplinary research project “iQ – intelligent reactive power management” was a one year lasting cooperation between research institutes of information technology, power supply and control theory with industrial partners of grid operators and IT consulting [20]. The main research question of the project was to analyze and optimize the control and stability of reactive power provision of DG units regarding requirements for the reactive power exchange at the main HV/MV-transformer for specific set-points.. Different approaches and methodologies have been evaluated by the use of both software analyses and a co-simulation set-up. An industrial control-hardware was used to be evaluated for the different control tasks within the project. First the interconnection of the simulation models was established via software interfaces. Second a real-time simulator was used in order to establish the communication with the hardware-based control strategy (realized with an industrial controller). The main task for the software set-up was the incremental development of both the co-simulation and hardware setup with the use of an industrial computer [21].

The input parameters of the research project, in this project the grid models and load data, have been analyzed in characteristic distribution grids in different scenario setups of the reactive power provision of the DG units in stationary time-series simulations (see chapt. III). These results have been the basis of the evaluation of optimized reactive power exchange of the rural grid regarding the HV level and the co-simulation approach and evaluation of control strategies (see chapt. IV and [20]).

3.1. Implementation of Typical Grid Data

To cover the high divergence of medium-voltage grids four typical MV grids (see TABLE 1 and TABLE 2) have been selected and modeled with the power system modeling and simulation tool DIgSILENT PowerFactory [22]. In the first project stage a common rural grid from a literature source was used to have a quick set-up [8], [9]. Additionally the project partners (an urban and a rural grid operator) provided all needed grid specifications (see TABLE 1) for one rural 20-kV-grid, one urban 10-kV-grid and one suburban 20-kV-grid. The data included measured data at the HV/MV-transformer. All data had been transferred and implemented in PowerFactory to enable a manageable data exchange between all research partners.

TABLE 1, Structural parameters of the analyzed MV grids

grid	power lines	local substations
urban 10 kV	41.5 km	67
urban 20 kV	95.2 km	113
rural 20 kV	134.5 km	113
literature [8], [9]	199 km	121

All grids show different characteristics for as well the topological data (see TABLE 1) as well as the installed power of DG and the particular peak load (see TABLE 2). In the rural grid one wind farm close to the HV/MV-transformer with eleven wind turbine generators (WTG) with 22 MVA installed power in total is notable. Whilst in the grid of previous works [9] a mix of WTG and photovoltaic (PV) units was used, the urban grids have only a few DG units including combined heat and power units (CHP) installed in the current state.

TABLE 2, INSTALLED POWER OF DISTRIBUTED GENERATION UNITS IN THE ANALYZED MV GRIDS IN MVA

grid	WTG	PV	CHP	loads
urban 10 kV	0	0	0	17.64
urban 20 kV	3.7	1.74	5.37	39.44
rural 20 kV	22.15	3.2	0.23	35.22
literature [8], [9]	6	19.1	0	25

Because the research focus of the project was the control of DG units, the urban 10-kV-grid without any DG was not analyzed in detail. The grid operators provided the measured data of active and reactive power at the high-voltage side of the main HV/MV-transformer at the substation. Hence different configurations of the DG units should be analyzed in time series simulations, all loads and generation units needed data for one year. The source of the normalized time series of the loads was the parent project *Smart Nord* [12], the normalized generation data was determined from public data of a transmission system operator [23], [24].

With these synthetic load and generation data in combination with the nominal data in the grid models the original grid behavior has been reproduced [21]. However the simulated grid behavior at the main transformer differs from the measured data, because of a higher simultaneousness of the loads and DG as well as missing information of further influencing factors.

The maximum values of active power have been used to determine the need of scaling factors analog to the simultaneity factor in standard grid analyses. The implemented time series leads to specific grid characteristics shown in TABLE 3. With the combination of the normalized time series the dates for typical high and low load states could be determined.

TABLE 3, CHARACTERISTIC POINTS IN TIME OF HIGH AND LOW LOAD

date dd.mm.yyyy	time hh:mm	wind in %	solar in %	loading in %
21.03.2015	13:00	55	99	68
20.12.2015	19:00	89	0	72
18.07.2015	13:00	0	87	81
30.10.2015	20:00	0	0	67
11.05.2015	11:00	70	59	39
23.12.2015	04:00	95	0	15
07.06.2015	09:00	0	72	29
01.10.2015	05:00	0	0	12

These points are not the maximum/minimum load states or maximum/minimum feed-in of the DG, but typical points within the correlation of all load and generation data. The time points are useful to compare different scenarios or grid analyses, thus the shown color classification is used to highlight these specific load states in the results (cf. Fig. 4 to Fig. 7).

3.2. SCENARIO DEFINITION

Time series simulations within different scenarios have been used to evaluate the reactive power capability of distribution grids. The aim is to determine the operational area of these grids and thus the possible adjusting range for a potential control of reactive power provision [8]. According to the latest grid codes four scenarios were defined for the simulations (see TABLE 4).

TABLE 4, SCENARIOS FOR DG UNITS AND LOADS IN THE STATIONARY GRID ANALYSES

scenario	WTG	PV	loads
1	1	0.95 ind.	0.98 ind.
2	0.95 ind.	0.95 ind.	0.98 ind.
3	0.95 cap.	0.95 ind.	0.98 ind.
4	$\cos(\varphi)(P)$	0.95 ind.	0.98 ind.

To reduce the problem on the comparison of control of reactive power through a single control unit in different set-ups the photovoltaic units have been simulated with fixed power factors according to the current grid codes [3], [4], irrespective of nominal power or date of installation. The different reactive power provision of the wind turbines is therefore the main research task, because for the rural grid the control hardware was set up to optimize the wind farm at the main busbar and the results shall be comparable [20], [21].

The scenario 4 with the function $\cos(\varphi)(P)$ describes a reactive power supply proportional to the active power P with two boundaries for low and high power provision according to the current grid codes for generation units in medium-voltage grids [4].

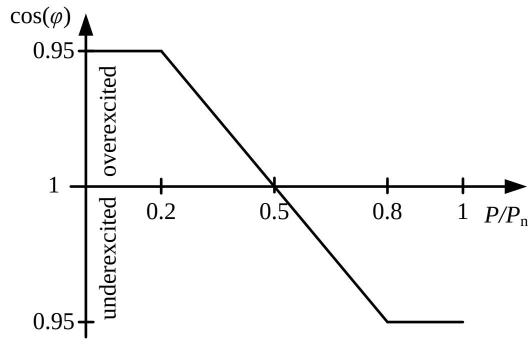

Fig. 3, $\cos(\varphi)(P)$-characteristic for scenario 4 according to [4]

In this paper the characteristic is defined with limits of 0.2 and 0.8 for the ratio of P/P_n (ratio of active power P to nominal power P_n) and 0.95 as limitation for the inductive or capacitive load factors.

3.3. Reactive Power Management of typical Medium-Voltage Grids in different Scenarios

For the modelled medium-voltage grids all scenarios were simulated in time series of one year in one-hour steps. The results are shown for all grids (except the urban 10-kV-grid) with the characteristic points of high and low load highlighted in the diagrams. For the reactive power capability analyses the shown diagrams provide a good indication [8]. The results of the time series simulations are plotted with each reactive power Q_N to the corresponding active power P_N at the main transformer for every single point in time. In this way *PQ*-clouds or -curves can be determined from the load flow calculations, which describe the stationary grid behavior for the different grids over one year precisely and allow a comparison of different input parameters [8].

20-kV-rural grid (literature)

At points in time with high load and only little generation the reactive power follows the active power demand proportionally (see Fig. 4 – high load case 4). The high share of PV units in this grid leads to a constant reactive power provision within all scenarios. Hence the grid behavior is not varying significantly between all analyses. Low loading of lines brings out the capacitive characteristic of the power cables, especially for a rural grid with long circuit lines (see Fig. 4 – low load case 4). The results show primarily for scenario 1 and scenario 2 a typical grid behavior of medium-voltage grids with a high share and balanced mixture of DG units [8], [9].

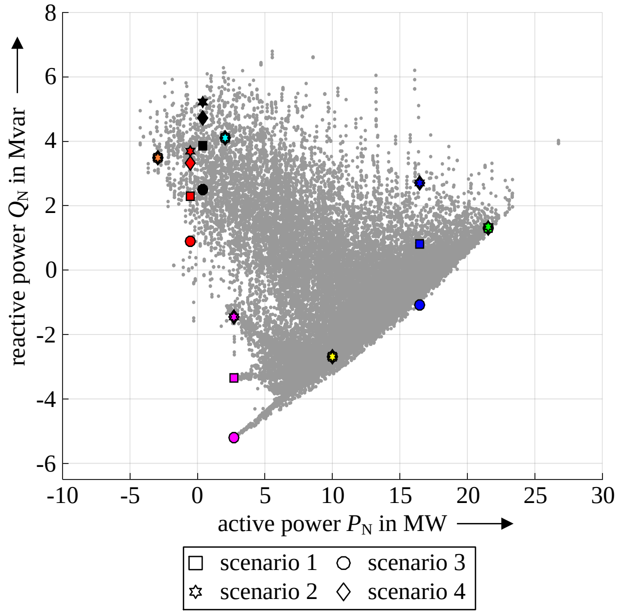

Fig. 4, Results for the 20-kV-rural grid in the scenario analyses

The unusual capacitive power factor in scenario 3 (the wind turbines provide reactive power and increase the nodal voltages) leads to the most negative operational points for the reactive power exchange at the main transformer (see Fig. 4 – low load case 2). Due to possible voltage band problems this scenario is not practically reasonable in all points in time, but works as negative boundary for the capability analyses. The scenario 4 with the cos(φ)(P) characteristic is always between the limitations of 0.95 underexcited and 0.95 overexcited (see Fig. 3) and thus between scenario 2 and scenario 3 (see e.g. Fig. 4 – high load case 1).

For this grid model detailed analyses have been published in several studies [8], [9], hence it was used as benchmark for the simulation set-up.

20-kV-urban grid

The urban grid with 20 kV nominal voltage has only very few DG units installed. Thus in all scenarios a very proportional behavior of active and reactive power to the load states was obvious. Additionally, because of the shorter length of lines and higher load density, the minimum value of Q_N is only about -3.5 Mvar (see Fig. 5 – low load case 2).

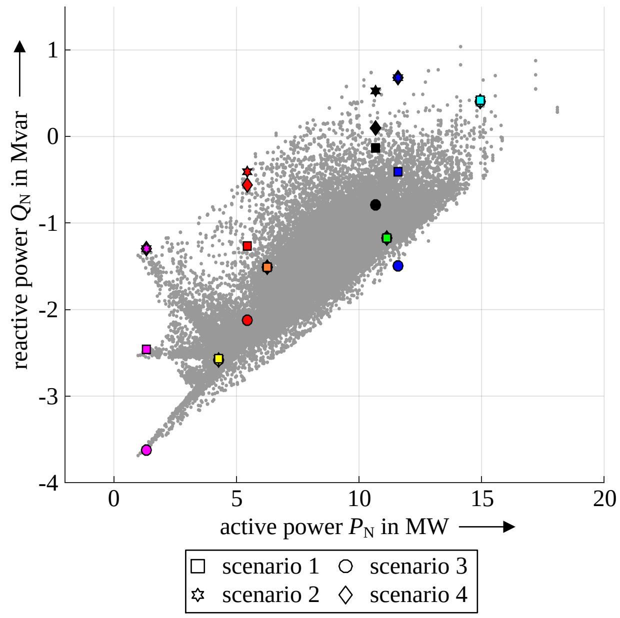

Fig. 5, Results for the 20-kV-urban grid in the scenario analyses

To match the measured data of the grid operator a scaling factor of 0.6 had to be used for all loads, because the simultaneousness of the used load time series did not exactly recreate the original data. The results show a typical overall grid behavior for nearly all points in time with a negative reactive power balance to the upper voltage level. Potential scenarios for reactive power optimization could be a more optimized grid behavior or a minimization of the impact on the upper voltage levels, if more DG units are installed with a future expansion of RES in urban grids like this.

20-kV-rural grid

The rural grid including the measured data from the grid operator was the main simulation subject of the research project "iQ". With a 22 MVA wind farm installed at the main busbar a good practice-oriented set-up could be build up, especially for the co-simulation approach with the control-hardware. The results of the stationary grid analyses (see Fig. 6) show a different characteristic of active to reactive power behavior as the other observed grids (cf. Fig. 4 and Fig. 5).

Contrary to the other grid simulations, the measured data and the results did first not match either qualitative or quantitative. This can be explained with different input parameters in the load flow calculation, the aggregation of some subgrids (as e.g. the cables of the wind farm and a few bigger industrial loads), different voltage set-points at the main transformer and of course a much more individual behavior of all loads within the real grid in comparison to the simulation. As a solution a base load of 5 Mvar had to be installed to match the measured data quantitative.

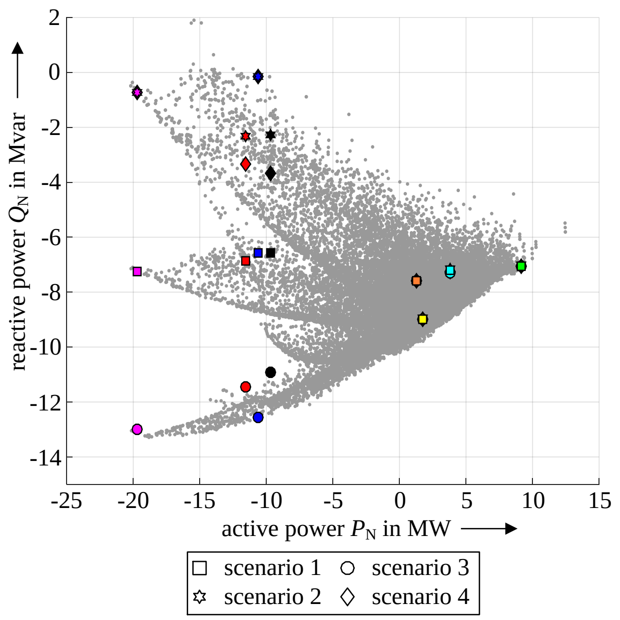

Fig. 6, Results for the 20-kV-rural grid in the scenario analyses

The qualitative behavior could not be matched satisfactorily. The exact operation for active and reactive power of the wind farm in the time span of the measured data could not be elaborated. However independent from the actual operation of the wind turbines in the comparison between the measured data and the results of the four scenarios (see Fig. 6) the best match has been most likely an operation between either scenario 2 ($\cos(\varphi)$ = 0.95 ind.) or scenario 4 ($\cos(\varphi)(P)$) to reproduce a most matching overall grid behavior.

An improved methodology of recreating measured grid data and the influence of further possible improvements for emulating the original grid behavior as e.g. different grid switching states and more individual loads is still a missing task (see chapt. VI). Furthermore the grid model was supplemented with 400 mm² AL cables with a standard two-string-topology for the wind farm to consider the influence of the connecting cables to the reactive power exchange. This was also an important parameter of the control hardware.

In comparison of all scenarios the results show the high influence of all DG units and especially the wind farm (see Fig. 6):

- the original grid as well as the simulation results show a high negative behavior of the reactive power for most points in time (compensators have not been considered in the simulations)
- all scenarios have a big influence on the overall grid behavior (power exchange and voltage bands)
- scenario 1 differs from the results of the literature grid because of different WTG/PV and load ratio
- scenario 2 and 3 are primarily proportional of wind-farm active power to reactive power (the influence of the PV units is diminished)
- scenario 4 differs as in Fig. 4 between scenario 2 and 3 because of the used $\cos(\varphi)(P)$-characteristic
- the reactive power ability differs significantly with the available active power of the DG units
- the difference between the characteristic points in time varies from only a few Mvar up to 14 Mvar at weak load and high wind generation

The 14 Mvar difference at the peak generation approximate the overall reactive power ability of the wind farm. In the optimization of the reactive power exchange (see 4.1 and 4.2) a typical operation diagram of wind turbines was used to determine this characteristic more detailed. Within the project this results were used as framework for the further studies with the control hardware, complemented also with analyses of control values and system stability [20].

3.4. Comparison of the Stationary Grid Analyses

All results combined with a synthetic simulation of the urban 10-kV-grid, which was supplemented with a WTG for comparison purposes, give a good overview of the high divergence of the stationary grid behavior (see Fig. 7).

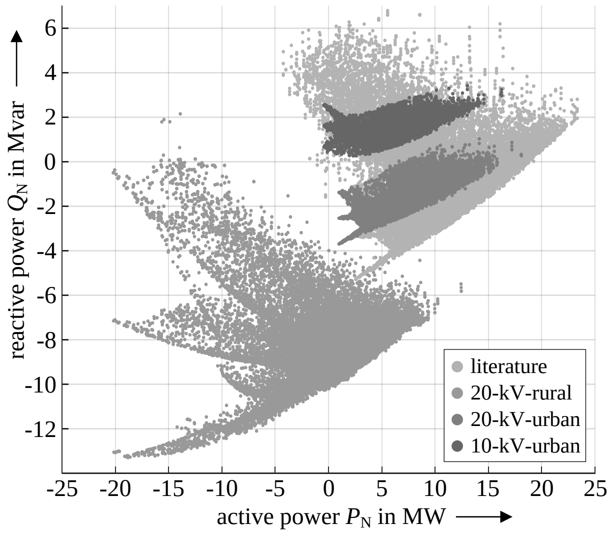

Fig. 7, Results of all medium-voltage grids combined

Especially the 20-kV-rural-grid is deviating from the average grid behavior. The specific points in time of high and low load allow a good and quick approximation of the active to reactive power characteristic, but only the simulation for one year, even with time characteristics with a higher simultaneousness than real loads and generation units, describe the grid behavior sufficiently. Additional approaches as e.g. the variation of photovoltaic units, alternating voltages at the 110-kV-busbar, automatic tap-changing of the main transformer or different load characteristics have also been simulated for selected grids, but will be content of future work (see chapt. VI).

IV. REACTIVE POWER EXCHANGE OPTIMIZATION

After the stationary analyses of all presented medium-voltage grids, the optimization of reactive power exchange between the high-voltage grid and one single medium-voltage grid (the rural 20-kV-grid) has been analyzed. Two different approaches have been realized. First a simulative analyses was implemented in PowerFactory, to give a theoretical basis of comparison to the experimental approach. Second, a co-simulation with the integration of a control-hardware was set up (see Fig. 8).

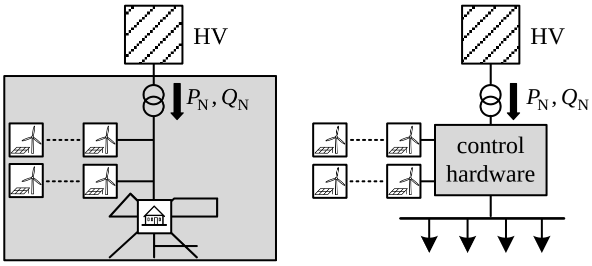

Fig. 8, Set-up for the reactive power exchange optimization approaches in section 4.1 and 4.2

The aim of both approaches was to fulfil definite set-points at the high-voltage side of the main transformer for the reactive power Q_N, which is equal to the reactive power exchange between these two voltage levels as well as the overall medium-voltage reactive power consumption of the considered MV grid model. The differences of both approaches are within the details of the grid model (see Fig. 8) and different optimization methods.

4.1. THEORETICAL REACTIVE POWER ABILITY

Three different set-points at the main transformer have been simulated in 15-minutes steps to evaluate first the reactive power ability on the basis of the maximum and minimum reactive power exchange values of the overall grid behavior and second the ability of the wind farm to achieve one single set-point.

- set-point 1: $Q_N = Q_{max}$
  (maximum demand of the MV grid to the HV grid)
- set-point 2: $Q_N = Q_{min}$
  (maximum provision of the MV grid to the HV grid)
- set-point 3: $Q_N = 0$
  (a neutral grid behavior to the HV grid is desired)

The results show the ability of the wind farm within typical operational limitations of the wind turbines to fulfil these set-points (see Fig. 9). In PowerFactory the maximum, minimum or exact needed reactive power provisions for all wind turbines are calculated automatically in several iterations with knowledge of all the complete grid data with the use of a control method for all wind turbines.

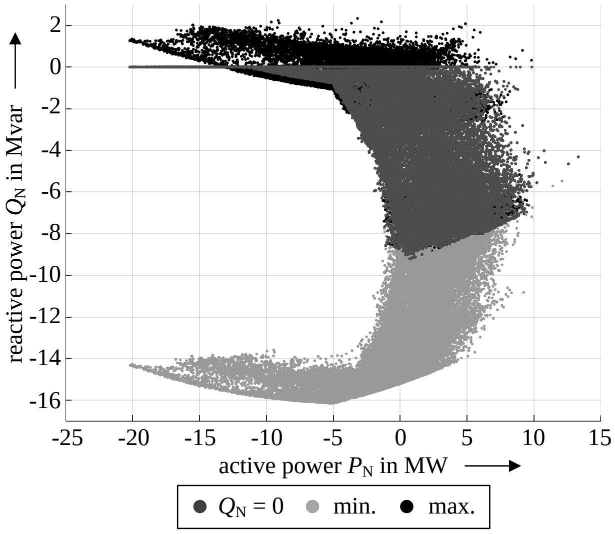

Fig. 9, Results for the 20-kV-rural grid for specific set-points

With the use of the complete grid model in the points in time with high wind generation and thus high reactive power reserve the set-point $Q_N = 0$ could be fulfilled exactly. This is divergent to the results of the co-simulations with the control hardware, which was using an aggregated grid model and had limitations in accurateness because of closed source libraries (see 4.2 and [20]).

Nevertheless, for most points in time the reactive power reserve of all wind turbines was too small to exceed the overall grid behavior (capacitive character of the power lines) so it was not possible to fulfil the set-point of zero reactive power exchange for every grid state. Additionally the PV units have been considered in the same optimization, but provided no significant effect on the general relations of the results. To improve the reactive power ability more control variables would be needed within the optimization (see chapt. VI).

4.2. CO-SIMULATION SET-UP WITH A CONTROL-HARDWARE

Co-simulation is defined as the interconnection of two or more models in a coordinated fashion. The set-up can be comprised of software, hardware models or a combination of both. The iQ project utilizes a software co-simulation set-up [25] that integrates three distinctive models as virtual machines (VM) to evaluate the practical operation of control units in combination with a wind farm for reactive power optimization [21]. The first is the distribution grid modeled in PowerFactory (as discussed in the previous sections). The second is a time series that contains the power production of the entire wind farm within the grid model. The final model is an industrial controller overseeing the reactive power provision for grid stabilization. Fig. 10 portrays a graphical representation of the interconnection of the three models described.

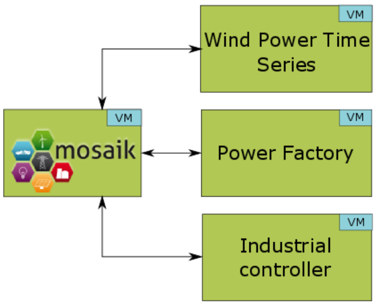

Fig. 10, Software in the loop architecture

The scenarios, grid models and results from the previous analyses are used as input parameters. This means that the previously defined PowerFactory models are reused and connected together with the industrial controller. In addition, the simulation model of the control strategy uses an internal load flow calculator for the set-point calculation. This requires a description of the grid topology within the model of the industrial controller. However a reduced grid topology is employed in order to reduce the complexity of the grid (i.e. the current grid model contains over 700 nodes). Therefore, the grid model within the industrial controller is reduced to the wind farm, main busbar and main transformer.

The complete analysis of the results is shown in [20] and [21], from these two scenarios are selected. In the presented case 1 there is a predominantly high load contribution (approximately 68 % at its peak) and a moderately contribution from the wind farm (55 % of power provision). The case 2 studies the scenario of a low load contribution (29 % of loading) and low power provision (0 % at the lowest point in time). In addition, the set-point $Q_N = 0$ (see 4.2) has been defined. This entails that the industrial controller is measuring the reactive power values at the distribution transformer busbar and controlling the wind farm to provide the required reactive power in order to reach 0 Mvar. The results of the co-simulation set-up are compared with the results from the scenario 4, which has been assumed as the most suitable to represent the original grid behavior from the measured load data supplied by the grid operator. The simulation time for the scenarios has been defined for 24 hours in steps of one hour.

Case 1: high load case 1 (21.03.):

For this specific load case the wind farm supplied 11.796 MW active power in average. Thus a reactive power reserve of $\pm$ 8.104 Mvar with the implemented capability curve was available on average. These values are varying within the simulated 24 hours (see Fig. 11).

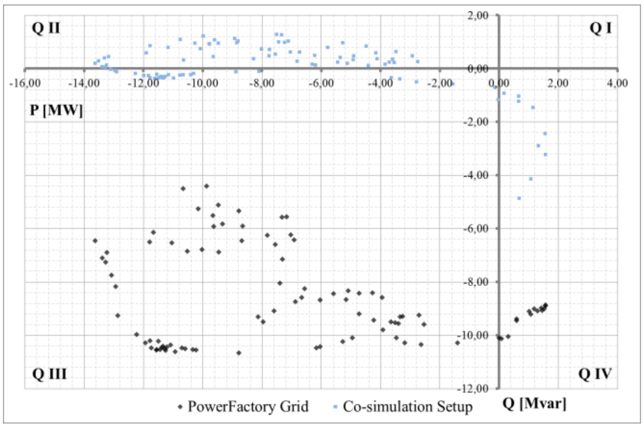

Fig. 11, Results for the 20-kV-rural grid in the high load case 1 with the control-hardware in comparison with the stationary analyses

The results show, that in points in time with high reactive power reserve as high load case 1 the industrial controller was able to configure all wind turbines in the farm in such way, that the set-point value ($Q_N = 0$) was approximated in most of the time. Deviations are notable and for some points in time the set-points could not be achieved at all. This was also notable at the theoretical approach (see Fig. 9)

Case 2: low load case 3 (07.06.)

For this specific load case the wind farm supplied 0.842 MW active power in average. Thus a reactive power reserve of $\pm$ 2.247 Mvar with the implemented capability curve was available on average. These values are varying within the simulated 24 hours (see Fig. 12).

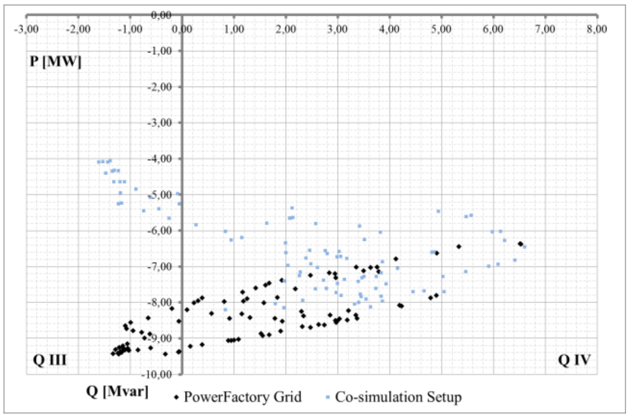

Fig. 12, Results for the 20-kV-rural grid in the low load case 3 with the control-hardware in comparison with the stationary analyses

In Fig. 12 it is observed that the industrial controller attempts to improve the reactive power demand as best as possible taking into consideration the required set-point. However, the set-point value is not reached. This occurs because there is a small amount of power reserve (0 % at its lowest point) coming from the wind farm.

 ©2016 North Sea

4.3. Comparison of Reactive Power Ability Results

The results of the theoretical approach with PowerFactory (see 4.1) and the software integration of the control-hardware (see 4.2) deviate in quality and quantity. The theoretical approach was calculated for one year, thus more values are available, also apart from the characteristic points in time. Furthermore the approach with PowerFactory in contrary to the control-hardware was able to fulfil the set-point $Q_N = 0$ exactly. This deviation can be explained with several reasons:

- the control-hardware uses an aggregated grid model of the detailed grid model, thus deviations in the load flow calculations are naturally
- the theoretical approach had full knowledge of the grid model and was allowed to iterate as often as needed
- the control-hardware is a closed source industrial product, thus not all configurations could be changed as needed

The deviations in the results show some limitations in the used approach. This is the result of being unable to access the control algorithm of the industrial controller. On the other hand, the co-simulation set-up enables the interaction among interdisciplinary simulation models which paves the way for inexpensive testing of multiple scenarios involving several control strategies with different grid topologies.

V. Conclusion

Because reactive power provision is a correlated problem of all voltage levels both system levels (transmission and distribution system) have to be analyzed for future power system management concepts. The continuance of the research work after the interdisciplinary research project *Smart Nord* in the follow-up project "iQ" lead to promising results. With the successful collaboration of research and industrial partners within the project the evaluation of realistic and practical approaches has been realized. This paper describes the results of the research project "iQ" and the relation of reactive power supply of medium-voltage grids to the high-voltage level in the current research field of reactive power management.

The detailed analyses of the medium-voltage grids have been evaluated considering current grid codes and the VDE FNN guidelines for reactive power management. It is important to consider the diversity of distribution grids in the research of reactive power management, thus rural and urban grids have been considered in the study. The medium-voltage grids have been simulated with time series for loads and generation units in four defined scenarios for parametrization of the reactive power supply of generation units.

The grid models and simulation results were used as input parameters within the research project and for comparison of different approaches for the evaluation of the reactive power supply ability of a wind farm in a rural 20-kV-grid. With the use of DIgSILENT PowerFactory an optimized power supply of generation units for given set-points could be determined. This is used as theoretical best case scenario in comparison with the use of an industrial control-hardware in a co-simulation approach. The results show differences in the accuracy of fulfillments of the set-point. The dependence of reactive power supply of current load situation and active power reserve is significant in both approaches.

The grid models, simulation frameworks and results can be used in further analyses with different control tasks, continuing studies of reactive power exchange within all voltage levels and reactive power management of distribution and transmission system.

VI. Outlook

With the ongoing transformation of the electrical energy supply system, the reactive power exchange will continue to vary in quantity and quality in future grid states with high shares of distributed generation units. Also the reactive power provision within all voltage levels and in the large-scale view within all system levels will have to be evaluated.

Hence voltage collaborating models and methodologies are needed to analyze not only the possibilities but also the boundaries of the use of DG units to supply ancillary services, as e.g. the reactive power provision. The approaches of this paper in the software simulation as well as in the co-simulation of the hardware component are proper methodologies to analyze different scenarios and requirements for control of several DG units, as e.g. a wind farm. Furthermore other hardware components or different control tasks could be analyzed in the co-simulation, which would allow several interdisciplinary research questions also in the field of control-strategies and system stability [20].

The simulative approach could be extended with the use of various different medium-voltage grids or different scenarios, respectively different reactive power behaviors of the grid components with more generic data as described in [8]. The current work in DIgSILENT PowerFactory has been validated with load flow studies in Matlab based on Newton-Raphson method and the same scenario data as described. With all data transferred to Matlab more flexibilities arise within the field of power supply. The further integration of the underlying voltage levels in the existing grid and market model of the ENTSO-E transmission model would allow large-scale analyses with the use of a broad data base [13], [16]. The regional data for characteristics of economy, market, population, industry or geography for different regions from this model could be used for an advanced approach for generic analyses of the reactive power exchange of different characteristic distribution grids.

An improved reproduction of the measured grid data as often provided from grid operators (15 minutes mean values of active and reactive power at the main transformer) with aggregated loads and DG units could enhance the performance and quality of the scenario analyses.

Furthermore the optimization of the reactive power provision as well as the exchange within all voltage levels has to be continued to analyses within the interconnection of distribution and transmission system and therefore between the HV and UHV level. This could be elaborated with e.g. the use of optimal power flow methodologies, to implement also the flexibilities of other grid components as FACTS, transformer tap-changers and static VAR compensators.

Acknowledgments The *Smart Nord Transferprojekt iQ Intelligente Blindleistungssteuerung für Verteilnetze* acknowledges the support of the Lower Saxony Ministry of Science and Culture (MWK) (Grant number VWZN3002).

REFERENCES

[1] E. Handschin, “Optimale Netzführung unter Berücksichtigung von Sicherheitsbedingungen“, *Springer Fachmedien*, Wiesbaden, 1980

[2] ZVEI - Zentralverband Elektrotechnikund Elektronikindustrie e. V. :Fachverband Starkstromkondensatoren, “Beitrag industrieller Blindleistungs-Kompensationsanlagen und -Verbraucher für ein innovatives Blindleistungs-Management in der Stromversorgung Deutschlands“, Frankfurt am Main, November 2013

[3] VDE Verband der Elektrotechnik Elektronik Informationstechnik e. V. Forum Netztechnik/Netzbetrieb im VDE (FNN), “VDE-AR-N 4105:2011-08 - Erzeugungsanlagen am Niederspannungsnetz - Technische Mindestanforderungen für Anschluss und Parallelbetrieb von Erzeugungsanlagen am Niederspannungsnetz“, 2011

[4] BDEW Bundesverband der Energie- und Wasserwirtschaft e.V, “Technische Anschlussbedingungen für den Anschluss an das Mittelspannungsnetz“, Berlin, Ausgabe Mai 2008

[5] D. Echternacht, D. Heuberger, C. Breuer, C. Linnemann and A. Moser, “Advantageous Positions for HVDC Terminals in Europe”, *IEEE EnergyTech 2013*, Cleveland, USA, 21.05.-23.05.2013

[6] X.-P. Zhang, C. Rehtanz and B. Pal, “Flexible AC Transmission Systems: Modelling and Control”, revised and extended edition, *Springer-Verlag*, 2nd. edition, Feb. 2012

[7] A. Panosyan, “Modeling of Advanced Power Transmission System Controllers”, Hannover, 2010

[8] Forum Netztechnik/Netzbetrieb im VDE (FNN), “Blindleistungsmanagement in Verteilnetzen“, Berlin, Juli 2014

[9] E. Kämpf, S. Schmidt, B. Walther, S. Wildenhues, R. Eggemeyer, J. Brantl and M. Braun, “Einhaltung definierter Blindleistungsbänder an HS/MS-Übergabestellen durch Einsatz der Blindleistungsfähigkeit dezentraler Einspeiser”, *VDE ETG Kongress*, Berlin, 2013

[10] V. Calderaro, G. Conio, V. Galdi, G. Massa and A. Piccolo, “Optimal decentralized voltage control for distribution systems with inverter-based distributed generators”, *IEEE Trans. Power Syst*., vol. 29, no. 1, pp. 230–241, Jan. 2014

[11] European Commission, “COMMISSION REGULATION (EU) 2016/631 of 14 April 2016 establishing a network code on requirements for grid connection of generators”, Brussels, April 2016

[12] L. Hofmann, M. Sonnenschein, “Smart Nord – Final Report”, Hanover, April 2015

[13] T. Breithaupt, S. Garske, T. Rendel and L. Hofmann, “Methodological Approach for Integrated Grid and Market Simulation of Coherent Distribution and Transmission Systems”, *EnviroInfo 2013*, Hamburg, Germany, 02.-04. September 2013

[14] F. Marten, K. Diwold, L. Löwer, L. M. Faiella, P. Hochloff, L. H. Hansen and M. Braun, “Analysis of a reactive power exchange between distribution and transmission grids,“ in *IEEE 2013 International Workshop on Intelligent Energy Systems*, pp. 52-57

[15] F. Fuchs, R. Dietz, S. Garske, T. Breithaupt, A. Mertens and L. Hofmann, “Challenges of Grid Integration of Distributed Generation in the Interdisciplinary Research Project Smart Nord”, *IEEE 5th International Symposium on Power Electronics for Distributed Generation Systems (PEDG)*, Galway, Ireland, 24.-27. June 2014

[16] T. Rendel, “Erweiterung und Plausibilisierung eines Modells für die integrierte Simulation des europäischen Verbundnetzes und Strommarktes”, *Verlag Dr. Hut*, München, 2015

[17] T. Breithaupt, S. Garske, T. Rendel, and L. Hofmann, “Work Package 4.1 Interconnected System”, *Smart Nord – Final Report*, pp. 169-183, Hanover, April 2015

[18] M. Blank, T. Breithaupt, J. Bremer, A. Dammasch, S. Garske, T. Klingenberg, S. Koch, O. Lünsdorf, A. Nieße, S. Scherfke, M. Sonnenschein and L. Hofmann, “Work Group: Scenario Design”, in *Smart Nord – Final Report*, pp. 21-30, Hanover, April 2015

[19] K. Rudion, A. Orths, Z. A. Styczynski, K. Strunz, “Design of Benchmark of Medium Voltage Distribution Network for Investigation of DG Integration”, *IEEE Power Engineering Society General Meeting*, 2006

[20] S. Lehnhoff, S. Garske, S. Lampke, K. Piech, J. Velasquez, “iQ – Abschlussbericht”, Oldenburg, 2016, to be published

[21] J. Velasquez, K. Piech, S. Lehnhoff, L. Fischer, S. Garske, “Incremental Development of a Co-Simulation Setup for testing a Generation Unit Controller for Reactive Power Provision”, *5th D-A-CH+ Energy Informatics Conference*, 2016

[22] DIgSILENT, http://www.digsilent.com/-index.php/products-powerfactory.html, last access 15.07.2016

[23] 50Hertz Transmission GmbH, “Hochrechnungsistwerte Windenergieeinspeisung 2014“, http://www.50hertz.com, last access 31.07.2015

[24] 50Hertz Transmission GmbH, “Hochrechnungsistwerte Photovoltaik 2014”, http://www.50hertz.com, last access 31.07.2015

[25] Offis, “A flexible Smart Grid co-simulation framework”, https://mosaik.offis.de/, last access 20.07.2016

Journal of Energy Challenges and Mechanics
http://www.nscj.co.uk/JECM/
ISSN 2056-9386
Volume 3 (2016) issue 3, article 4

Performance analysis of a hybrid storage system for electric vehicles

电动汽车混合存储系统之性能分析

Carl Michael Odulio*, Rovinna Janel F. Cruzate, Martin S. Reyes III, Leo Allen S. Tayo

Electrical and Electronics Engineering Institute, University of the Philippines Diliman, QC 1101, Philippines

codulio@ieee.org

Accepted for publication on 25th August 2016

Abstract - **One of the major concerns in electric vehicles is the performance and maintenance of the battery as the storage system. The vehicle load requirements have a great impact on the life and cost of the batteries. High power pulses during acceleration and regenerative breaking requires large amounts of discharge and charge currents. A small capacity battery will result to a lower cycle life due to high current charging and discharging rates. An increase in the capacity of these batteries to meet the current requirements will result in expensive and bulky battery banks. Batteries have the capacity for very high energy storage but low power densities. To compensate for this, a high-power density device in the form of ultra-capacitor is used with the battery to form a hybrid energy storage system. However, it has the disadvantage of having a low energy density.**

This research implemented a hybrid energy storage system with a single bidirectional dc-dc converter between the battery and an ultracapacitor. This configuration lets the converter control the power derived from the battery more efficiently as it controls the discharge to let the battery operate at the optimum levels. The ultracapacitor is connected directly to the load and will deliver peak currents directly to the bank and can absorb the regenerative energy during braking conditions.

The system was modeled in Simulink to determine the energy distribution of the two storage sources. The results show that the ultracapacitor delivers the required power surges of the load with the battery delivering an average power that is at optimum levels. An actual drive cycle was tested and showed that the configuration chosen maximized the benefits of using the ultracapacitor

Keywords - **hybrid energy storage system, lithium ion, electric vehicles.**

I. INTRODUCTION

The study of the different configurations of energy storage systems have been done in different research activities. These have proven to be beneficial in electric vehicle systems in terms of performance and cost implications. One of the major concerns in electric vehicles is the performance and maintenance of the battery as the storage system. The load requirements of these vehicles have a great impact on the life and cost of the battery systems. High power pulses due to acceleration and regenerative breaking require large amounts of discharge and charge currents in the batteries. A small capacity battery results to a lower cycle life due to these high current charging and discharging rates. An increase in the capacity of these batteries to meet the current requirements results in very expensive and bulky battery banks. Batteries have the capacity for very high energy storage but low power densities. In order to compensate for this, a high power density device is used with the battery to form a hybrid energy storage system. A device with this characteristic is the ultracapacitor, but has the disadvantage of having a low energy density. The hybrid system lets the battery supply the energy required by the load and the capacitor delivers the high power pulses due to acceleration and absorbs the power from braking of the vehicle.

This project implements a hybrid energy storage system using the configuration in Fig. 1. This configuration allows the converter to control the power derived from the battery more efficiently as it controls the discharge to let the battery operate at the optimum levels. The ultracap will be connected directly to the load and delivers peak currents directly to the bank and is able to absorb the regenerative energy during braking conditions. The voltage variation is larger than the battery voltage variations but operates within the limits of the motor controller. In some configurations, another converter is connected between the capacitor and the load to stabilize the voltage but this adds to the losses in the system because of the added conversion stage.

©2016 North Sea

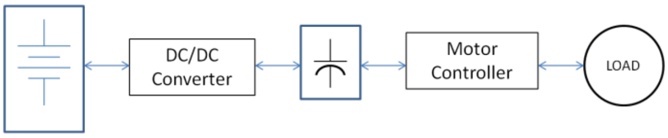

Fig.1, HESS System Configuration

II. Components of a Hybrid Energy Storage System

2.1. Battery

Energy storage systems for both electric vehicles and hybrid electric vehicles have been lenient on using batteries as the main storage component. Different types have been used but the lead-acid and lithium-ion are the most used kinds in this application.

Lead-acid has the advantage of low cost, low maintenance requirements, and ease of use. It's mostly used for hybrid buses [4] [7] but is not very ideal for low speed vehicles such as electric tricycles because of its weight and low energy density. For low speed vehicles, lithium ion batteries are more commonly used. With higher energy density, the lighter lithium ion cells are more favorable for smaller electric vehicles. This paper presents the simulation results for an energy storage system using the lithium ion battery pack.

Applications such as motor drives for electric vehicles have a different power requirement due to different modes of operation. Acceleration and regenerative energy or braking require higher power from the battery which in turn increases the power rating needed as well as decrease battery life [7] [8]. These moments of high-current pulses cause higher cost due to decrease in battery life as well as the need to increase battery capacity [2]. These limit the capabilities of the lithium ion battery pack, hence the need for hybridization or an additional storage element.

2.2. Ultracapacitor

The electrolytic double layer capacitor, also called ultracapacitor, is known for its high capacitance, very high energy storage density, smaller capacity, and long cycling life. [8] With these characteristics, the ultracapacitor becomes a complementary storage component to batteries.

In EV applications, the ultracapacitor will be able to handle the peak power requirements of the motor as well as utilize the regenerative energy from breaking [2] [4] [5] [7] [9]. With the same application, the lower limit of the ultracapacitor voltage is chosen at 50% since the energy stored below that threshold is only 25% [1] [3].

2.3. Bidirectional DC-DC Converter

Different bidirectional dc-dc converter topologies have been used with the same goal of facilitating power transfer between the ultracapacitor and battery as well as to the power train of the EV. Buck-boost is one popular topology that can address the power requirements needed in a HESS [6].

The specifications of voltage and power levels for this converter are often dictated by the sizing of both the battery and the ultracapacitor.

For this paper, several assumptions regarding the operation of the DC-DC converter are enumerated. It should have a Constant Current (CC) – Constant Voltage (CV) charging characteristic that depends on the voltage level of the load side. Upon reaching the target voltage at the load side, the converter will automatically switch from CC mode to CV mode. Along with this, the converter should have a generation and regeneration mode to be able to fully utilize the functionality of the ultracapacitor.

III. Existing HESS Configurations

Several HESS configurations have already been proposed. This section discusses the basic configurations used.

3.1. Passive Parallel Connection To DC Link

To achieve the target operation of the HESS, the most basic connection of the ultracapacitor and battery is in parallel. The two components can be interchanged as shown in Fig. 2 and Fig. 3. This kind of configuration has no possibility of controlling the power flow between the ultracapacitor, battery and the DC link. The internal resistances and voltages of the components are the sole determinants of current distribution. Voltage across the two components and the DC link are always equal [3][4][9].

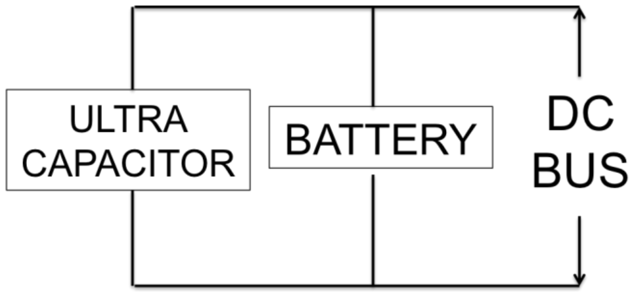

Fig.2, Ultracapacitor – Battery Direct Connection.

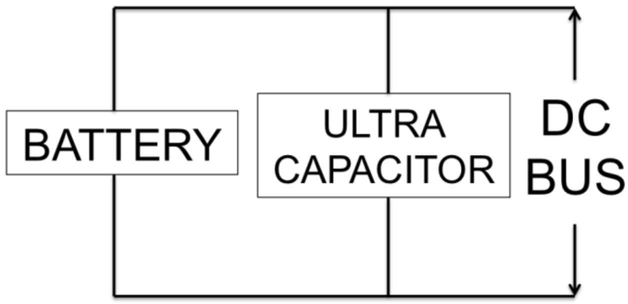

Fig.3, Battery – Ultracapacitor Direct Connection.

Shown in Fig. 4 and Fig. 5 are other passive configurations of HESS. These figures are considered passive because the power flows between the two storage components are still not controllable [9]. The battery and ultracapacitor are also interchangeable while maintaining similar operation. In these passive configurations, the ultracapacitor becomes a low pass filter.

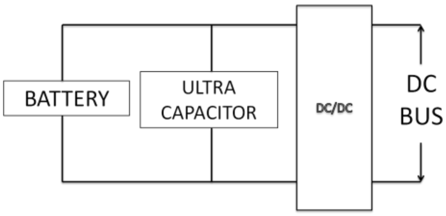

Fig.4, Battery – Ultracapacitor with DC-DC interface to DC Bus.

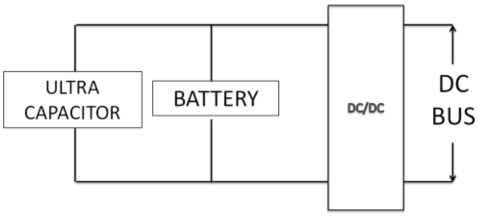

Fig.5, Ultracapacitor – Battery with DC-DC interface to DC Bus.

Ease of implementation and minimal power converter requirement are the advantages of these passive configurations. However, one major issue is pre-charging the ultracapacitor. Directly connecting them without pre-charging would cause extremely high currents within that loop [4]. Aside from this, the energy provided by the ultracapacitor is not utilized effectively [3]. Hence, the hybridization is considered inefficient.

3.2. Active Parallel Connection To DC Link

To address the lack of power flow control in the previous configurations, a more active hybrid energy storage system was developed [3]. The main difference from the previous section is the bidirectional dc-dc block that facilitates and controls the power exchange between the battery and the capacitor as shown in Fig. 6 and Fig. 7.

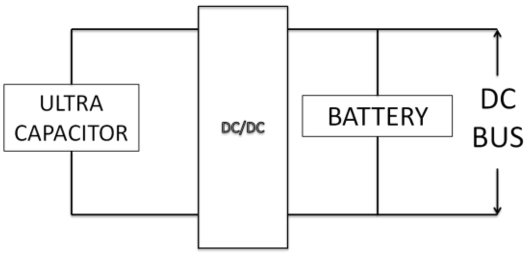

Fig.6, Active Ultracapacitor – Battery Configuration.

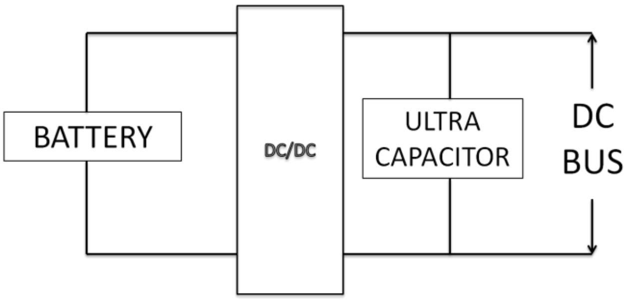

Fig.7, Active Battery – Ultracapacitor Configuration.

The configuration in Fig. 6 has a more stable voltage in the DC bus because of the direct connection to the battery [9]. Another advantage is that the voltage level of the ultracapacitor is not limited by the requirements of the motor controller. However this configuration is demanding on the specifications and ratings of the DC-DC converter, since the peak power provided by the ultracapacitor has to be interfaced with that block [3].

The swapped version of the active topology shown in Fig. 7 addresses the disadvantages presented in the original configuration. Since the ultracapacitor is directly connected to the DC link, the DC-DC converter is only required to interface the average power provided by the battery bank. The battery voltage level can also be varied and not tied down to the requirements of the motor controller. To ensure stability in the DC link, this topology allows the bus voltage level to swing depending on the operation of the ultracapacitor [3].

In this paper both active parallel configurations are going to be investigated and simulated to confirm the advantages and disadvantages presented in this section.

IV. Drive Cycle Profile

Drive cycle profile is an important tool to evaluate the configuration of the hybrid energy storage system. This will determine the operation and performance of the simulation. It is important to choose a suitable profile that will demonstrate the modes of operation where using only the battery, as the storage system, is disadvantageous: start-up, acceleration, and breaking.

4.1. Most Common Profiles Used for EVs and HEVs

The New European Driving Cycle (NEDC) was originally used for fuel-based vehicles. However, due to lack of standard test drive cycle, this profile has been applicable to EVs and HEVs in the recent times [10]. This cycle is more concerned with testing the overall efficiency of the vehicle versus simulating real life driving conditions. It also does not satisfy the portrayal of high current pulse generating operations discussed in the previous section.

Due to the lack of a standard driving cycle for electric vehicles, a number of papers opted to develop their own drive cycles using actual EV on-road test recorded by means of data acquisition [5] [6]. By doing so, the simulations are closer to real life driving situations. It also increases the accuracy by using an actual drive cycle by electric vehicles or hybrid electric vehicles. Several tools can be used to migrate these data to actual simulations such as the Aerovironment ACB-150 Power processing system and the Advanced Vehicle Simulator (ADVISOR) [5] [6] [7].

4.2. Actual Drive Cycle Profile

The drive cycle shown in Fig 8 was acquired from on-road testing of an electric vehicle under Philippine conditions. It simulates the actual start-and-stop driving characteristics of an electric vehicle. The regenerative capability of an EV is also incorporated in the drive cycle to further observe the dynamics of the electric storage systems under test. The profile statistics are shown in Table 1.

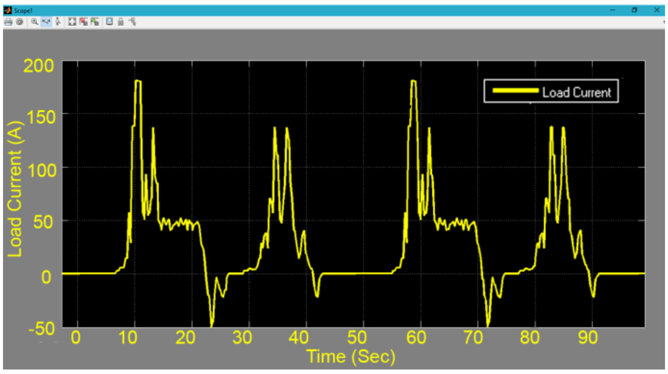

Fig.8, Drive Cycle Snippet.

TABLE 1, DRIVE CYCLE PROFILE CHARACTERISTICS

Parameter	Value	Unit
Peak forward current	200	A
Peak forward power	60	kW
Average forward current	31.34	A
Average forward power	9.4	kW
Minimum forward power	0	kW
Peak regenerative current	50	A
Peak regenerative power	15	kW
Average regenerative current	1.96	A
Average regenerative power	586.96	kW
Maximum current slew rate	364	A/sec
Simulation time	2.7	h
Peak forward power time	5	sec

V. METHODOLOGY

5.1. SYSTEM COMPUTATIONS

For this paper, the sizing of the ultracapacitor and the battery are based on the assumption that the HEV or EV system is using a high voltage to high voltage energy storage system. Table 2 shows the specifications of each component of the HESS.

TABLE 2, SIMULATION SYSTEM SPECIFICATIONS

Parameter	Value
Battery Rating	$360V_{NOM}$, 100Ah, Lithium-ion bank
Ultracapacitor Rating	$340V_{MAX}$, 65 Farads
Bidirectional DC/DC Rating	20kW

The simulation time ($T_{simulation}$) at 2.7 hours and the average forward current ($I_{average}$) at 31.34 A are considered in computing for the minimum battery capacity ($Batt_{capacity}$) needed for both configurations shown in Eq. (1).

$$Batt_{capacity} = I_{average} \times T_{simulation} \tag{1}$$

$Batt_{capacity}$ = 31.34A x 2.7 hours

$Batt_{capacity}$ = 84.618 Ah

The minimum battery capacity needed for both configurations is 84.618 Ah. For a more standard capacity rating, a 100 Ah lithium ion battery specification was used.

For the ultracapacitor sizing, the voltage swing is assumed to be 50% at max. The voltage rail is assumed to be at 340V max. Therefore the minimum capacitance requirements can be computed.

$$E_{initial} = \tfrac{1}{2} CV_{initial}^2 \tag{2}$$

$E_{initial}$ = initial capacitor energy

C = capacitance

$V_{initial}$ = initial voltage of capacitor

$$E_{final} = \tfrac{1}{2} CV_{final}^2 \tag{3}$$

E_{final} = final available energy of capacitor

V_{final} = final voltage of capacitor

$$E_{initial} - E_{final} = ((P_{peak} - P_{ave}) \times T_{peak}) \tag{4}$$

P_{peak} = peak power

P_{ave} = average power

T_{peak} = time during peak power

Using Eq. (2), Eq. (3) and Eq. (4) and plugging in the parameters from the drive cycle profile to get the minimum capacitance needed:

$\tfrac{1}{2} CV_{initial}^2 - \tfrac{1}{2} CV_{final}^2$ = (60kW – 9.4kW) x 5 sec

$\tfrac{1}{2} C(340V)^2 - \tfrac{1}{2} C(170V)^2$ = (60kW – 9.4kW) x 5 sec

C_{min} = 5.83 F

The minimum capacitance needed is 5.83F. However, this is not a standard value and is difficult to find commercially. Therefore, a more standard value was used to carry-on with the simulation as shown in Table 2. A total of 65F with a maximum voltage of 340 V is used.

Lastly, the rating of the DC-DC converter was dictated by the peak regenerative power, which is at 15kW. A surplus of 5 kW was added for margin.

VI. MODELLING AND SIMULATION

The following figures show the two configurations used in the simulations of the system. Figure 9a shows a bidirectional converter connected between the battery and ultracapacitor with the ultracapacitor connected to the load side. The other configuration switches the locations of the two sources and puts the battery at the load side. In both cases, the ultracapacitor is intended to handle the peak currents that the load presents to the source.

The flowchart for the configuration in Fig. 9a is shown in Fig. 10a. The ultracapacitor is always connected across the load of the system. The load voltage is allowed to swing within the operating range of the motor driver. This requires the ultracapacitor to be rated beyond the maximum allowable voltage for the motor driver. With a motor driver connected as the load of the energy storage system, there are different characteristics of the load that the ultracapacitor addresses like high peak load currents and regenerative power.

As the motor drive is started, corresponding to an electric vehicle accelerating, there is a high peak current that the load draws from the source. This peak current is naturally supplied by the ultracapacitor because it is connected across the load. The battery delivers only an average power as limited by the constant current mode of the bidirectional converter. During the accelerating condition, the load current is the sum of the battery current and ultracapacitor current. After acceleration, the vehicle is expected to be coasting or in braking mode. In the first mode, the vehicle is drawing a more or less constant current from the battery. The bidirectional converter is operating at a current limit level such that it can be higher than the average current that the motor driver is drawing. The excess current is used to charge the capacitor to replenish the expended energy during the peak current discharge of acceleration. When the vehicle brakes, there is regenerative energy that flows back to the source. Since the ultracapacitor is already across the load, it automatically absorbs this energy and prevents the battery from having very large charging currents. The state of charge of the ultracapacitor is always monitored determine whether it needs to be charged by the battery or if it is operating beyond a threshold where the energy should be transferred back to the battery.

The ultracapacitor is expected to have a threshold of 90% of the state of charge. Whenever the load is not requiring high peak currents, the ultracapacitor is charged from the battery using the bidirectional converter. The state of charge is limited to 90% so that the ultracapacitor still has capacity to absorb a fair amount of braking power when the vehicle suddenly brakes and delivers regenerative power to the source.

The configuration in Fig. 9b has a control scheme that is shown in the flowchart of Fig. 10b. This configuration has a battery system connected directly across the load. The ultracapacitor is still intended to deliver and absorb high peak currents but is dependent on the operation of the bidirectional converter. During accelerating conditions, the high peak currents drawn by the load have to be sensed right away by the system in order to signal the bidirectional converter to operate and source the peak power from the ultracapacitor. This is also the same requirement during braking conditions where the load current has to trigger the converter to operate in the opposite direction and discharge the high regenerative energy into the ultracapacitor. There are also limits to the operating state of charge of the ultracapacitor in order to ensure availability of storage capacity during the peak current charging and discharging conditions. The ultracapacitor excess energy is discharged to the battery system when the state of charge is greater than 90%. When the state of charge is less than 90%, the battery charges the capacitor to replenish the extinguished energy during the accelerating condition of the vehicle. The lower limit of the ultracapacitor state of charge is 25% because the operating voltage is already at 50% during this level of state of charge. This is the recommended minimum voltage for operating an ultracapacitor. When this condition is met, the battery is the only source delivering energy to the load and bidirectional converter will be disabled.

These two control schemes may operate using an integrated logic controller in the bidirectional converter or it may be triggered and controlled by an external circuit. Current sensors are used to monitor load current levels and voltage sensors are used for state of charge estimation.

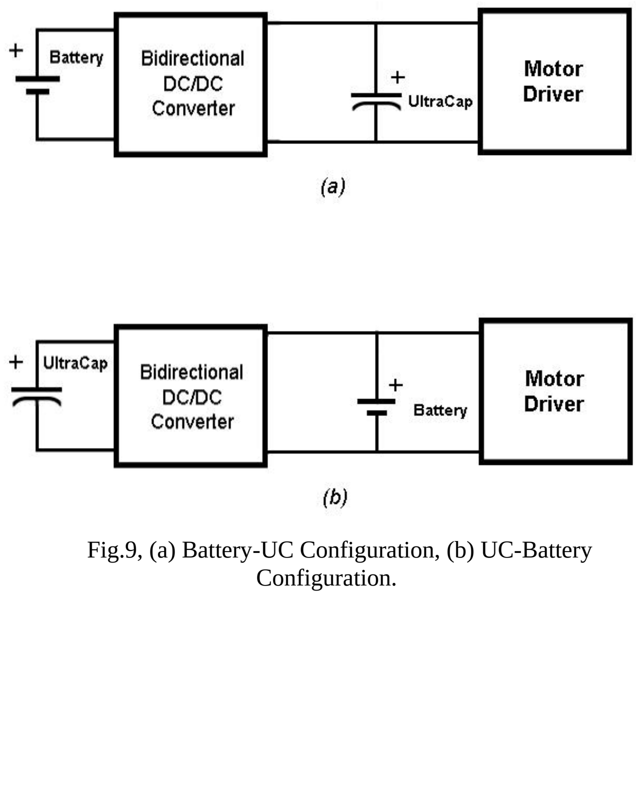

Fig.9, (a) Battery-UC Configuration, (b) UC-Battery Configuration.

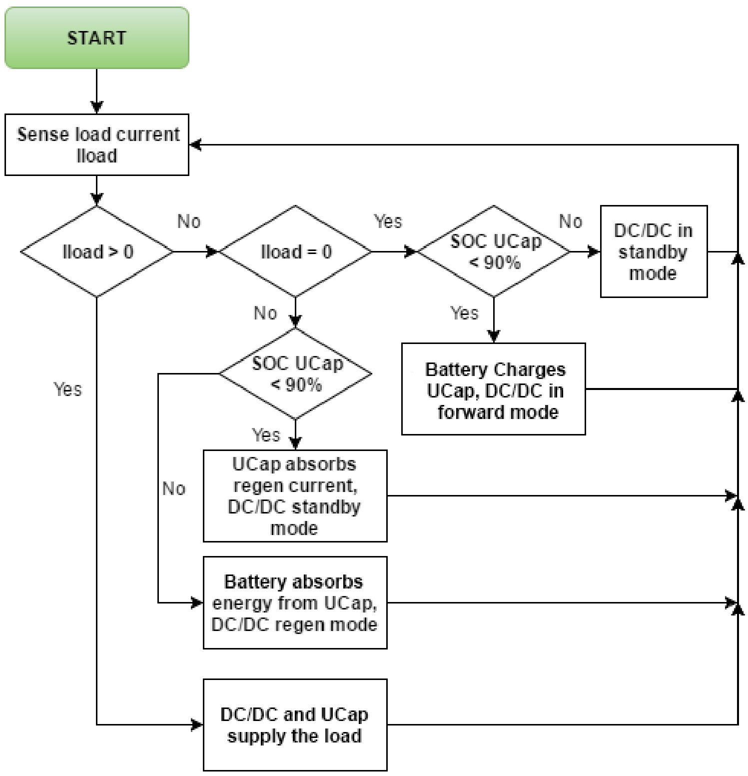

(a)

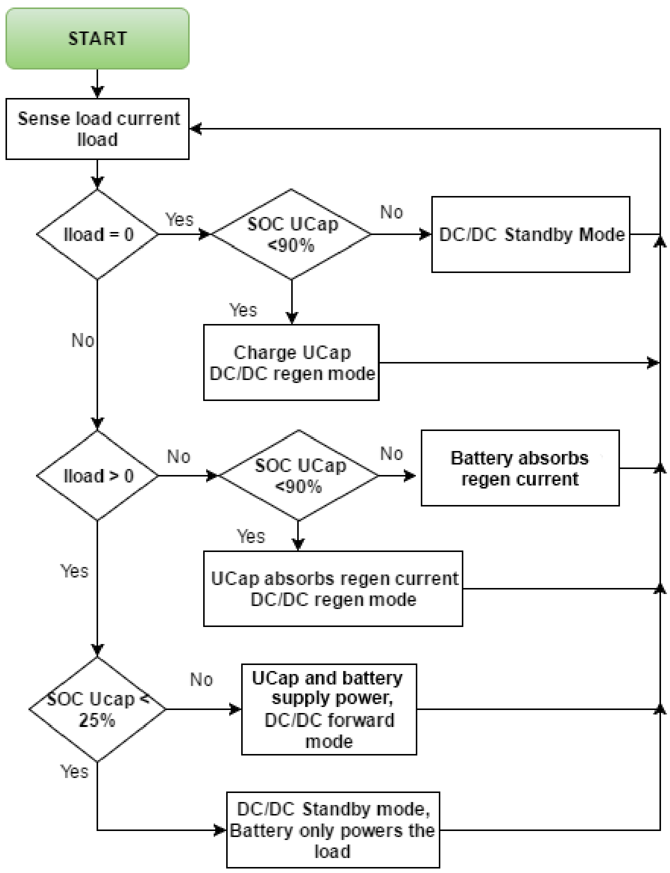

(b)

Fig.10, (a) Battery-UC Configuration Flowchart, (b) UC-Battery Configuration Flowchart.

where

Iload = load current
SOC = state of charge
UCap = ultracapacitor

VII. Results And Discussions

The graphs in the following figures show the performance of the two different configurations when subjected to the given drive cycle in Fig. 8. The curves in Fig. 11 and Fig. 12 show the three currents from the battery, ultracapacitor and the load. The peak current drawn by the load is around 190A. A standalone battery system is required to deliver this peak current. If the required battery system cannot deliver this kind of current level, the battery ampacity is increased to the appropriate level. With the configuration in Fig. 9a, this load current is divided between the two sources. The peak current from the ultracapacitor is around 125A and the battery current peaks at around 65A. This shows that the ultracapacitor is able to deliver the required peak current of the load and prevents the battery from operating at very high peak current discharges.

The next part of the waveform in Fig. 11 shows that the current of the load drops to around 50A. This is divided between the battery and the ultracapacitor with the battery delivering 40A and around 10A coming from the ultracapacitor. This is then followed by a braking condition as seen from the negative current at the load. This is again distributed between the sources with the bidirectional converter operating in the opposite direction to charge the battery with the regenerative power. The bidirectional converter is still current limited in order for the battery to have a limited amount of peak charging energy. The excess energy that is delivered back to the source is absorbed by the ultracapacitor.

This is again followed by another accelerating condition that is shown with the peaking of the load current. The distribution of the currents shows that the battery is still delivering a lower level of current than the ultracapacitor. This again shows that the battery is limited to a safe current level that will not damage nor decrease the life of the battery. A brief braking condition ends one period of the drive cycle. The drive cycle is a periodic waveform that can show the different conditions in an electric vehicle road load. The important thing to consider in the selection of the system is that the battery system is selected properly in order to provide enough energy to cover the target driving range of the vehicle.

The second configuration shows waveforms in Fig. 13 and Fig. 14 that are very similar to the first set of waveforms in terms of current sharing. The capacitor is also able to supply a portion of the load current effectively reducing the load on the battery. The intention of both configurations has been achieved but have some differences that greatly affect the design of the system.

One difference in the performance of the two configurations is the wave shape of the ultracapacitor current. The ultracapacitor current from Fig. 11 shows that this is very similar in shape as the load current. This is the effect of having the ultracapacitor connected across the load. The current sourced from the ultracapacitor is automatically delivered. This lets the ultracapacitor to have a very fast response time in delivering the required current.

The ultracapacitor current waveform from Fig. 13 shows that it has a rectangular shape that is very different from the load current waveform. The ultracapacitor cannot respond right away to the fast transient that the load requires. This is because of the dependency of the delivery of the current to the response time of the bidirectional converter. The system has to sense the load current first and determine whether the ultracapacitor has to deliver current or not. Once this has been determined, the system enables the bidirectional converter to transfer energy from the ultracapacitor to the load. This has a finite time delay that is not present in the first configuration.

The two minimum features of the bidirectional converter of the second configuration are high slew rate and low time delay. The high slew rate will enable the ultracapacitor to deliver peak currents that can handle the rise times that the load current presents. This has to be fast enough so that the battery current does not have to support these transient conditions. The waveforms show that the battery current for the second configuration has a wave shape that follows the load current. This shows that the transient condition is supported by the battery and not by the ultracapacitor. A very fast converter may rectify this in order to account for these rise time requirements at the expense of a more expensive converter.

The time delay or response time of the converter has to be negligible so the battery does not have to deliver short burst of high peak currents when the output of the converter is not yet enabled because of the response time.

Another drawback of the second configuration is the power rating of the bidirectional converter. It is shown in the first configuration that the converter operates at a current limit level that is near the operating current of the battery. There are no peak currents expected since these current are supplied and absorbed by the ultracapacitor. In the second configuration however, the high peak current delivered by the ultracapacitor goes thru the bidirectional converter and in to the system. This means that the current rating of the converter has to be greater than the normal level that is being supplied by the battery. This peak current is repetitive but effectively has a low duty cycle. Even with a high peak current rating, the total power delivered by the converter is not as high as the power rating of the converter.

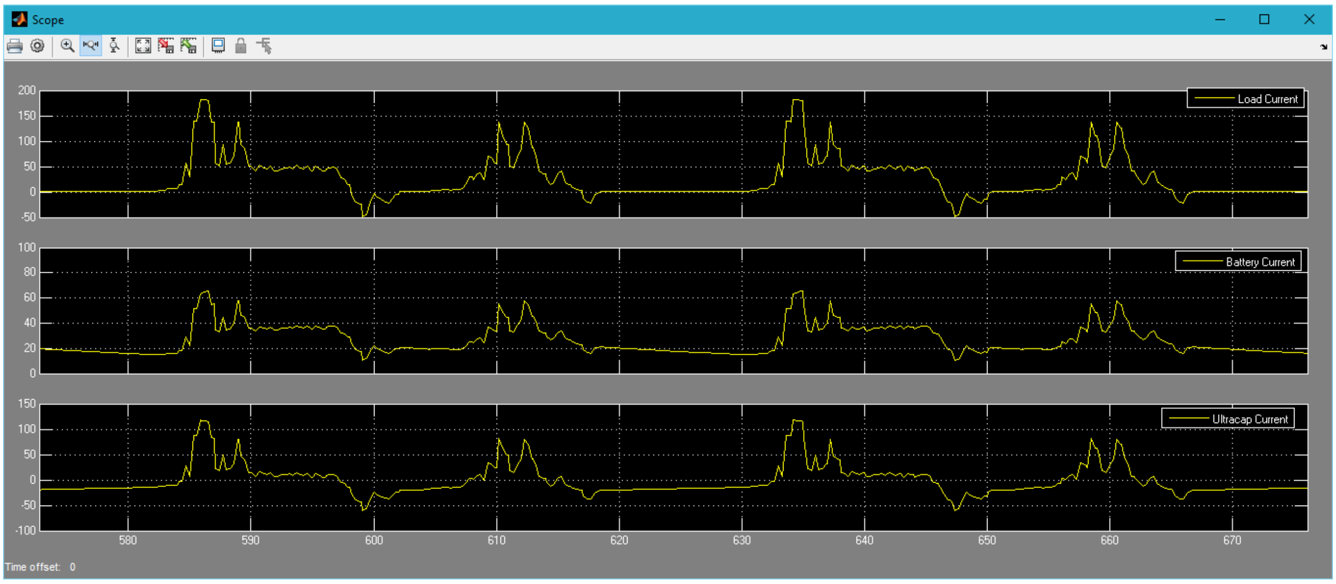

Fig.11, Simulation Results for the Battery – UC Configuration

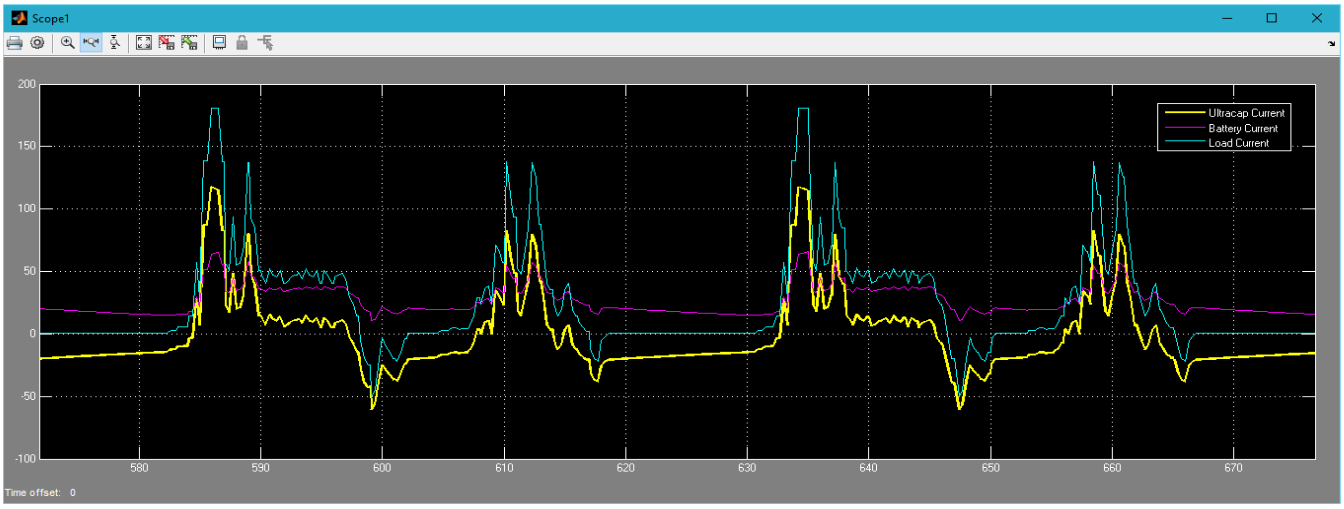

Fig.12, Battery – UC Overlaid Simulation

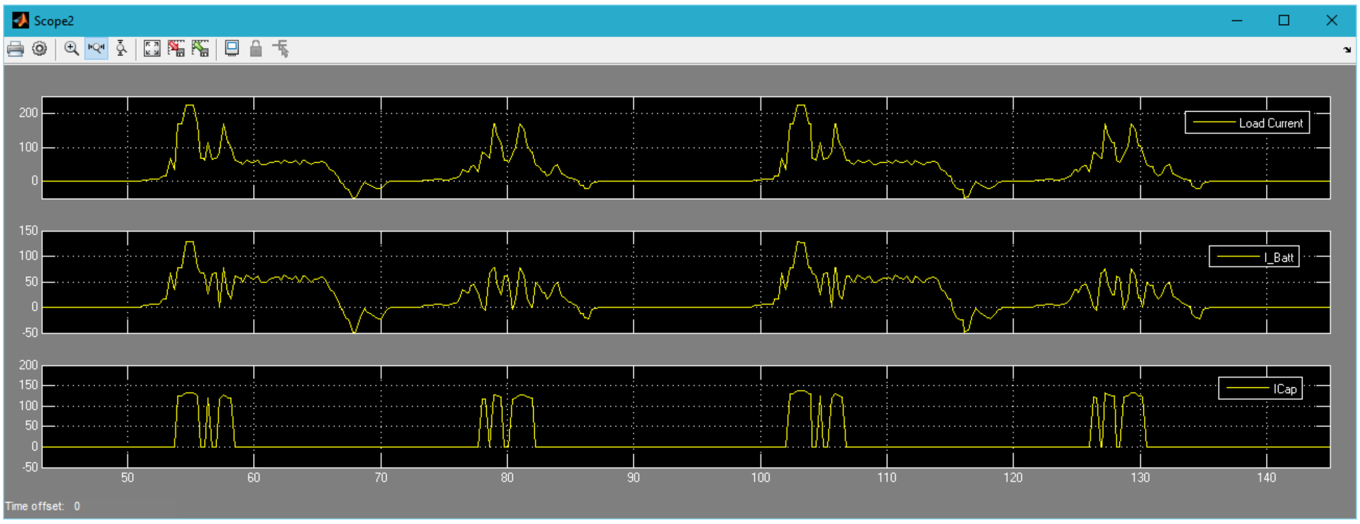

Fig.13, Simulation Results for the UC – Battery Configuration

 ©2016

Fig.14, UC - Battery Overlaid Simulation

VIII. Conclusion

This paper presented a performance comparison of two different configurations of a hybrid energy storage system for electric vehicles. The basic elements of the hybrid energy storage system have been discussed. The functionality of two different configurations has been compared. The two configurations were used in a simulation setup using an actual drive cycle of an electric vehicle to verify the performance of the two systems.

The two systems have both performed as intended. The ultracapacitor in both systems has contributed to the sharing of the load current and reduced the current delivered by the battery system. The HESS with an ultracapacitor connected across the load has shown advantages in overall system specifications and design. Although the intention for both systems has been achieved, there is a clear advantage in choosing one over the other.

In the second configuration, the power rating of the bidirectional converter is largely dependent on the expected peak current that the ultracapacitor is going deliver into the system. If the battery system is limited to a maximum of 1C discharge rate of the battery and the load requires 3C, the converter is rated at a current level of 2C but will only deliver this power level during the accelerating condition.

In the first system, the bidirectional converter is operating at a current limit that will be at an almost constant level and significantly lower than the peak current of the load. This allows the converter to be specified at a lower current and power rating and can be operated continuously at the target power rating. This let the converter operate at the optimum level without being over rated.

The preferred configuration is the first system where the ultracapacitor is connected directly across the load. This maximizes the benefits of having an ultracapacitor in a hybrid energy storage system not only in its electrical performance, but in the impact of the system design as well.

Acknowledgment

The authors acknowledge the financial support of the Department of Science and Technology – Engineering Research and Development for Technology (DOST-ERDT).

References

[1] Abo-Elyousr, F., RM, K., Abo-zeid, H., & Abd-elbar, F. (2013). Characterization and effectiveness of an ultracapacitor bank to enhance a battery electric vehicle energy storage system dynamics. *2013 International Conference on Electrical Machines and Systems*, (pp. 235-241). Busan. doi:10.1109/ICEMS.2013.6754420

[2] Ahmadkhanlou, F., & A, G. (2011). Hybrid Lithium-ion/Ultracap energy storage systems for plug-in hybrid electric vehicles. *EEE Vehicle Power and Propulsion Conference*, (pp. 1-7). Chicago, IL. doi:10.1109/VPPC.2011.6043196

[3] Cao, J., & A, E. (2009). A new battery/ultra-capacitor hybrid energy storage system for electric, hybrid and plug-in hybrid electric vehicles. *IEEE Vehicle Power and Propulsion Conference*, (pp. 941-946). Dearborn, MI. doi:10.1109/VPPC.2009.5289744

[4] Haifeng, D., & Xueyu, C. (2010). A Study on Lead Acid Battery and Ultra-capacitor Hybrid Energy Storage System for Hybrid City Bus. *International Conference on Optoelectronics and Image Processing*, (pp. 154-159). doi:10.1109/ICOIP.2010.321

[5] Jarushi, M., & Schofield, N. (2010). Battery and supercapacitor combination for a series hybrid electric vehicle. *th IET International Conference on Power Electronics, Machins and Drives*, (pp. 1-6). Brighton, UK. doi:10.1049/cp.2010.0100

[6] Liu, X., Zhang, Q., & Zhu, C. (2009). Design of battery and ultracapacitor multiple energy storage in hybrid electric vehicle. *IEEE Vehicle Power and*

 ©2016 North Sea Conference & Journal

Propulsion Conference, (pp. 1395-1398). Dearborn, MI. doi:10.1109/VPPC.2009.5289462

[7] Stienecker, A., T., S., & C., A. (2005, July). A Combined ultracapacitor- lead acid battery storage system for mild hybrid electric vehicles. *IEEE Vehicle Power and Propulsion Conference.* doi:10.1109/VPPC.2005.1554582

[8] Rade, M., & Dhamal, S. (2015). Battery-Ultracapacitor combination used as Energy Storage System in Electric Vehicle. *International Conference on Emerging Research in Electronics, Computer Science and Technology*, (pp. 230-234). Mandya. doi:10.1109/ERECT.2015.7499018

[9] Xiang, C., Wang, Y., Hu, S., & Wang, W. (2014, April 8). A New Topology and Control Strategy for a Hybrid Battery-Ultracapacitor Energy Storage System. *Energies*, 2874-2896. doi:10.3390/en7052874

[10] TJ, B., S, L., IS, M., & PG, B. (n.d.). *A Reference Book of Driving Cycles For use in the Measurement of Road Vehicle Emissions.* Retrieved July 2016, from https://www.gov.uk/government/uploads/system/uploads/attachment_data/file/4247/ppr-354.pdf

Journal of Energy Challenges and Mechanics

http://www.nscj.co.uk/JECM/

ISSN 2056-9386
Volume 3 (2016) issue 3, article 5

Energy Harvesting Circuit for Radio Frequency Application

无线电频率应用之能量收集电路

Haruichi Kanaya

Department of Electronics, Graduate School of Information Science and Electrical Engineering, Kyushu University, Fukuoka 819-0395, Japan

kanaya@ed.kyushu-u.ac.jp

Accepted for publication on 3rd September 2016

Abstract - **Battery-free or autonomous wearable electronics have attracted great interest in both information communication and medical research. Energy harvesting systems for the radio frequency (RF) region feature long-range energy transmission. However, because the RF receiving signal is so weak, the conversion efficiency is low. In this study, to enhance the amplitude of the RF receiving signal, a resonant circuit is constructed in front of the boosting circuit. The impedance matching circuit, the resonant circuit, and the Cockcroft–Walton (CW) circuit are connected to each other. Moreover, the proposed circuit is mounted on the backside of a one-sided directional antenna on a flexible substrate. This antenna is composed of a coplanar waveguide and a slot on the top metal surface and the bottom floating metal layer. The simulated output DC voltage is 2.89 V for an input of 100 mV and a 50-Ω power source at 900 MHz, and the power efficiency is 58.7% for a 10-MΩ load resistance. In our design method, it is easy to increase the output voltage by optimizing the element number of the CW circuit and the quality factor of the LC resonant circuit.**

Keywords - **Energy harvesting circuit, impedance matching circuit, booster circuit, flexible antenna, one-sided directional antenna.**

I. Introduction

Recently, battery-free or autonomous wearable electronics have attracted great interest in medical, infrastructure and factory monitoring, and information communication devices [1]–[4]. Radio frequency (RF) energy harvesting systems are suitable for long-range or indoor operation.

Radio frequency identification (RFID) systems in the UHF (ultrahigh frequency) band have become very popular in various applications, such as distribution logistics and human tracking. UHF band RFID systems have long-range identification ability and high-speed data rate compared to other frequency regions. However, they have a disadvantage in their limited amount of RF power and low conversion efficiency.

A number of booster circuits have been reported for a radio frequency identification (RFID) system [5]–[7]. The Cockcroft–Walton circuit (CW circuit) [8] and the modified CW circuit are composed of diode and capacitor pairs and are easy to implement as on-board circuits. In the RF region, there are a number of parasitic elements in the diode and capacitor that degrade the RF boosting properties. Moreover, the RF receiving signal is so weak that an enhancement circuit, such as an LC resonance circuit, and an impedance matching circuit are needed in the RF region.

If an omnidirectional antenna such as a slot antenna that receives RF signals is mounted on a metallic object surface or non-planar object surface such as a can or bottle, its radiation properties are remarkably deteriorated because of electro-magnetic interference. There are several reports about tag antennas such as patch- or label-type antennas for metallic object applications [9–12]. Kanaya et al. [13–15] presented the design method of a one-sided directional slot antenna for IMS band (@2.4 GHz) applications, with an attached floating metal layer on the bottom side and optimized length of the metal layer. An impedance matching circuit is also realized by using an interdigital gap and conductor-backed coplanar waveguide (CPW) transmission line [16, 17]. Based on this design theory, a one-sided directional slot antenna for 900-MHz band RFID systems has been reported on a flexible substrate [18].

In the present study, a resonant circuit was constructed in front of the booster circuit to enhance the amplitude of the RF signal. Moreover, this harvesting circuit was mounted on the backside of a one-sided directional slot antenna. The proposed antenna was designed with the aid of a commercial three-dimensional electromagnetic field simulator (Ansoft; HFSS).

©2016 North Sea

The antenna was fabricated and measured to verify the RF properties. We also successfully lit an LED without connecting it to the power source using wires. This paper is organized as follows. Section II describes the booster circuit design. Section III shows the design method of the impedance matching circuit. Section IV describes the antenna design. The implementation and measurement results are provided in Section V and Section VI. Finally, the conclusion is presented in Section VII.

II. CIRCUIT DESIGN

Figure 1 shows a block diagram of the proposed energy harvesting circuit with a one-sided directional flexible antenna. The antenna, the impedance matching circuit, the resonant circuit, and the CW circuit are connected to each other. The resonant circuit can enhance the RF signal. The individual circuit blocks are described in more detail in the following paragraphs.

Figure 2 shows the unit cell of the CW circuit. The CW circuit comprises two pairs of capacitors and diodes. When the input voltage reaches its negative peak, current flows through the diode charge the left side of the capacitor to an input voltage. When the input voltage reverses polarity and reaches its positive peak, it is added to the left side capacitor's voltage, and the right side capacitor is charged to the double of the input voltage [8].

The output voltage of the CW circuit (V_{out}) is represented theoretically as follows:

$$V_{out} = V_{in} \times 2N \tag{1}$$

where V_{in} represents the input voltage, N is the number of capacitors and the diode unit structure, and V_{out} is multiplied by $2N$.

$$|I_S| = \frac{E}{\sqrt{R_S^{\,2} + (X_{LS} - X_{CS})^2}} \tag{2}$$

where X_{LS} and X_{CS} represent ωL_S and $1/\omega C_S$, respectively.

At the resonance condition, resonance current I_0 is given by

$$I_0 = E / R_S \tag{3}$$

In this case, the normalized voltage of L_S or C_S is described as

$$\frac{E_L}{E} = \frac{E}{R_S} X_{LS} \cdot \frac{1}{E} = \frac{X_{LS}}{R_S} \tag{4}$$

and

$$\frac{E_C}{E} = \frac{E}{R_s} X_{CS} \cdot \frac{1}{E} = \frac{X_{CS}}{R_S} \tag{5}$$

Thus, the quality factor of this circuit (Q_S) is given by

$$Q_S = \frac{X_{LS}}{R_S} = \frac{X_{CS}}{R_S} \tag{6}$$

We can obtain the output voltages E_L and E_C, which are Q_S times larger than E. In our energy harvesting circuit, the input RF voltage signal is enhanced by using the above LCR series resonance circuit.

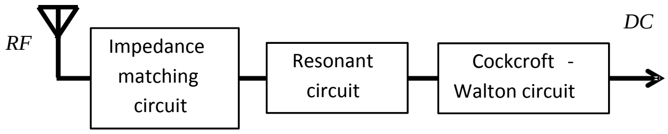

Fig.1. Block diagram of the proposed booster circuit.

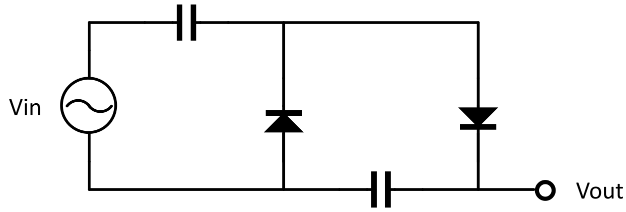

Fig.2. Unit cell of the CW circuit.

Figure 3 shows the circuit model of the LCR series circuit. The output voltage is obtained from both sides of L_S or C_S with a high impedance load. The absolute value of the current I_S ($|I_S|$) in this circuit is given by

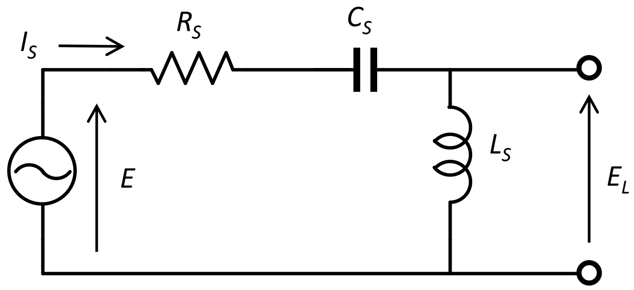

Fig. 3. Circuit model of the LCR series circuit.

Figure 4 shows the circuit model of the proposed booster circuit [19]. In Fig. 4, the input impedance is set to 50 Ω. To enhance the RF voltage amplitude, L (= 15 nH) and C_C (= 0.3 pF) are used in the main resonant circuit. C_1 (= 0.3 pF) is the tuning block for compensating the tolerance of the discrete components and obtaining a high voltage swing at the centre frequency. Here, C_2 (= 0.3 pF) is an impedance matching capacitor. The two-stage CW circuit is composed of a diode (HSMS-286Y, Avago), C_2 and C_3 (= 15 pF). In the input section, an AC voltage source and a 50-Ω internal resistance (R) are connected in place of the antenna. The DC output of the proposed circuit is numerically analysed using the ADS (Keysight technologies) circuit simulator.

Figure 5 shows the typical simulation results of the relationship between V_{out} / V_{LC} and N, where V_{LC} represents the output voltage of the resonant circuit—namely, the input of the CW circuit. From Fig. 5, Eq. (1) is not satisfied because of the parasitic elements of the diodes, and there is an optimized number for the unit structure in the RF region. The input impedance of the booster circuit is changed slightly by increasing *N*; hence, the capacitance values are optimized as mentioned in the previous paragraph.

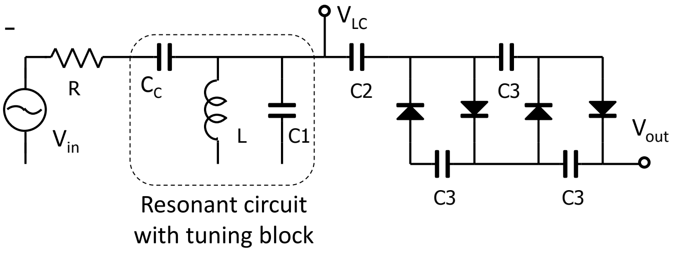

Fig.4. Circuit of the proposed booster circuit.

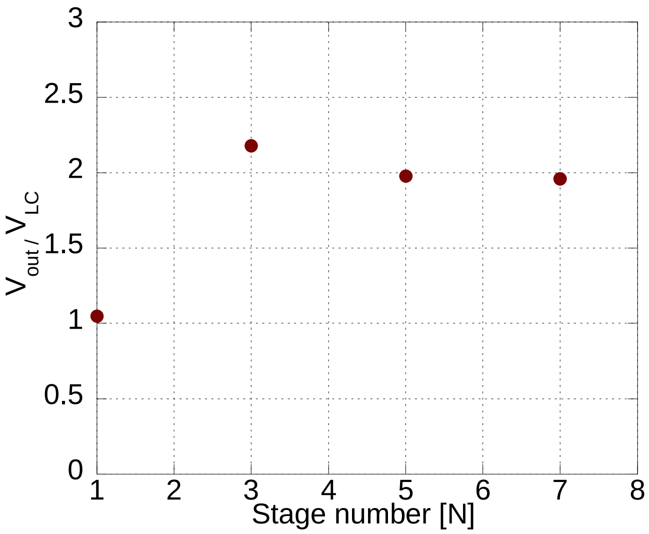

Fig. 5. Simulation results of the relationship between V_{out} / V_{LC} and *N*.

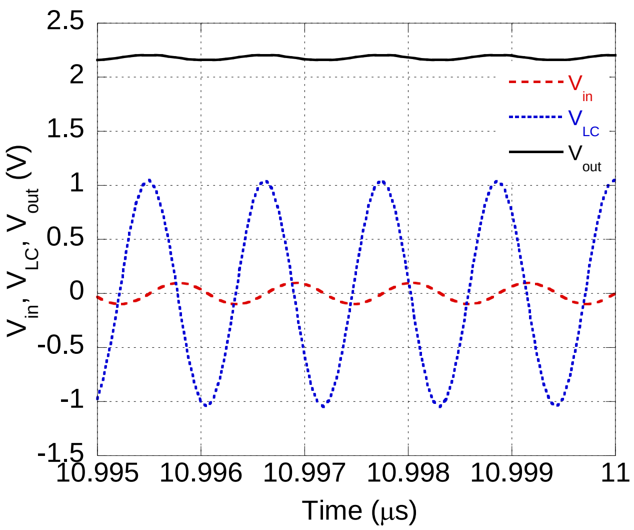

Fig. 6. Transient analysis of V_{in}, V_{LC} and V_{out} at 900 MHz.

Figure 6 shows the simulated voltage of the source (V_{in}), V_{LC}, and V_{out} in the booster circuit. Here, V_{in} is 100 mV at 900 MHz, and V_{LC} is set to be 10 times greater than V_{in} by passing it through the resonant circuit. Because the RF signal is boosted and rectified by the CW circuit, V_{out} is 23 times greater than V_{in}, and the proposed energy harvesting circuit generates an approximately time-independent output voltage.

The RF-to-DC power conversion efficiency (η) is defined as follows [20]:

$$\eta = \frac{DC\ output\ power}{RF\ input\ power} \tag{7}$$

Figure 7 shows the simulated power conversion efficiency dependency on the load resistance (R_L), where the RF input power is –10 dBm. The maximum η in this study is 57.8% for R_L=1.0 × 10^7 Ω.

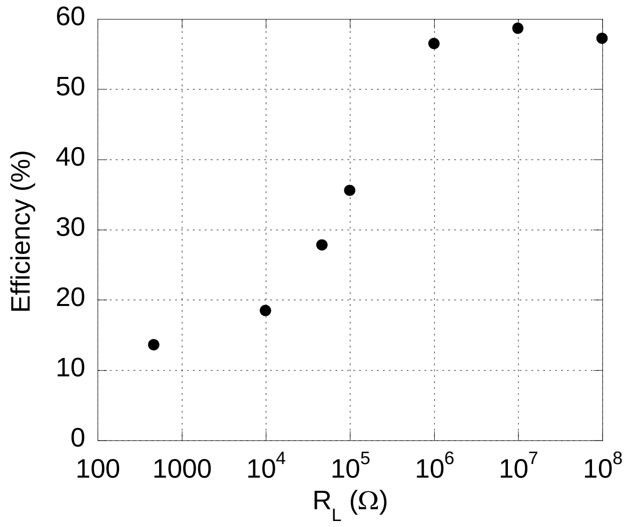

Fig. 7. Power conversion efficiency dependency on load resistance (R_L) at 900 MHz

III. Impedance Matching Circuit Design

Our proposed energy harvesting circuit is placed on the backside of a one-sided directional planar antenna fabricated on a flexible substrate. A slot dipole antenna was chosen for our system. To miniaturize the slot size of the antenna, an impedance matching circuit is necessary. This antenna is called an electrically small antenna (ESA). The impedance matching circuit in the ESA that we propose is composed of a CPW transmission line and interdigital gap, and the design method is the same as was proposed previously [13].

Our proposed impedance matching circuit is based on a Chebyshev bandpass filter (BPF) [22, 23]. The BPF is composed of a resonance circuit and impedance inverter (K-inverter, $K_{i,\,i+1}$). A one-stage BPF is used to reduce the circuit size.

Figure 8 shows the one-stage BPF composed of K-inverters given by

$$K_{0,1} = \sqrt{w}\sqrt{\frac{Z_0 x_1}{g_0 g_1}}, \quad K_{1,2} = \sqrt{w}\sqrt{\frac{x_1 Z_0}{g_1 g_2}} \qquad (8)$$

$$X_1 = x_1\left(\frac{\omega}{\omega_0} - \frac{\omega_0}{\omega}\right) \qquad (9)$$

where X_1 is the reactance of the transmission line, which has a reactance slope parameter x_1. w is a relative bandwidth, and g_i is the filter parameter. ω and ω_0 are the angular velocity and the resonance angular velocity, respectively.

At the centre frequency, the equivalent circuit model is described as shown in Fig. 9. In this case, the resonance condition is given by

$$R'_L = \frac{K_{0,1}^2}{Z_0} = \frac{w x_1}{g_0 g_1} \qquad (10)$$

$$R'_S = \frac{K_{1,2}^2}{Z_0} = \frac{w x_1}{g_1 g_2} \qquad (11)$$

A quality factor of this resonance circuit (Q) is obtained by

$$Q = \frac{x_1}{R'_S + R'_L} = \frac{g_0 g_1 g_2}{w\left(g_0 + g_2\right)} \qquad (12)$$

Substituting Eq. (10) for Eq. (11), the resistance ratio is given by

$$\frac{R'_L}{R'_S} = \frac{g_0}{g_2} \ . \qquad (13)$$

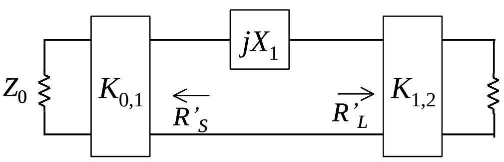

Fig. 8. Circuit model of the one-stage BPF with a K-inverter.

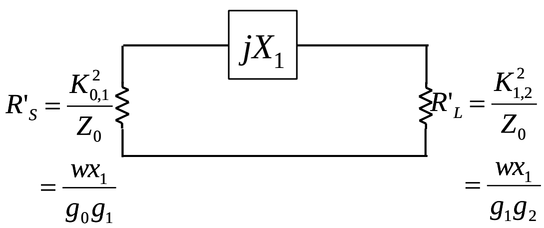

Fig. 9. Equivalent circuit of the circuit shown in Fig. 8 at the resonance frequency.

Next, the design of the miniaturized impedance matching circuit using a quarter-wavelength (λ/4) transmission line was presented.

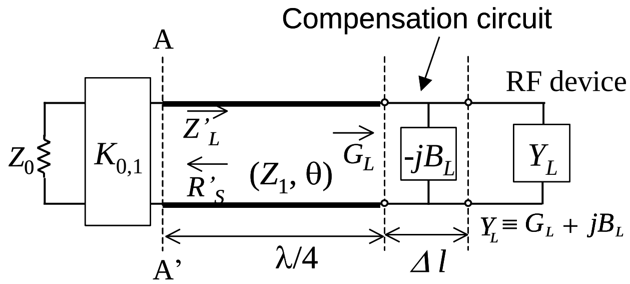

Fig. 10. Circuit model of the proposed impedance matching circuit.

Figure 10 shows the circuit model of the proposed transmission-line-based impedance matching circuit. Generally, an RF device has an admittance Y_L of

$$Y_L = \frac{1}{Z_L} \equiv G_L + jB_L \qquad (14)$$

To compensate B_L, the length of the transmission line is optimized by

$$\Delta l = -\frac{B_L}{\omega_0 C} \qquad (15)$$

where C [F/m] is the capacitance per unit length in the transmission line.

In Fig. 10, Z_L' and R_S' are described as

$$Z_L^{'} = Z_1^2 G_L + jX_1 \equiv R_L^{'} + jX_L^{'} \qquad (16)$$

$$X_1 = -Z_1 \cot\theta \equiv x_1\left(\frac{\omega}{\omega_0} - \frac{\omega_0}{\omega}\right) \qquad (17)$$

$$x_1 = \frac{\pi}{4} Z_1 \qquad (18)$$

$$R_S^{'} = \frac{K_{0,1}^2}{Z_0} \qquad (19)$$

where Z_1 and θ are the characteristic impedance and electrical length of the transmission line, respectively. The admittance (Y_L) of the RF device is assumed to be $|Y_L| << Y_0$. At the resonance frequency, X_1 in Eq. (17) goes to zero. In this case, the equivalent circuit model at A-A' in Fig. 10 can be modified as shown in Fig. 11.

Considering the resonance condition of Eqs. (12) and (13), we can obtain the resistance ratio and Q value at the resonance frequency as follows.

$$\frac{R'_L}{R'_S}=\frac{Z_0}{K_{0,1}^2}Z_1^2G_L=\frac{g_0}{g_2} \tag{20}$$

$$Q=\frac{x_1}{R'_S+R'_L}=\frac{Z_0}{K_{0,1}^2}\frac{x_1}{\left(1+\frac{g_0}{g_2}\right)}=\frac{g_0g_1g_2}{w(g_0+g_2)} \tag{21}$$

By solving Eqs. (20) and (21), the final design equations are given by

$$Z_1=\frac{\pi}{4}\frac{w}{g_1g_2G_L} \tag{22}$$

$$K_{0,1}=\sqrt{w}\sqrt{\frac{Z_0x_1}{g_0g_1}},\quad \left(x_1=\frac{\pi}{4}Z_1\right) \tag{23}$$

The input impedance is matched by using the λ/4 transmission line, which has a characteristic impedance (Z_1) and K-inverter ($K_{0,1}$).

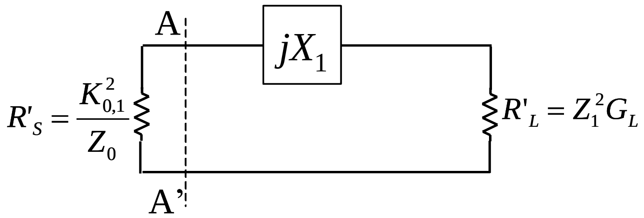

Fig. 11. Equivalent circuit model of the circuit shown in Fig. 10 at the resonance frequency.

IV. Antenna Design

Our proposed impedance matching circuit is implemented in an antenna. Figure 12 shows the layout of the one-sided directional slot antenna on the flexible substrate (Duroid RT6010, Rogers). The designed centre frequency is the 900 MHz band. The cross-sectional view of this antenna is also shown in Fig. 12. To suppress the backward radiation, the floating metal layer is attached to the bottom of the substrate. The substrate has dielectric constant ε_r=10.2 and tanδ = 0.0023. The thickness of the substrate and both copper metals are 1.27 mm and 18 μm, respectively. Figure 13 shows a close-up of the interdigital gap. To realize the 50-Ω impedance matching, the number of teeth, tooth length, and tooth width are optimized.

The simulated electric field distribution of a top metal and a bottom floating metal layer are shown in Fig. 14. The top layer resonates; however, the bottom floating metal layer does not resonate. Thus, this floating metal layer can suppress the radiation of the backward radiation (bottom side), and the directivity of the forward direction is greater than that of the backward direction.

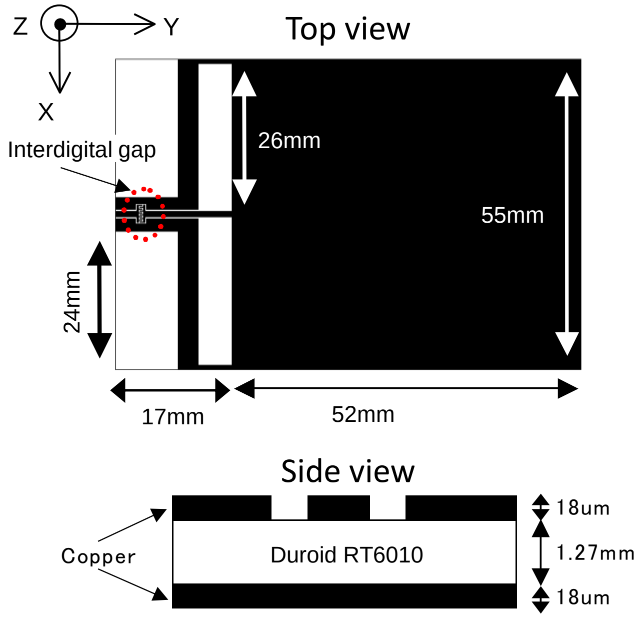

Fig. 12. Layout of the one-sided directional slot antenna on the flexible substrate.

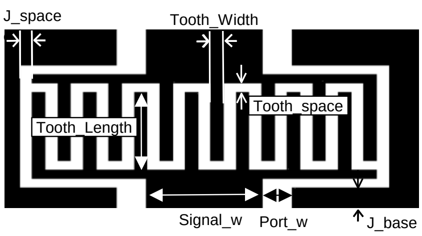

Name	Size [mm]
J_space	0.12
J_base	0.12
Tooth_length	0.95
Tooth_width	0.12
Tooth_space	0.12
Signal_w	1.00
Port_w	0.26

Fig. 13. Close-up of the interdigital gap.

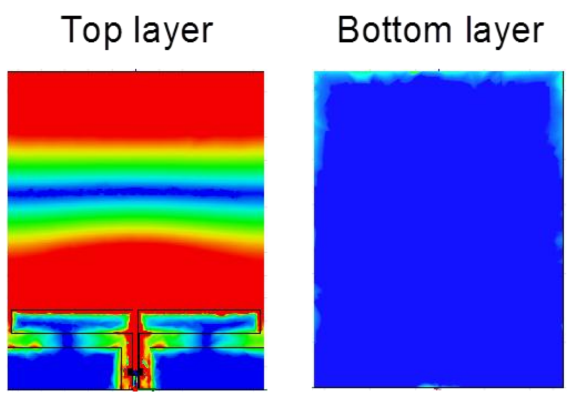

Fig. 14. Electric field distribution of a top metal and a bottom floating metal layer.

Figure 15 shows the input impedance (Z_{in}) of this antenna. At 900 MHz, Z_{in} is 47.94 – j 0.65 Ω, which is almost the same as 50 + j 0 Ω. Thus, the impedance matching circuit is deemed operational.

Because this substrate is flexible, the return loss and radiation characteristics of this antenna were simulated as if this antenna were bent. Figure 16 shows the cross-sectional view for the simulation condition. In the figure, θ is the bending angle. Figures 17 and 18 show the frequency responses and radiation patterns of our proposed antenna with different values of θ. The matching frequency (centre frequency), matching bandwidth, and radiation patterns are almost the same over the different θ values. This antenna maintains the one-sided directional radiation if it is bent.

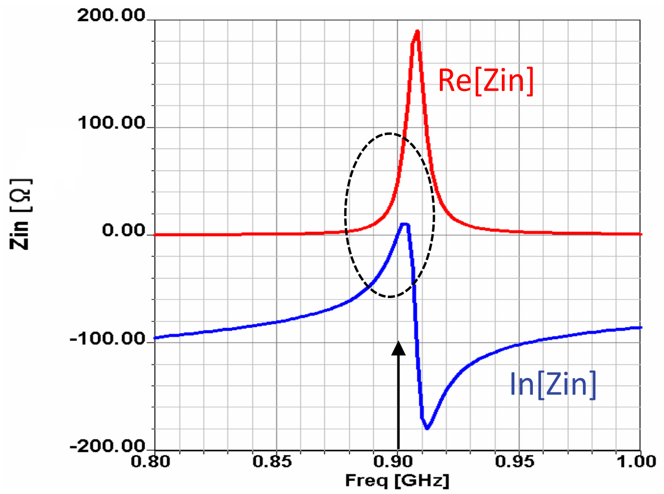

Fig. 15. Simulated input impedance of the proposed antenna.

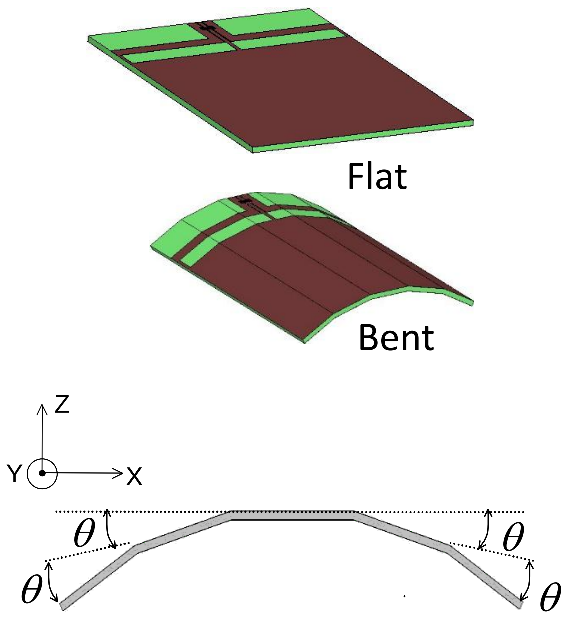

Fig. 16. Simulation condition of the bending angle.

V. Measurement Results of the Circuit

Figure 19 shows a photograph of the booster circuit, which has an input impedance = 50 Ω. All capacitors, inductors, and diodes are placed on the top metal of the microstrip transmission line and are connected by solder. The dimensions of the booster circuit are 2.0 mm × 1.6 mm. The ground metal plane is placed on the backside of this circuit. Figure 20 shows the frequency dependence of the output voltage of the proposed energy harvesting circuit. In the figure, the solid line shows V_{out} calculated from Fig. 4—namely, without parasitic components—where the RF input is 100 mV. The dotted line shows the measured results. Compared with the ideal values, the measured centre frequency and peak voltage are lower, and the bandwidth is wider. The measured power efficiency is 44%. Because of the parasitic components due to the resistance of electrical contacts to the printed circuit board (PCB), the characteristic impedance of the transmission line on the PCB, inductance of the RF feed lines, and tolerance of the chip components, the centre frequency and quality factor of the circuit are reduced. The tolerances of the capacitor and inductor are 0.1 pF and 5%, respectively. The characteristic impedance and metal loss of the microstrip transmission lines, which have a 1 mm line width, are also considered. The broken line shows the simulation results with the above parasitic components. The measured results are good agreement with the simulation results of parasitic components.

Table I summarizes the performance of the proposed circuit compared with the recently published work. The efficiency is higher than those in previous research. In each case, the input power is similar to and lower than a similar wireless power transfer system, and the efficiency is less than 50%. From the results of our proposed circuit, the series resonance circuit and impedance mating circuit in front of the CW circuit are strong tools for enhancing a weak RF input signal such as that in a wireless telecommunication system.

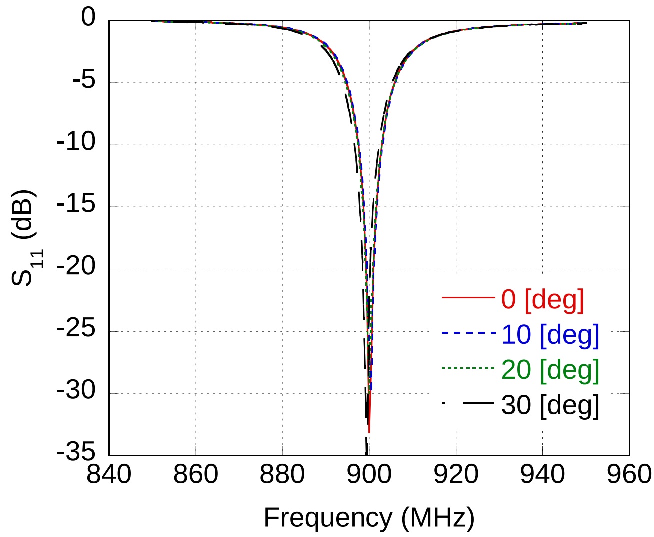

Fig. 17. Frequency responses of the slot antenna with different bending angles.

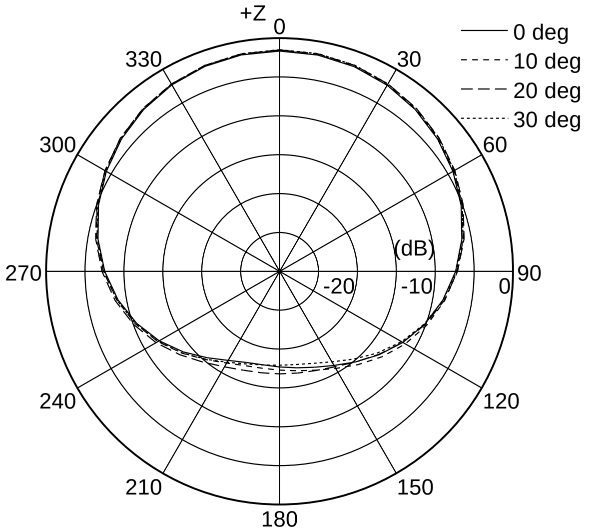

Fig. 18. Simulated radiation patterns of the slot antenna with different bending angles.

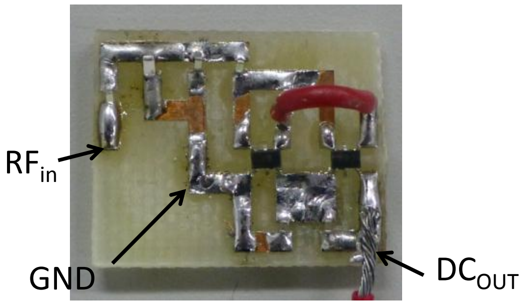

Fig. 19. Photograph of the proposed booster circuit.

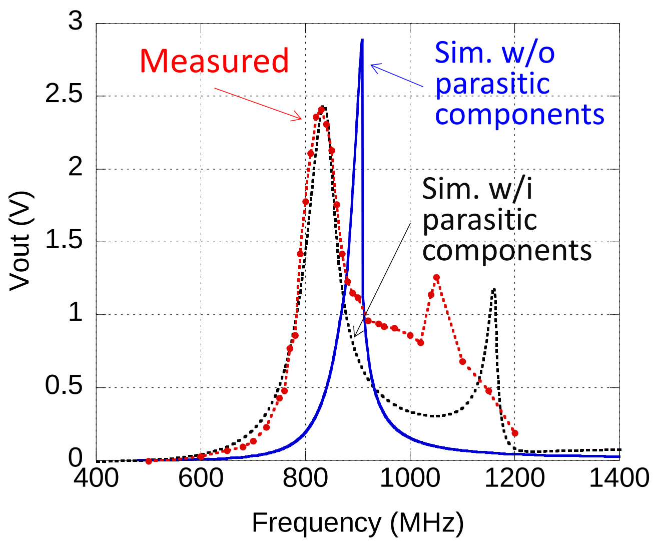

Fig. 20. Frequency responses of the output voltage of the proposed energy harvesting circuit.

Table.1. Comparison of the measured efficiency of the energy harvesting circuit for the UHF band

Ref.	Freq.(MHz)	Pin (dBm)	Efficiency (%)
[2]	850	-10	35
[3]	550	-10	45
[5]	896	-19	18
This work	830 900*	-10	44 58.7*

* Simulation w/o parasitic components.

VI. MEASUREMENT RESULTS OF THE ANTENNA

Our proposed antenna was fabricated by using CAD-controlled milling machine. Figure 21(a) shows a photograph of this machine. Figure 21(b) shows a close-up of the drill section. There is a ϕ = 0.1 mm drill in this system. Figure 22 shows the photograph of the proposed antenna. The top metal layer (a) and bottom floating metal layer (b) are shown. The bottom floating metal layer is not connected. A close-up of the interdigital gap composed of impedance matching circuit (c) is also shown. The MMCX connector is attached at the input port.

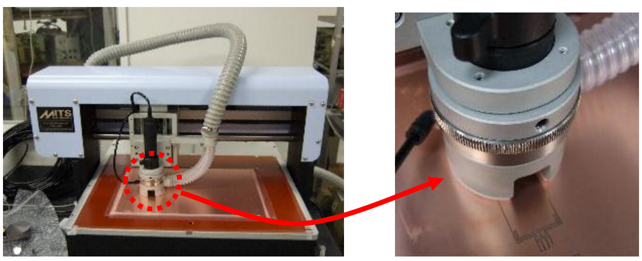

(a) Milling machine (b) Close-up of the drill

Fig. 21. Photograph of the proposed antenna.

The radiation patterns of this antenna are measured in the anechoic chamber. Figure 23 shows the layout of this chamber. Our proposed antenna was placed on the turntable on the left, and the angular dependence of the receiving signal was measured by rotating the turntable. Figure 24 shows a photograph of the chamber. A wideband horn antenna (up to 18 GHz) was used as a reference transmitting antenna. The distance between the reference antenna and our proposed antenna is 2.5 m.

Figure 25 shows a photograph of the flat antenna and the antenna after being bent. This antenna is flexible; hence, it is easy to revert to the original flat structure. Figure 26 shows a comparison of the return loss with different values of θ. These data are similar and agree with the simulation results in Fig. 17. However, the centre frequency is slightly shifted to a lower region because of the error in the dielectric constant of the substrate. Figure 27 shows the measured radiation patterns at 900 MHz, where "Flat" represents θ = 0 degree and "Bend" represents θ = 17 degrees, respectively. The measured front-to-back ratio (F/B ratio) is approximately 10 dB. As shown in Fig. 27, our proposed antenna maintains the one-sided directional radiation if θ increases. Thus, we can realize the one-sided directional antenna on a flexible substrate. This antenna can work if it is mounted on nonplanar objects. The booster circuit can be connected to the backside of this antenna.

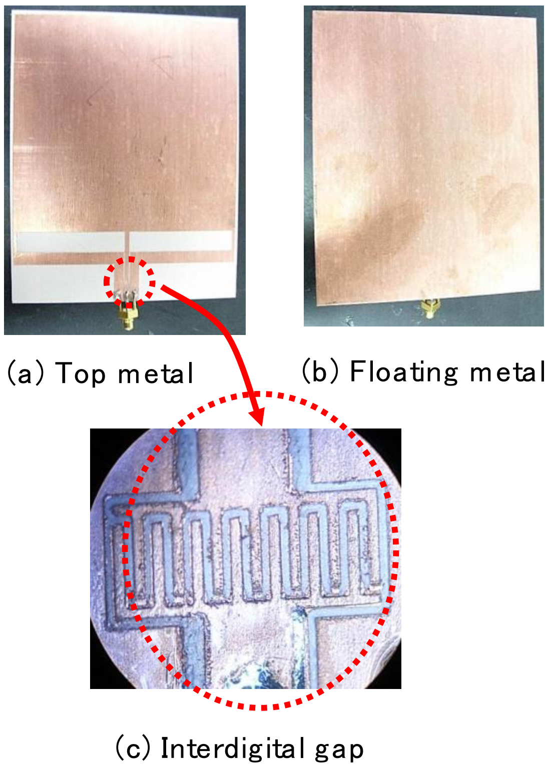

Fig. 22. Photograph of the proposed antenna.

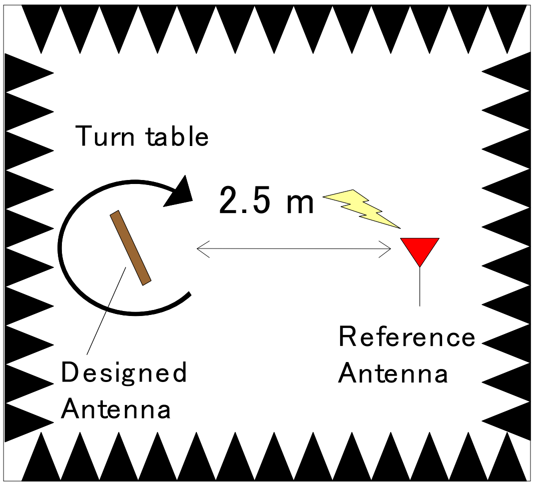

Fig. 23 Layout of the measuring setup.

We also attempted to light an LED without connecting it to a power source by wires.

The 900 MHz band is one of the ISM (industry, science, medical) bands that are operated without licenses. UHF RFID tag systems operating at the 900 MHz band are used worldwide. The output power of the UHF RFID transmitter is 250 mW, which is suitable for the RF energy harvesting system, because it is higher than the Wi-Fi transmitter power.

Figure 28 shows a photograph of the LED light-up demonstration with the energy harvesting circuit on the backside of the antenna. The antenna gain of both the transmitting and receiving antennas is -0.7 dBi. The distance between antennas is 0.2 m. The transmission signal power at the output port of a signal generator is 20 dBm. As can be seen, the LED is operational. Because the V_f (forward voltage) of this LED is 2.0 V, our proposed energy harvesting system generates at least 2 VDC of voltage, confirming the data in Fig. 6.

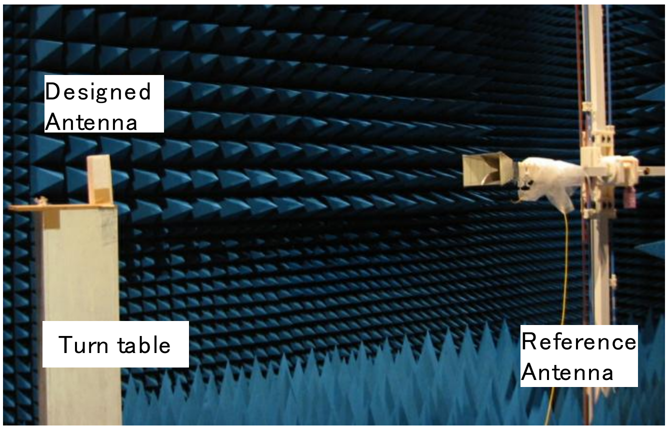

Fig. 24 Photograph in the anechoic chamber.

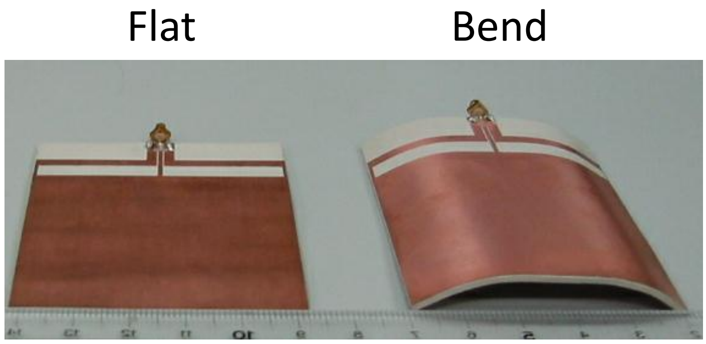

Fig. 25. Photograph of the flat antenna and the antenna after being bent.

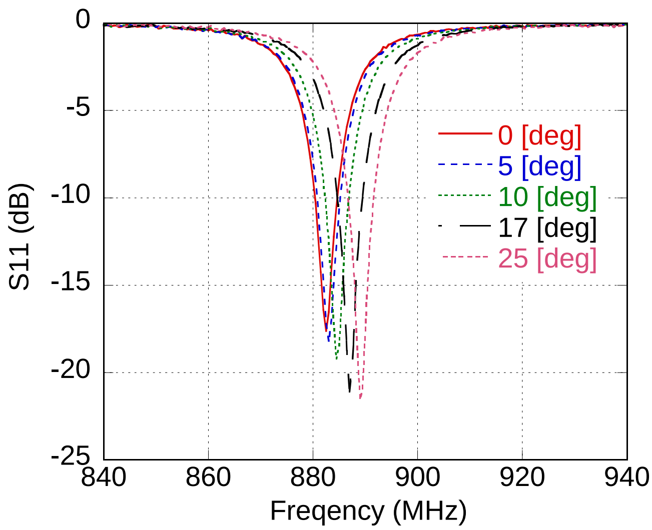

Fig. 26. Comparison of the return loss with different θ values (measured).

VII. Conclusions

This paper describes the design of an RF-to-DC energy harvesting circuit. The circuit was composed of a one-sided directional antenna on a flexible substrate, an impedance matching circuit, a resonant circuit, and a booster circuit for converting and boosting radio frequency power into DC voltage. A transmission-line-based impedance matching circuit was implemented on the one-sided directional slot antenna. This antenna is composed of a top metal layer and a bottom floating metal layer. The measured F/B ratio is approximately 10 dB, and the antenna gain is –0.7 dBi. The simulated conversion efficiency of the proposed boosting circuit without any parasitic elements is 58.7%. Owing to the effect of the parasitic components in the circuit, the measured efficiency was 44%. By using the backside of the proposed antenna on the flexible substrate, the DC voltage is directly generated, and the LED is operated.

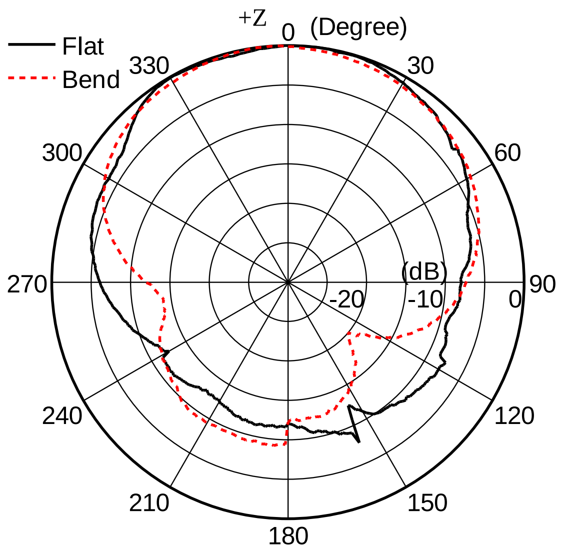

Fig. 27. Measured radiation patterns at 900 MHz.
(θ = 0 deg (Flat) and θ = 17 deg, (bend))

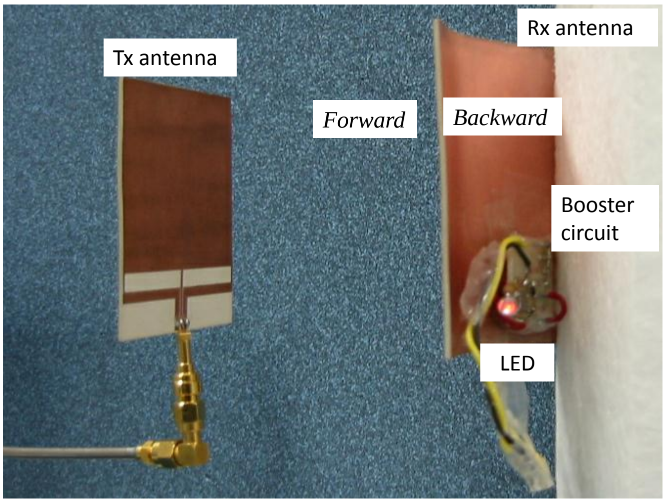

Fig. 28. Photograph of the LED light-up demonstration for the power harvesting circuit on the antenna.

Acknowledgements

This work was partly supported by the VLSI Design and Education Center (VDEC), the University of Tokyo in collaboration with CADENCE Corporation and Keysight Corporation. This work was partially supported by the Grant-in-Aid for Scientific Research (KAKENHI) from Japan Society for the Promotion of Science, JSPS. This research was also partially supported by the Grant-in-Aid for Collaborative Research Program Based on Industrial Demand, CREST and Matching planner program from Japan Science and Technology Agency, JST.

The author would like to express thanks to Miss Yuharu Shinki and Mr. Kyohei Shibata in Kyusshu University, Japan and Mr. Mohamed Mansour at the Electronics Research Institute, Dokki, Egypt, for their help and support.

References

[1] A. Shameli, A. Safarian, A. Rofougaran, M. Rofougaran, and F. D. Flaviis, "Power harvester design for passive UHF RFID tag using a voltage boosting technique", *IEEE Trans. Microwave. Theory Tech.*, vol. 55, no. 6, pp. 1089–1097, June 2007.

[2] A. Georgiadis, A. Collado, S. Via, and C. Meneses, "Flexible hybrid solar/EM energy harvester for autonomous sensors", *IEEE IMS 2011 Digest*, pp. 1–4, June 2011.

[3] C. Mikeka and H. Arai, "Microwave tooth for sensor power supply in battery-free applications", Proc. Asia Pacific Microw. Conf., pp. 1802–1805, Dec 2011.

[4] A. Sample, and J. R. Smith1, "Experimental results with two wireless power transfer systems", *Proc. IEEE Radio and Wireless Symposium*, pp. 16–18, Jan. 2009.

[5] U. Karthaus and M. Fischer, "Fully integrated passive UHF RFID transponder IC with 16.7-uW minimum RF input power", *IEEE J Solid-State Circuits*, vol. 38, no. 10, pp. 1602–1608, Oct. 2003.

[6] J. P. Curty, N. Joehl, F. Krummenacher, C. Dehollain, and M. J. Declercq, "A model for u-power rectifier analysis and design", *IEEE Trans Circuit Systems*, vol. 52, no. 12, pp. 2771–2779, Dec. 2005.

[7] H. Kitayoshi and K. Sawaya, "Long range passive RFID-tag for sensor networks", *Proc. IEEE Vehicular Tech. Conf.*, pp. 2696–2700, Sept. 2005.

[8] Cockcroft-Walton generator, http://en.wikipedia.org/wiki/Cockcroft Walton generator

[9] C. Cho, H. Choo, and I. Park, "Design of planar RFID tag antenna for metallic objects", *Electron. Lett.*, vol. 44, pp. 175–177, 2008.

[10] Q. Z. Chen and B. J. Hu, "Novel UHF RFID tag antenna with shorted stubs mountable on the metal objects", *Microwave and Millimeter Wave Technology.*, pp 1822–1824, 2008.

[11] D. D. Arumugam, and D. W. Engels, "Characteristics of passive UHF RFID tags on metalslabs", *Proc. IEEE Antennas and Propagation Society International Symposium*, pp.1–4, June, 2009.

[12] T. W. Koo, D. Kim, J. I. Ryu, J. K. Kim, J. G. Yook, and J. C. Kim, “Design and Implementation of Label-type UHF RFID Tags for the Metallic Object Application”, *Proc. IEEE Antennas and Propagation Society International Symposium*, 206.6, June, 2010.

[13] H. Kanaya, R. Nabeshima, R. K. Pokharel, K. Yoshida, M. Tsujii, and R. Iino, “Development of an Electrically Small One-Sided Directional Antenna with Matching Circuit”, *Proc. 2008 IEEE Radio and Wireless Symposium*, pp. 739–742, 2008

[14] H. Urabe, R. K. Pokharel, H. Kanaya, K. Yoshida, A. Ishikawa, S. Fukagawa, and A. Tahira, “Design and Performance of 800MHz/2GHz Dual Band Small Planar Antenna”, *Asia-Pacific Microwave Conference Proceedings*, pp. 1508, Dec. 2009.

[15] H. Kanaya, M. Kato, R. K. Pokharel, and K. Yoshida, “Development of 2.4GHz One-Sided Directional Planar Antenna with Quarter Wavelength Top Metal”, *Proc. 2010 IEEE International Symposium on Antennas & Propagation*, 404.1, 2010.

[16] H. Kanaya, J. Fujiyama, G. Urakawa, and K. Yoshida, "Design and Performance of High Tc Superconducting Coplanar Waveguide Matching Circuit for RF-CMOS LNA", *IEICE transactions on electronics*, vol. 86, no. 1, pp. 37–42, 2003.

[17] H. Kanaya, T. Shinto, K. Yoshida, T. Uchiyama, and Z. Wang, "HTS coplanar waveguide bandpass filters with highly packed meanderlines", *IEEE Trans Appl. Supercond.*, 11, pp. 481–484, 2001.

[18] T. Hirabaru, H. Kanaya, D. Kanemoto, R. K. Pokharel, K. Yoshitomi, and K. Yoshida, "Development of 900MHz band one-sided directional antenna on flexible substrate", *Proc. IEEE Antennas and Propagation Society International Symposium*, pp. 1008–1011, July 2011.

[19] H. Kanaya, S. Tsukamoto, T. Hirabaru, D. Kanemoto, R. K. Pokharel, and K. Yoshida, "Energy Harvesting Circuit on a One-Sided Directional Flexible Antenna", *IEEE Microwave and Wireless Components Letters*, vol. 23, no. 3, pp. 164–166, 2013.

[20] V. Mariani and M. Thevenot, "Efficient design of rectifying antennas for low power detection", *IEEE IMS 2011 Digest*, pp. 1–4, June 2011.

[21] H. Kanaya, Y. Koga, G. Urakawa, and K. Yoshida, “Design of HTS Coplanar Waveguide Matching Circuit for Low Noise CMOS-HTS Receiver”, *IEEE Trans Appl. Supercond.*, vol. 13, pp. 1031–1034, 2003.

[22] G. Matthaei, L. Young, and E. Jones, “Microwave Filters, Impedance-Matching Networks, and Coupling Structures”, New York: *McGraw-Hill*, 1964, pp. 427–440.

[23] H. Kanaya, J. Fujiyama, R. Oba, and K. Yoshida, “Design method of miniaturized HTS coplanar waveguide bandpass filters using cross coupling”, *IEEE Trans Appl. Supercond*., vol. 13, pp. 265-268, 2003.

Journal of Energy Challenges and Mechanics
http://www.nscj.co.uk/JECM/

ISSN 2056-9386
Volume 3 (2016) issue 3, article 6

Study on the Gear Ratio for a Tidal Current Power Generation System using the Constant Turbine Output Control Method

使用恒定涡轮输出控制方法的潮汐流发电系统之齿轮比研究

Kentaro Tsuji[1*], Kazuhisa Naoi[1], Mitsuhiro Shiono[1]

[1] *Department of Electrical Engineering, College of Science and Technology, Nihon University, Chiyoda-ku, Tokyo 101-8308, Japan*

tsuji.kentaro@nihon-u.ac.jp

Accepted for publication on 14th September 2016

Abstract - **Tidal current is the flow of sea water due to the tidal phenomenon. Therefore, it is possible to predict power output of the tidal current power generation system, which is more advantageous than other renewable energy sources, when the tidal current power generation system is connected to the power grid and operated.**

Power generation method of tidal current power generation systems is a fixed-speed method or a variable-speed method. The authors have examined the gear ratio and generator capacity of the tidal current power generation system using the maximum power point tracking (MPPT) control scheme. The capacity factor of the system which influences cost of power generation was about 14%. To increase the capacity factor of tidal current power generation systems, we propose the tidal current power generation system which can be controlled to constant turbine output and we examined a method of deciding the gear ratio and generator capacity which maximize generated energy.

First, this paper examines the speed control model which is operated using the constant turbine-output control scheme. The target value of the speed control model is rotational speed of generator for each current speed. Second, this paper examines the gear ratio and generator capacity which maximize generated energy, when the tidal current power generation system is operated using constant turbine-output control scheme.

This paper shows that the constant turbine-output control scheme increases generated energy, capacity factor and energy conversion efficiency in comparison with the MPPT control scheme. On the other hand, the constant turbine-output control scheme decreases generator capacity in comparison with the MPPT control scheme. The results of the speed control model using calculated the gear ratio and generator capacity show a good dynamic response to variation of current speed.

Keywords - **tidal current power generation, Darrieus type water turbine, DFIG, constant turbine-output control method, gear ratio**

I. INTRODUCTION

Methods for generating electricity from renewable energy sources are of growing interest for achieving a stable energy supply and as countermeasures against global warning. One form of renewable energy is tidal currents, flows of sea water caused by the rise and fall of the tide. The direction of these flows reverses every half-period; the length of the period varies with location, and is either about half a day or a full day [1]. Thus, tidal current power generation offers advantages in terms of connecting to a power grid, as the power output is predictable and little influenced by the weather.

The authors have investigated a Darrieus turbine-based tidal current power generation system whose generator transforms the rotational energy of the turbine into electrical energy. We have conducted water channel tests and open water tests of the characteristics of a Darrieus-type water turbine and of the electric power it can generate [2][3], in preparation for use of this turbine in a tidal current power generation system.

The power input to a tidal current power generation system varies in a similar way to a wind power generation system. Power generation method of tidal current power generation

©2016 North Sea

systems is a fixed-speed method or a variable-speed method. Variable-speed methods have received the most attention, as they are more efficient in converting tidal current energy to electrical energy. Two types of generators are used in variable-speed methods, doubly fed induction generators (DFIGs) and synchronous generators. In a DFIG-based system, an inverter is placed between the rotor circuit of the generator and the power grid; this has the advantage of allowing the inverter to be of lower capacity than that for a synchronous generator [4]. Thus, the tidal current power generation system we have investigated employs a variable-speed DFIG.

As mentioned above, in the field of wind power generation, there have been investigations of systems incorporating DFIGs [5][6] and models of speed controls for generators [7-9], just as in the case of tidal current power generation. However, those investigations all examined systems in which the gear ratio, the generator capacity, or both, were fixed. The present investigation addressed gear ratios and generator capacities for tidal current power generation systems to maximize the generated energy without overloading it. One of our previous investigations revealed that the annual capacity factor of this system was about 14% while operated with maximum power-point tracking (MPPT) [10]. For comparison, figures of 12% and 20% are commonly quoted for solar and wind power generation systems, respectively [11]; thus, this annual capacity factor exceeds that for solar power generation systems.

Nonetheless, when operating with MPPT, the generator must be large enough to accommodate the maximum current speed occurring during the year, and this detracts from economic efficiency. We propose reducing the generator capacity and, in order to further improve the annual capacity factor of this tidal current power generation system, to implement a constant turbine-output control scheme. The objective of this study was to identify the optimal gear ratio and the generator capacity providing the maximum generated energy without overloading the generator while the tidal current power generation system is operated under this control scheme.

This study is presented as follows: First, a method of approximating the characteristics of the water turbine and a probability density function for the occurrence of current speeds are described. Then, a model of the speed controller for the tidal current power generation system is examined. A procedure is investigated for identifying the gear ratio and the generator capacity that will allow maximizing the generated energy without overloading the generator while the tidal current power generation system is operated under this control scheme. Finally, the response of a system incorporating the identified gear ratio and generator capacity operating in currents of varying speeds is examined.

II. Tidal Current Power Generation System Based on Darrieus Water Turbine

2.1. Power output characteristics of Darrieus water turbine

We have developed and conducted experiments in a water channel and in the ocean with a tidal current power generation system based on a Darrieus water turbine [2][3]. This turbine contained straight blades, and is referred to as a "straight-bladed vertical-axis water turbine" (Fig. 1(a)). The profile for these blades was based on the symmetric

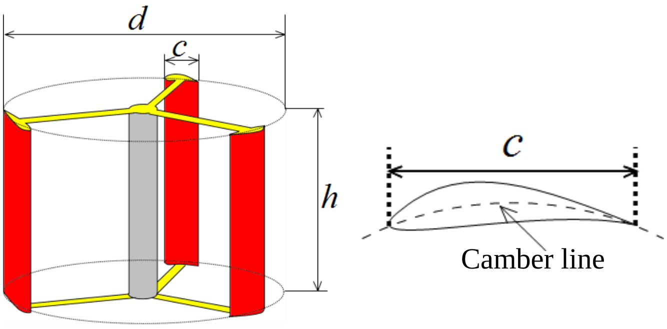

(a) Turbine configuration (b) Shape of blade

Fig. 1, Schematic diagram of Darrieus water turbine.

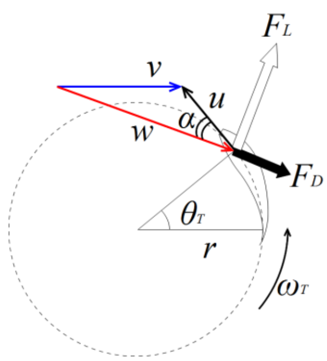

Fig. 2, Forces exerted by flow.

NACA63$_3$-018 [12], but on a camber line fitting the blade path (Fig. 1(b)). The blades were placed at uniform intervals around the circumference of the turbine.

We first describe the operating principles of the Darrieus water turbine. We begin with a simple 2-dimensional view of the plane of rotation in Fig. 1(a). A single blade rotates with a circumferential speed u about a blade path of radius r at an angle θ_T in a flow field moving at velocity v. Figure 2 shows the relation between u and v. The relative flow (relative velocity) w at the blade is given by the vector sum of v and u:

$$w = v\sqrt{1+2\lambda\cos\theta_T+\lambda^2} \tag{1}$$

where λ is the tip speed ratio (= u/v = $r\omega_T/v$), r is the turbine radius, ω_T is the angular speed of the turbine.

When the fluid strikes the blade, it exerts a force against it. This force can be resolved into two components, the drag force F_D acting in the same direction as the relative fluid velocity, and the lift force F_L acting in a direction perpendicular to F_D. These forces are given by Eqs. (2) and (3), using the fluid density ρ and blade area A.

$$F_L = \frac{1}{2} C_L \rho A w^2 \quad (2)$$

$$F_D = \frac{1}{2} C_D \rho A w^2 \quad (3)$$

C_L and C_D are the coefficients of lift and of drag, respectively, and are influenced by many factors including the blade profile, angle of attack, Reynolds number, and blade surface roughness. α is the angle of attack and is given by Eq. (4) on the basis of Fig. 2.

$$\alpha = \tan^{-1}\left(\frac{\cos\theta_T}{\sin\theta_T + \lambda}\right) \quad (4)$$

The torque T_1 arising in a single blade is given by:

$$T_1 = \frac{1}{2} \rho r A w^2 \left(C_L \sin\alpha - C_D \cos\alpha\right) \quad (5)$$

The mean torque T_q generated by n blades during a single revolution of the turbine is then:

$$T_q = \frac{n}{2\pi} \int_0^{2\pi} T_1 d\theta_T \quad (6)$$

The dimensionless torque coefficient C_T in Eq. (7) is introduced to evaluate the torque:

$$C_T = \frac{T_q}{0.5 \rho S r v^2} \quad (7)$$

where S (=d×h) is the swept area of the water turbine, d is the turbine diameter, and h is the blade height. The turbine output power P_{To} is estimated using:

$$P_{To} = \omega_T T_q \quad (8)$$

If the input fluid power over the swept turbine area S is P_{Ti}, this is given by:

$$P_{Ti} = \frac{1}{2} \rho S v^3 \quad (9)$$

The water turbine efficiency, i.e., its power efficiency C_P, is expressed as

$$C_P = \frac{P_{To}}{P_{Ti}} \quad (10)$$

2.2. APPROXIMATION OF WATER TURBINE CHARACTERISTICS WITH A SPLINE FUNCTION

We now consider the method for approximating the water turbine characteristics, which will be needed in order to calculate the generated energy and to examine the turbine speed control model. These characteristics are approximated using a (2m–1)-dimensional spline smoothing function. The turbine characteristics obtained from the water channel tests were the turbine speed and the torque [3]; in this study, the torque coefficient C_T is approximated with a spline smoothing function.

The smooth curve close to the data points obtained in the experiment is designated $f_s(x)$, the coordinate system of the obtained data is (x_1,y_1), (x_2,y_2), …, (x_n,y_n), and ε defined in Eq. (11) is employed as the evaluation indicator showing how faithfully and smoothly $f_s(x)$ reproduces the data points.

$$\varepsilon = \sum_{i=1}^{n} w_i \left\{ f_s(x_i) - y_i \right\}^2 + g \int_{x_1}^{x_n} \left\{ f_s^{(m)}(x) \right\}^2 dx \quad (11)$$

Here, $f_s^{(m)}(x)$ is the m^{th} derivative of $f_s(x)$, and w_i and g are weighting coefficients with values $0 < w_i \leq 1$ and $g > 0$. The first term in this index denotes how faithfully $f_s(x)$ reproduces the data points. The second term indicates how smooth $f_s(x)$ is. Thus, when ε has been minimized, $f_s(x)$ has reached its smoothest possible shape under coefficient g. The (2m-1)-dimensional spline smoothing function is given by:

$$f_s(x) = p_{m-1}(x) + \sum_{i=1}^{n} c_i \left(x - x_i\right)_+^{2m-1} \quad (12)$$

Here, $\left(x - x_i\right)_+^{2m-1}$ is the (2m-1)$^{\text{th}}$ truncated power function and $p_{m-1}(x)$ is a (m-1)$^{\text{th}}$ polynomial given by

$$p_{m-1}(x) = \sum_{i=0}^{m-1} b_i x^i \quad (13)$$

The c_i in Eq. (12) are constants satisfying m conditions given by

$$\sum_{i=1}^{n} c_i x_i^{\,k} = 0 \quad (k=0, 1, 2, \ldots, m\text{-}1) \quad (14)$$

It has been shown [13] that Eq. (11) is a function minimizing ε when the n conditions in Eq. (15) are satisfied by the spline smoothing function $f_s(x)$ in Eq. (12).

$$f_s(x_j) + (-1)^m \cdot g \cdot (2m-1)! c_j w_j^{-1} = y_j \quad (j=1, 2, \ldots, n) \quad (15)$$

Table 1 presents the specifications of the water turbine constructed for water channel experiments, in which the turbine characteristics were identified. Using w_i=1 in Eq. (11), g was varied until a minimum value for ε was found; this is shown in Table 2. Here, ε_w represents the first term and ε_g represents the 2nd term in Eq. (11). The value for g in Table 2 was employed to approximate C_T, and the results are shown in Fig. 3. C_T is described by the following cubic (m=2) spline smoothing function:

$$C_T = d_0 + d_1\lambda + d_2\lambda^2 + d_3\lambda^3 \quad (16)$$

Here, $d_0 - d_3$ are constants which differ in every sector of the approximated data. C_P is a function of λ and C_T, (Eq. (17)) and is shown in Fig. 4:

$$C_P = \lambda C_T \quad (17)$$

TABLE 1, SPECIFICATIONS OF TESTED WATER TURBINE

Number of blades n	3
Diameter d [mm]	300
Height h [mm]	200
Chord length c [mm]	55.3
Solidity σ	0.176

TABLE 2, MINIMUM VALUES OF ε AND g
FOR DIFFERENT CURRENT SPEEDS

Current speed v [m/s]	Weighting factor g	Evaluation index ε	ε_w	ε_g
1.0	2.7×10^{-2}	2.6×10^{-2}	2.8×10^{-4}	2.6×10^{-2}
1.2	3.1×10^{-2}	2.2×10^{-2}	2.6×10^{-4}	2.2×10^{-2}
1.4	3.9×10^{-2}	2.9×10^{-2}	4.5×10^{-4}	2.8×10^{-2}

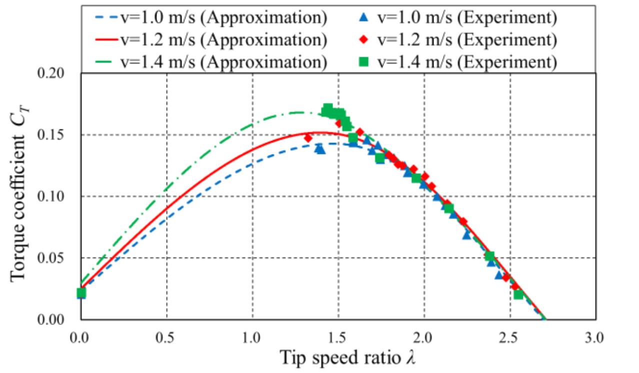

Fig. 3, Approximation of C_T characteristics using spline.

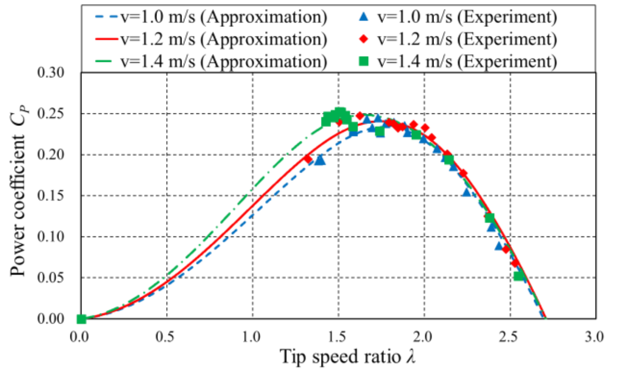

Fig. 4, Approximation of C_P characteristics using spline.

From Table 2, the data are most closely and smoothly approximated when ε is minimized; ε is lowest at a current speed of v = 1.2 m/s. Thus, the investigation in this study was carried out using the approximation curve for v = 1.2 m/s.

2.3. PROBABILITY DENSITY FUNCTION FOR OCCURRENCE OF CURRENT SPEEDS

Generally, the direction and speed of tidal currents change every 6 hours. The estimated values for current speed near the center of Akashi Strait [14] provided by the Japan Coast Guard Hydrographic and Oceanographic Department from January to December in 2003 and 2004 were used as data samples. Figure 5 presents those speed data.

We created a histogram as a representative probability distribution of these speeds v_j. A linear interpolation was performed to find the times t_j, t_{j+1} at which speeds v_j, v_{j+1} occur. This procedure was carried out throughout the observation time T. A Darrieus turbine rotates in the same direction, regardless of the direction of the incoming flow, so only the absolute value (i.e., speed). The symbols denoting absolute values will be omitted below. The probability of occurrence of a v value between v_j and v_{j+1} during time T is given by:

$$F(v_j \le v \le v_{j+1}) = \frac{\sum \Delta T_j}{T} \tag{18}$$

where $\Delta T_j = t_{j+1} - t_j$ and $\Sigma \Delta T_j$ is the sum of the time intervals when speeds between v_j and v_{j+1} occurred.

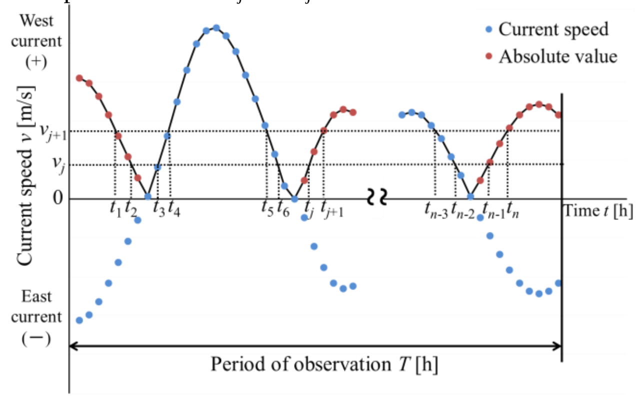

Fig. 5, Examples of tidal current speed.

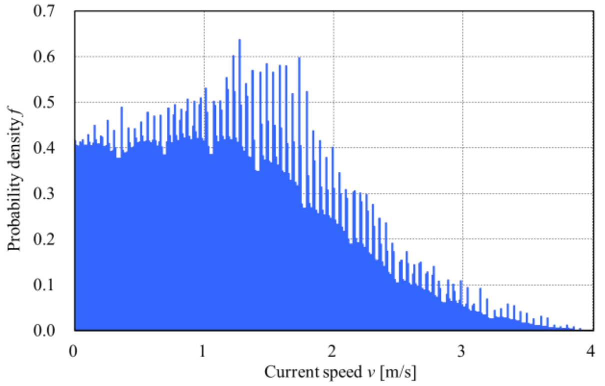

Fig. 6, Probability density function for current speed (2003).

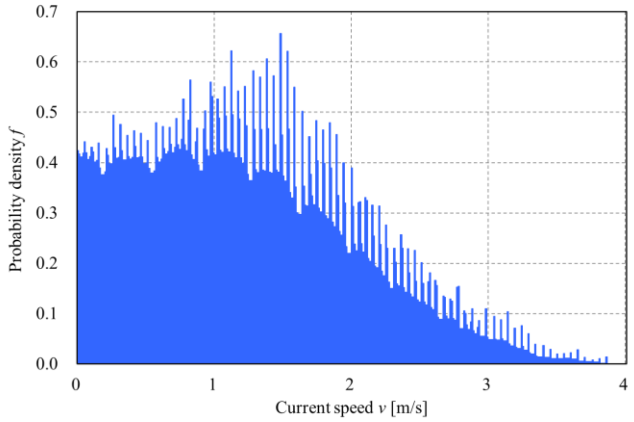

Fig. 7, Probability density function for current speed (2004).

The probability density function for the current speed is written as:

$$f(v) = \frac{F(v_j \le v \le v_{j+1})}{\Delta v} \tag{19}$$

where $0 \le v \le v_m$ and $\Delta v = v_{j+1} - v_j$. v_m is the maximum current speed during time T. Figures 6 and 7 show $f(v)$ for the years 2003 and 2004, respectively, where Δv was 0.01 m/s.

 ©2016 North Sea Conference & Journal

2.4. DFIG-BASED TIDAL CURRENT POWER GENERATION SYSTEM

Figure 8 shows a schematic illustration of the tidal current power generation system incorporating a DFIG. Here, P_{To} is

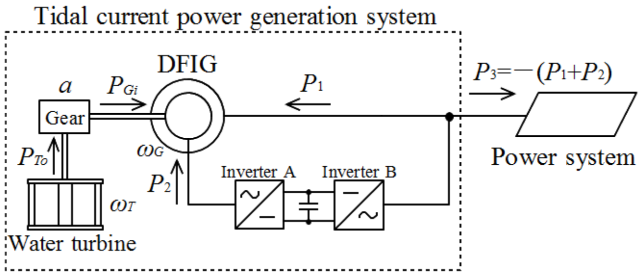

Fig. 8, Schematic illustration of tidal current power generation system.

the power output of the water turbine, ω_T is the angular speed of the water turbine, a is the gear ratio, P_{Gi} is the power supplied to the generator, ω_G is the angular speed of the generator, P_1 is the stator active power, and P_2 is the rotor active power. The power input to the generator is defined as positive for P_1 and P_2, while P_3 is defined as the power generated by the system, which consists of the DFIG and the inverter. Inverter B, which is attached to the rotor side, could also be used to compensate for reactive power, but in this study, the inputs and outputs were controlled to ensure it only supplied active power.

III. INVESTIGATION OF SPEED CONTROL MODEL

This section describes the construction of a speed control model capable of controlling the generator angular speed ω_G so that any desired water turbine output power P_{To} can be obtained for any current speed v.

3.1. WATER TURBINE OUTPUT POWER AND SLIP

The water turbine output power P_{To} at speed v is given by Eq. (20), and is the product of the water turbine input power P_{Ti} and the power coefficient C_P.

$$P_{To} = C_P P_{Ti} \tag{20}$$

The water turbine angular speed ω_T is given by Eq. (21), using the water turbine radius r and the tip speed ratio λ corresponding to the power coefficient C_P.

$$\omega_T = \frac{v\lambda}{r} \tag{21}$$

The generator angular speed ω_G is expressed using ω_T and the gear ratio a as:

$$\omega_G = a\omega_T \tag{22}$$

Using Eq. (22), the slip s can be written:

$$s = 1 - \frac{\omega_G}{\omega_s} = 1 - \frac{a\omega_T}{\omega_s} \tag{23}$$

where ω_s is the synchronous angular speed.

Using the water turbine output power P_{To} in Eq. (20) and the target slip s^* in Eq. (23) the stator current, rotor current and supply voltage for rotor can be calculated.

3.2. SUPPLY VOLTAGE FOR ROTOR

Using Eq. (24), the voltage equation for an induction generator can be expressed in rotating d-q coordinates [15]. Here, the q-axis is defined as lagging 90° behind the d-axis:

$$\begin{bmatrix} v_{ds} \\ v_{qs} \\ v_{dr} \\ v_{qr} \end{bmatrix} = \begin{bmatrix} r_1 + PL_{s1} & X_{s1} & PM & X_M \\ -X_{s1} & r_1 + PL_{s1} & -X_M & PM \\ PM & sX_M & r_2 + PL_{s2} & sX_{s2} \\ -sX_M & PM & -sX_{s2} & r_2 + PL_{s2} \end{bmatrix} \begin{bmatrix} i_{ds} \\ i_{qs} \\ i_{dr} \\ i_{qr} \end{bmatrix} \tag{24}$$

where v_{ds} and v_{qs} are the stator d and q axis voltages, i_{ds} and i_{qs} are the stator d and q axis currents, v_{dr} and v_{qr} are the rotor d and q axis voltages, i_{dr} and i_{qr} are the rotor d and q axis currents, r_1 and r_2 are the stator and rotor resistances, and L_{s1}, L_{s2} and M are the self-inductances of the stator and rotor, and the excitation inductance, respectively. X_{s1}, X_{s2} and X_M are the self-reactances of the stator and rotor, and the excitation reactance, respectively, P is d/dt, and s is slip. All the values for the rotor side in the equations were calculated using the values on the stator side.

Next, values of the stator phase voltages e_{a1}, e_{b1} and e_{c1} on the d-q axes are converted using:

$$\begin{bmatrix} v_{ds} \\ v_{qs} \end{bmatrix} = \sqrt{\frac{2}{3}} \begin{bmatrix} \cos\omega t & \cos(\omega t - 2\pi/3) & \cos(\omega t + 2\pi/3) \\ \sin\omega t & \sin(\omega t - 2\pi/3) & \sin(\omega t + 2\pi/3) \end{bmatrix} \begin{bmatrix} e_{a1} \\ e_{b1} \\ e_{c1} \end{bmatrix} \tag{25}$$

where ω is the frequency of the power source. If e_{a1}, e_{b1}, and e_{c1} are the rated voltages and are maintained, they are given by:

$$\left.\begin{aligned} e_{a1} &= \sqrt{2}E_s \sin\omega t \\ e_{b1} &= \sqrt{2}E_s \sin(\omega t - \frac{2}{3}\pi) \\ e_{c1} &= \sqrt{2}E_s \sin(\omega t + \frac{2}{3}\pi) \end{aligned}\right\} \tag{26}$$

where E_s is the root mean square value of the stator phase voltage.

When the stator voltages in Eq. (26) are substituted into the d-q axes conversion expression in Eq. (25), we obtain Eq. (27), providing the stator d and q axis voltages v_{ds}, and v_{qs}:

$$\left.\begin{aligned} v_{ds} &= 0 \\ v_{qs} &= \sqrt{3}E_s \end{aligned}\right\} \tag{27}$$

In order to reduce the required capacity of the rotor inverter, an excitation current is supplied from the stator. The target stator d-axis current is then given by:

$$i_{ds}^* = -\frac{\sqrt{3}E_s}{r_1^2 + X_{s1}^2} X_{s1} \tag{28}$$

If it is assumed that gear losses can be neglected with regard to the water turbine output power P_{To} and the generator input power P_{Gi}, using Fig. 8 we obtain:

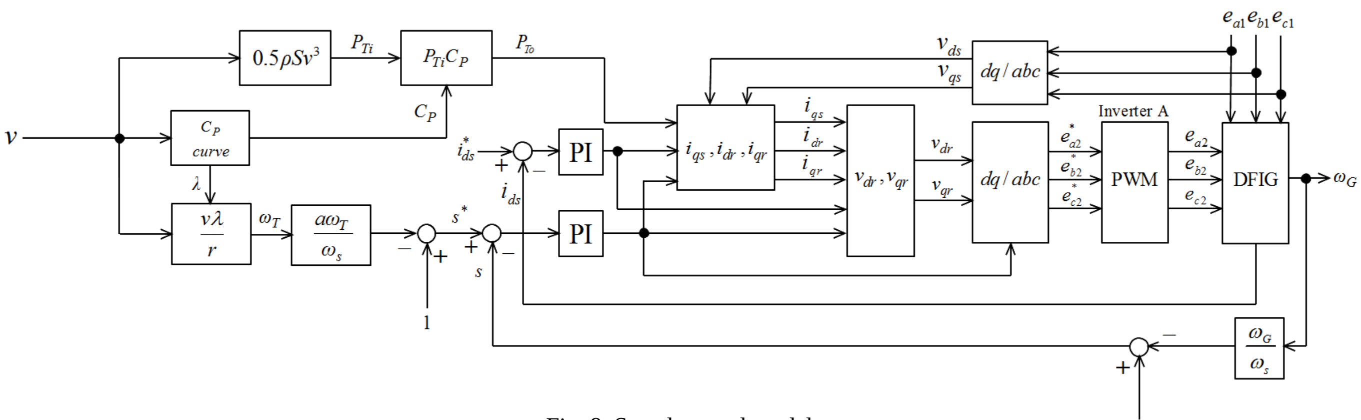

Fig. 9, Speed control model.

$$P_{To} = P_{Gi} = (1-s)X_M(i_{qs}i_{dr} - i_{ds}i_{qr}) \tag{29}$$

We find the stator and rotor currents i_{qs}, i_{dr}, i_{qr} from the target slip s^* in Eq. (23) and from the relations among the target stator d-axis current i_{ds}^* given by steady-state rows 1 and 2 in Eq. (24), and Eq. (28), the generator input power P_{Gi} in Eq. (29) and the water turbine output power P_{To}.

The d- and q-axes rotor voltages v_{dr} and v_{qr} are found using Eqs. (30) and (31), on the basis of rows 3 and 4 in Eq. (24).

$$v_{dr} = s^* X_M i_{qs} + r_2 i_{dr} + s^* X_{s2} i_{qr} \tag{30}$$

$$v_{qr} = -s^* X_M i_{ds}^* - s^* X_{s2} i_{dr} + r_2 i_{qr} \tag{31}$$

3.3. Equation of Motion

The generated torque T_e is obtained by dividing the generator input power P_{Gi} by the angular generator speed ω_G:

$$T_e = pM(i_{qs}i_{dr} - i_{ds}i_{qr}) \tag{32}$$

where p is the number of pole pairs of a DFIG.

The equation of motion is:

$$J\frac{d\omega_G}{dt} = T_T - T_e \tag{33}$$

where J is the total inertial moment of the turbine and the generator, and T_T is the turbine torque.

Figure 9 shows a schematic diagram of the complete speed control system model constructed in this study. As described above, the period of tidal fluctuations is long, so the compensation in this model is of the PI type.

IV. Investigation of Gear Ratio Maximizing Generated Energy

We now attempt to find a gear ratio and generator capacity that maximize the energy generated by the tidal current power generation system without overloading the generator during changes in the current speed while this system is operated under the above control schemes. Figure 10 shows the operating points of the MPPT control scheme and the constant turbine-output control scheme.

The MPPT system controls the system in order to maintain

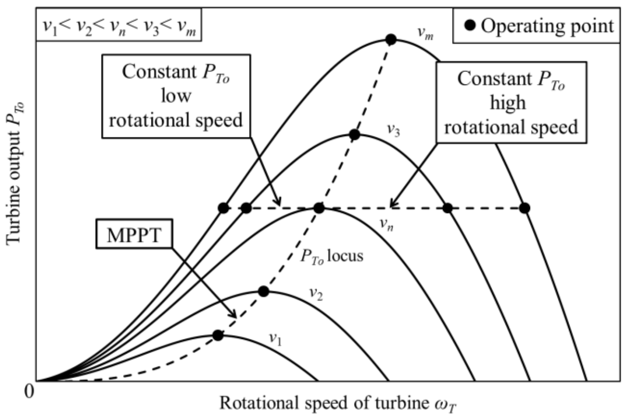

Fig. 10, Characteristics of turbine output.

the maximum possible water turbine power output up to the maximum current speed v_m, which gives the maximum annual energy production, as shown in Fig. 10. The constant turbine-output controller for the water turbine conducts MPPT at current speeds up to v (defined as the rated speed v_n) at which the stator current I_s or the rotor voltage E_r is at the rated value (1 pu), while at current speeds exceeding v_n, the operating point is controlled to hold the water turbine output constant. Constant turbine-output control can be performed in two ways: by maintaining the water turbine at a low speed with respect to v_n, the speed at which the water turbine output power would be maximized, or by maintaining it at a speed higher than v_n. If the turbine speed is kept low while the current speed exceeds v_n, there is a risk that I_s will exceed the rated value. However, if the turbine speed is kept high, there is a risk that E_r will exceed the rated value. Thus, when I_s or E_r exceed their rated values for any current speed below v_m, power generation is stopped, and that speed is subsequently designated as v_{max}, the maximum current speed at which power can be generated.

This will be described in detail below, but an iterative technique must be employed in order to identify the gear ratio a and the rated capacity of the generator S_B that provide the maximum generated energy W. In this process, S_B changes with a, but the generator constants given by the per-unit method will not change within the range of variation in this investigation, so this method was used for calculating the generator parameters. To calculate the generated energy W during the observation time T using the probability density function for current speeds $f(v)$, we use:

$$W(a,S_B)=S_B T\int_{v_0}^{v_{max}} P_3(v)\,f(v)\,dv \tag{34}$$

Here, v_0 is the cut-in current speed [m/s].

4.1. Maximum power point tracking control scheme

The values of a and S_B resulting in the maximum value for W in the MPPT scheme described in Eq. (34) are found by solving for $\partial W/\partial a = 0$, $\partial W/\partial S_B = 0$. However, there is a risk that the generator voltage or current could exceed their rated values at the identified a or S_B. The stator current I_s, rotor current I_r and rotor supply voltage E_r must be held within their rated values (within 1 pu). The conditions necessary in order to guarantee this are:

$$\left.\begin{aligned} h_1(a,S_B)&=I_s-1\le 0\\ h_2(a,S_B)&=I_r-1\le 0\\ h_3(a,S_B)&=E_r-1\le 0\end{aligned}\right\} \tag{35}$$

Identification of the gear ratio a and generator capacity S_B to maximize the generated energy W can be handled as an optimization problem using Eq. (34) as the objective function and Eq. (35) as an inequality constraint. The method of Lagrange multipliers can be used for optimization problems with inequality constraints [16]. The slack variable l is introduced into the inequality constraint to transform it into the equality constraint:

$$\left.\begin{aligned} h_i+l_i&=0\\ l_i&\ge 0\end{aligned}\right\}(i\text{=1~3}) \tag{36}$$

Next, using the penalty constant γ and the Lagrange multiplier ψ from the objective function in Eq. (34) and the equality constraint in Eq. (36), we obtain the modified penalty function:

$$Q(a,S_B,\boldsymbol{L},\boldsymbol{\psi})=-W+\sum_{i=1}^{3}\psi_i(h_i+l_i)+\frac{1}{\gamma}\sum_{i=1}^{3}(h_i+l_i)^2 \tag{37}$$

in which $\boldsymbol{L}=[l_1, l_2, l_3]^T$, $\boldsymbol{\psi}=[\psi_1, \psi_2, \psi_3]^T$ and γ is a constant ($\gamma>0$). The negative sign is placed on W in order to change this from a maximization to a minimization problem.

If we follow the calculation method for Lagrange multipliers, γ is fixed at a low constant value while $\boldsymbol{\psi}$ is set at an arbitrary value, and the a, S_B and $\boldsymbol{L}$ values yielding the minimum Q are found.

We begin by minimizing $\boldsymbol{L}$. Whenever l_i satisfies $\partial Q/\partial l_i = 0$, the non-positive elements of l_i (i.e. $l_i \le 0$) are set to 0. Positive elements of l_i are retained as they are and assumed to minimize Q. We then obtain:

$$l_i=-\left(h_i+\frac{\gamma\psi_i}{2}\right) \tag{38}$$

Substituting Eq. (38) into Eq. (37), Q becomes a function of only a, S_B, $\boldsymbol{\psi}$, and γ, and this simplifies to:

$$Q(a,S_B,\boldsymbol{\psi})=-W+\frac{1}{\gamma}\sum_{i\notin I}\left(h_i+\frac{\gamma\psi_i}{2}\right)^2-\frac{\gamma}{4}\sum_{i=1}^{3}(\psi_i)^2 \tag{39}$$

where $I = \{i \mid l_i>0\}$. For a and S_B to minimize Q, the following equations must be satisfied.

$$\frac{\partial Q}{\partial a}=-\frac{\partial W}{\partial a}+\frac{2}{\gamma}\sum_{i\notin I}\left(h_i+\frac{\gamma\psi_i}{2}\right)\frac{\partial h_i}{\partial a}=0 \tag{40}$$

$$\frac{\partial Q}{\partial S_B}=-\frac{\partial W}{\partial S_B}+\frac{2}{\gamma}\sum_{i\notin I}\left(h_i+\frac{\gamma\psi_i}{2}\right)\frac{\partial h_i}{\partial S_B}=0 \tag{41}$$

Solving Eqs.(40) and (41) allows us to find the values for the gear ratio a and the generator capacity S_B that minimize Q. However, since these are coupled nonlinear equations, initial values are estimated for a and S_B, and iterative calculations are performed until the following condition is satisfied:

$$\sum_{i=1}^{3}(h_i+l_i)^2+\left(\frac{\partial Q}{\partial a}\right)^2+\left(\frac{\partial Q}{\partial S_B}\right)^2\le\zeta \tag{42}$$

where ζ is a very small positive constant. If Eq. (42) is never satisfied, $\boldsymbol{\psi}$ is revised in accordance with the rules given in Eq. (43) and the calculations are resumed using Eq. (37).

$$\psi_i=\begin{cases}0 & ,i\in I\\ \psi_i+\dfrac{2h_i}{\gamma} & ,i\notin I\end{cases} \tag{43}$$

4.2. Constant turbine-output control scheme

Just as in MPPT, under constant turbine-output control, the a and S_B values that maximize W are found using Eq. (34) by solving $\partial W/\partial a$=0 and $\partial W/\partial S_B$=0. However, the control scheme changes under constant turbine-output control when the current speed surpasses the rated speed v_n, as shown in Fig. 10, so there is a discontinuity in the solution surface for W. Therefore, a genetic algorithm is employed to solve the maximization problem where the slope is discontinuous. Figure 11 shows the calculation process using the genetic algorithm in this study.

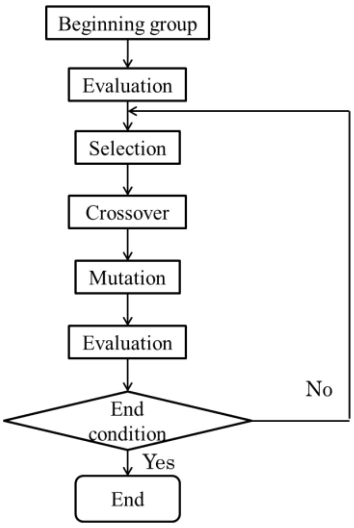

Fig. 11, Flow diagram for genetic algorithm.

4.3. Results of Calculations

Table 3 shows the parameters for the water turbine and DFIG obtained in the calculations to identify the gear ratio and generator capacity. The water turbine described in Table 3 is the model which the authors developed for use in an in-situ experiment, and is the largest we have ever tested [2]. Tables 4 and 5 present the results for the gear ratio and the generator capacity calculated for MPPT control and constant turbine-output control on the basis of the current speed data from 2003 and 2004. The annual capacity factor C_F shown in Tables 4 and 5 is defined as the ratio of the generated energy to that which would have been generated if the generator had operated for a full year at its full capacity. The energy conversion efficiency η_E is defined as the ratio of the annual generated energy to the annual tidal current energy passing through the swept area of the turbine S.

TABLE 3, Specifications and constants for tidal current power generation

Water turbine	
Number of blades n	3
Height h [m]	1.6
Diameter d [m]	1.6
Chord length c [m]	0.3
Solidity σ	0.179
DFIG	
Rated voltage [V]	200
Number of pole pairs p	3
Frequency f [Hz]	50
Stator resistance r_1 [pu]	0.054
Rotor resistance r_2 [pu]	0.078
Stator leakage inductance L_{l1} [pu]	0.100
Rotor leakage inductance L_{l2} [pu]	0.100
Excitation inductance M [pu]	1.754

TABLE 4, Results for gear ratio and rated capacity of generator (2003)

	MPPT	Constant P_{To} High rotational speed	Constant P_{To} Low rotational speed
Gear ratio a	25.24	25.50	28.59
Rated capacity of generator S_B [kVA]	9.93	9.63	9.28
Rated capacity of inverter S_{BI} [kVA]	9.01	8.73	6.29
Annual generated energy W [MWh]	10.54	10.55	10.58
Energy conversion efficiency η_E [%]	21.15	21.17	21.24
Annual capacity factor C_F [%]	14.38	14.85	15.45
Cut-in current speed v_0 [m/s]	0.81	0.80	0.79
Generation maximum speed v_{max} [m/s]	3.90	3.86	3.90

TABLE 5, Results for gear ratio and rated capacity of generator (2004)

	MPPT	Constant P_{To} High rotational speed	Constant P_{To} Low rotational speed
Gear ratio a	25.50	25.77	29.10
Rated capacity of generator S_B [kVA]	9.63	9.33	8.89
Rated capacity of inverter S_{BI} [kVA]	8.73	8.47	5.97
Annual generated energy W [MWh]	10.53	10.53	10.57
Energy conversion efficiency η_E [%]	21.19	21.20	21.28
Annual capacity factor C_F [%]	14.77	15.25	16.08
Cut-in current speed v_0 [m/s]	0.80	0.79	0.78
Generation maximum speed v_{max} [m/s]	3.86	3.82	3.86

Tables 4 and 5 provide a comparison between constant turbine-output control and MPPT control on the basis of the 2003 and 2004 data; constant turbine-output control required a higher gear ratio but had a lower generator capacity. It also yielded a higher annual generated energy, annual capacity factor, and energy conversion efficiency.

The C_F under constant turbine-output control was 1.07% higher than that under MPPT control with the 2003 data, and 1.31% higher with the 2004 data.

V. Response of Speed Control Model

The response of the speed control model was examined using the values for a and S_B in the constant turbine-output control scheme for maximizing W in each year for the control schemes shown in Tables 4 and 5. The results are given in Fig. 9. The inputs were the estimated tidal current speed data for Akashi Strait published by the Japan Coast Guard Hydrographic and Oceanographic Department from January to December of 2003 and 2004 [14]. The highest current speed for each year (occurring on November 25, 2003 and June 3, 2004) was selected from the two data sets and used as v_m. These sets provided discrete values at 10-minute intervals, and these values were linearly interpolated.

Figure 12 shows a plot of v for 2003. The simulation results are provided in Figs. 13-18. The simulations were performed using MATLAB/Simulink in this study.

Figures 13 and 14 show the target values and the controlled values for the slip s and d-axis stator current i_{ds}. Good agreement is seen for both parameters, even for t = 2.7 to t = 4.5 h, when the turbine was under constant-output control,

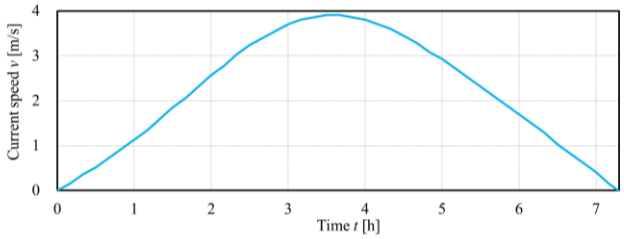

Fig. 12, Temporal change in current speed (2003).

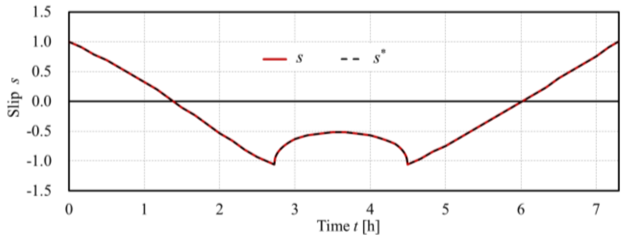

Fig. 13, Temporal change in slip (2003).

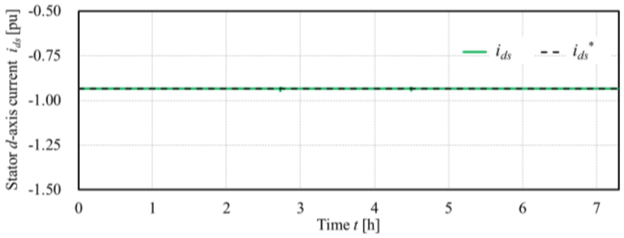

Fig. 14, Temporal change in stator d-axis current (2003).

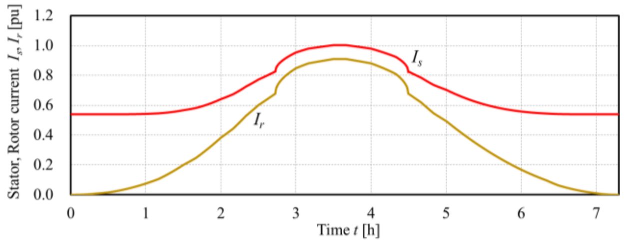

Fig. 15, Temporal change in stator and rotor currents (2003).

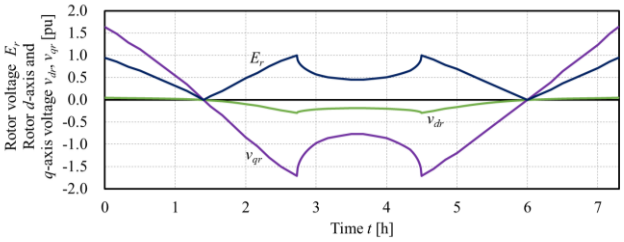

Fig. 16, Temporal change in rotor voltage, rotor d-axis voltage and rotor q-axis voltage (2003).

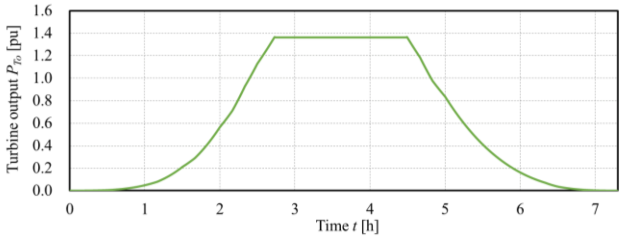

Fig. 17, Temporal change in turbine output (2003).

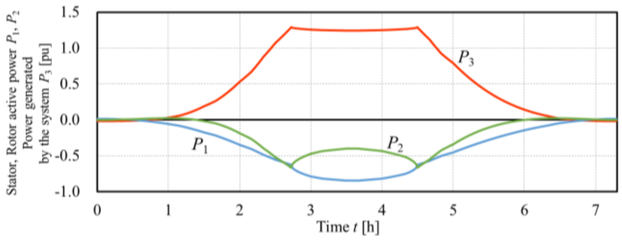

Fig.18, Temporal change in stator and rotor active power, power generated by the system (2003).

indicating a high degree of control. Figure 15 shows the stator and rotor currents I_s and I_r. As described above, I_s must supply excitation current from its d-axis current. Therefore, a current of 0.54 pu must always be flowing, and the stator current was held between 0.54 and 1.00 pu depending on the tidal current speed. The corresponding I_r values were between 0.00 and 0.91 pu. Figure 16 shows the d- and q-axes rotor voltages v_{dr} and v_{qr} and the rotor supply voltage E_r. v_{dr} varied between 0.05 and –0.30 pu and v_{qr} varied between 1.64 and –1.71 pu. E_r varied with current speed from 0.00 to 1.00 pu. Figure 17 shows P_{To} for the water turbine. P_{To} increased with current speed, and during constant turbine-output control, remained at a steady value of 1.37 pu. Figure 18 presents the stator and rotor active powers P_1 and P_2 and the power generated by the system P_3. P_1 was negative for nearly all current speeds, as it was supplying power to the power grid. P_2 was negative from t = 1.4 to 6.0 h; during this period, it was supplying power to the power grid through the inverter. P_3 increased with increasing current speed, reaching a maximum of 1.29 pu, and was approximately constant during constant turbine-output control. The value of P_3 with respect to P_{To}, i.e., the system efficiency η_s, for the current speed at which P_3 reached a maximum, was approximately 95%.

Turning to the 2004 data, Fig. 19 shows the temporal variation of v, and Figs. 20-25 show the simulation results.

Figures 20 and 21 show the slip s and the d-axis stator current i_{ds}, which both follow the target values well, even for t = 2.7 to 4.6 h during constant turbine-output control, indicating a high degree of control. Figure 22 presents the stator and rotor currents I_s and I_r. I_s varied between 0.54 and 1.00 pu depending on the current speed. Similarly, I_r varied from 0.00 pu to 0.91 pu. Figure 23 shows the d- and q-axes rotor voltages v_{dr} and v_{qr} and the rotor supply voltage E_r. As the current speed fluctuated, v_{dr} varied between 0.05 and –0.29 pu, v_{qr} varied between 1.64 and –1.71 pu, and E_r varied from 0.00 to 1.00 pu. Figure 24 shows the water turbine power output P_{To}; this parameter increased with current speed but was held constant at 1.35 pu during constant turbine-output control. Figure 25 presents the stator and rotor active powers P_1 and P_2 and the power generated by the system P_3. P_1 was negative for nearly all current speeds, as it was supplying power to the power grid. P_2 was negative from $t = 1.4$ to 6.1 h; during this period, it was supplying power to the power grid through the inverter. P_3 increased with increasing current speed, reaching a maximum of 1.28 pu, and was approximately constant during constant turbine-output control. The value of P_3 with respect to P_{To} system efficiency η_s, was about 95% for the current speed at which P_3 reached a maximum.

In closing, the reason that P_3 exceeded the rated capacity of the generator using the inputs from 2003 and 2004 was that the generated power came not only from the stator, but also from the rotor via the inverter. This probably increased η_s. However, this investigation did not account for losses at the inverter and elsewhere, so η_s for an actual system would be expected to be lower.

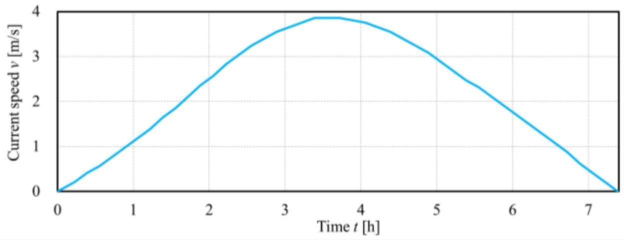

Fig. 19, Temporal change in current speed (2004).

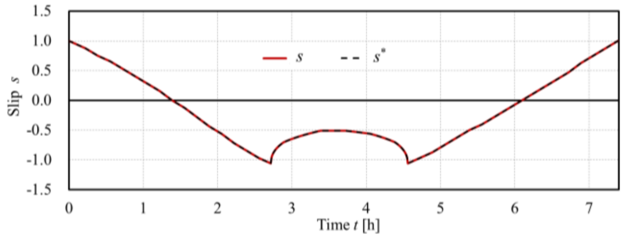

Fig. 20, Temporal change in slip (2004).

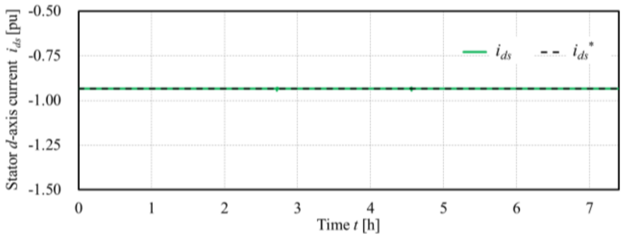

Fig. 21, Temporal change in stator d-axis current (2004).

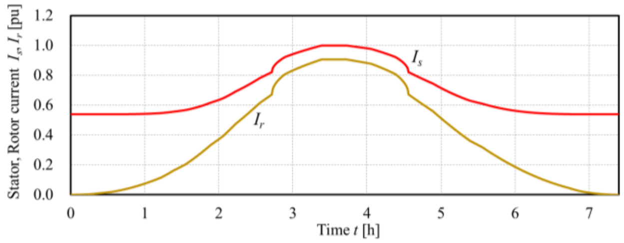

Fig. 22, Temporal change in stator and rotor currents (2004).

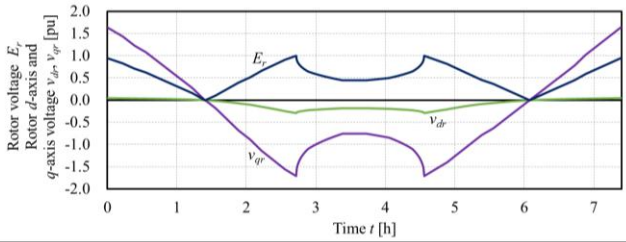

Fig. 23, Temporal change in rotor voltage, rotor d-axis voltage and rotor q-axis voltage (2004).

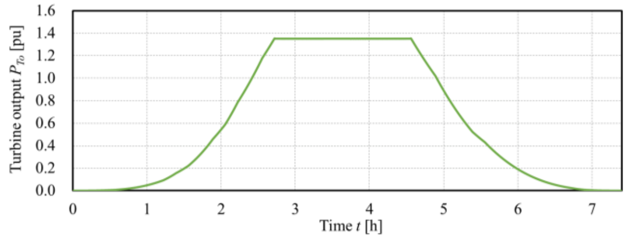

Fig. 24, Temporal change in turbine output (2004).

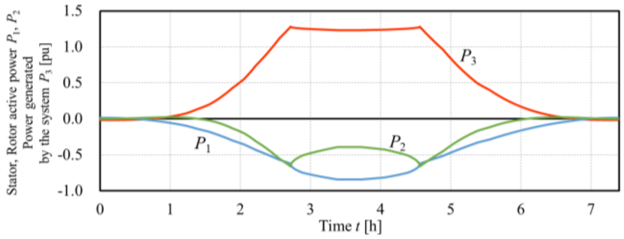

Fig. 25, Temporal change in stator and rotor active power, power generated by the system (2004).

VI. Conclusion

This study presented an investigation of a procedure for determining the gear ratio and the generator capacity for maximizing the generated energy without overloading a doubly-fed induction generator in a tidal current power generation system incorporating constant turbine-output control of the generator. A model was constructed for controlling the generator speed, while maintaining the water turbine at any desired speed during changes in current speed. The response of this model was examined with actual tidal current speed data. The following results were obtained in this study.

(1) The gear ratio and generator capacity resulting in the highest generated energy were calculated when a tidal current power generation system is operated under constant turbine-output control. This investigation indicated that constant turbine-output control results in higher electrical energy generation, allowing a generator with lower capacity, and a higher annual capacity factor of 16%, than a system operated under maximum power-point tracking.

(2) The response of a system operated under constant turbine-output control, with a gear ratio and generator capacity selected to generate the highest energy, was examined using actual varying tidal current speeds in a model of this controller. The target values for the slip and stator d-axis current were

followed well. The constant turbine-output control scheme was thus found to provide good control.

REFERENCES

[1] H. Kondo, H. Uehara, S. Kiho, T. Miyazaki, and K. Yano, *A Utilization Technology from Ocean Energy*, Tokyo: Morikita Publishing, 1996.

[2] S. Kihoh, M. Shiono, and K. Suzuki, "Power Generation from Tidal Currents," *International Symposium on Ocean Energy Development*, 1993, pp. 89-96.

[3] M. Shiono, K. Suzuki, and S. Kiho, "Experiments on the Characteristics of Darrieus Turbine for the Tidal Power Generation," *Proceedings of the Ninth International Offshore and Polar Engineering Conf.*, 1999, pp. 123-128.

[4] T. Ackermann, *Wind Power in Power Systems*, England: John Wiley & Sons, Ltd, 2005.

[5] R. Datta, and V. T. Ranganathan, "Variable-Speed Wind Power Generation Using Doubly Fed Wound Rotor Induction Machine - A Comparison With Alternative Schemes," *IEEE Trans. Energy Convers*., vol. 17, no. 3, pp. 414-421, Sep. 2002.

[6] M. Y. Uctug, I. Eskandarzadeh, and H. Ince, "Modeling and output power optimisation of a wind turbine driven double output induction generator," *IEE Proc.-Electr. Power Appl.*, vol. 141, no. 2, 1994, pp. 33-38.

[7] R. Datta, and V. T. Ranganathan, "Decoupled Control of Active and Reactive Power for a Grid-connected Doubly-fed Wound Rotor Induction Machine without Position Sensors," *Thirty-Fourth IAS Annual Meeting. Conference Record of the 1999 IEEE*, vol. 4, pp.2623-2630.

[8] A. Jain, and B. J. Reddy, "Control of Doubly Fed Induction Generator Connected to Variable Speed Wind Turbine," *2015 International Conference on Technological Advancements in Power and Energy*, pp. 500-505.

[9] A. Basak, K. Mukherjee, and P. Syam, "Speed Control of A Grid Connected Doubly-Fed Induction Generator System for Maximum Power Point Tracking with Improved Input Power Factor Employing Matrix Converter as a Slip Power Exchanger," *2016 IEEE First International Conference on Control, Measurement and Instrumentation*, pp. 42-47.

[10] K. Tsuji, K. Naoi, M. Shiono, and K. Suzuki, "Study on the Gear Ratio for a Tidal Current Power Generation System Using the MPPT Control Method," *Proceedings of the Twenty-fourth International Ocean and Polar Engineering Conf*., 2014, pp.568-574.

[11] Minister of Economy, Trade and Industry. Agency for Natural Resources and Energy. (2010) *Japan's energy 2010*. Available: http://www.enecho.meti.go.jp/about/pamphlet/energy2010html/policy/

[12] Ira H. Abbott, Albert E. Von Doenhoff, *Theory of wing sections*, New York: Dover Publications, Inc., 1959, p.339.

[13] K. Yoshimura, and F. Takayama. *The spline function by personal computer*, Tokyo: Tokyo Denki University Press, 1988.

[14] Japan Coast Guard, Hydrographic and Oceanographic Department. (2003, 2004) *Tide, tidal current information*. Available: http://www6.kaiho.mlit.go.jp/osakawan/index.htm

[15] D. W. Novotny, and T. A. Lipo, *Vector Control and Dynamics of AC Drives*, England: Oxford University Press, 1996.

[16] K. Shimizu, *System Optimization Theory*, Tokyo: CORONA Publishing Co., Ltd, 1976.

Journal of Energy Challenges and Mechanics
http://www.nscj.co.uk/JECM/
ISSN 2056-9386
Volume 3 (2016) issue 3, article 7

The National Drought Policy in Mexico

墨西哥國家乾旱政策

Felipe I. Arreguín Cortés[1*], Mario López Pérez[1], David Korenfeld Federman[2], David Ortega-Gaucin[1]

[1]*Mexican Institute of Water Technology, Paseo Cuauhnáhuac 8532, Col. Progreso, 62550, Jiutepec, Morelos, México*
[2]*Independent consultor*

felipe_arreguin@tlaloc.imta.mx

Accepted for publication on 11th August 2016

Abstract -. **Traditionally, drought effects in Mexico have been attended through governmental reactive efforts directed to provide water and food, to assure health protection, and to restore economic impact once the phenomena occurred. The Mexican Government through National Water Commission (CONAGUA, for its acronym in Spanish), interested in changing the paradigm for preventive actions to cope with droughts in Mexico in the past, decided to launch in 2013 the National Program Against Drought (PRONACOSE, for its acronym in Spanish) and created the Intersecretarial Commission on Droughts and Floods (CIASI, for its acronym in Spanish) to take charge of coordinating, implementing and following-up of the PRONACOSE. This program has its main focus on reducing vulnerability through the implementation of planned preventive actions under a comprehensive and participative approach. As a key part of the program, Programmes of Preventive and Mitigation Drought Measures (PMPMS, for its acronym in Spanish) for each one of the 26 river basin councils established in the country and for the principal cities of Mexico were developed. These programmes include the measures that can be implemented within the river basin councils and the cities to cope with drought in three ways: before the phenomenon occurs (strategic measures), when it is starting (tactical measures) or when it is already happening (emergency measures). Also, since 2014, the National Meteorological Service (SMN, for its acronym in Spanish) releases timely alerts and monitors the evolution of the drought including affected areas and level of severity of the phenomenon at a basin, state and municipality level. It is noteworthy that in all these activities the Mexican Institute of Water Technology (IMTA, for its acronym in Spanish) has played an important role, as this institute has provided the necessary technical support for the designing and implementation of the PRONACOSE. It is concluded that drought risk cannot be fully eliminated, nevertheless, the actions that are implemented as part of this program are useful to mitigate its effects.**

Keywords – **river basin council, drought, planning, prevention, vulnerability.**

I. INTRODUCTION

Drought is one of the most complex natural phenomena which affects a lot of people in the world [1]. Droughts in recent years have affected various socioeconomic sectors in Mexico, but especially the agricultural and livestock sectors as well as rural populations, leading to severe imbalances in the regional and national economies [2].

However, despite the frequency and recurrent droughts in Mexico, historically, attention to the effects of this phenomenon has been based on a reactive approach, where the primary importance has been the attention of crisis and not the risk management; in other words, in the last few decades have been implemented measures and response actions "emerging" only after is known each of the ravages caused by drought, without the time required to plan and properly assess the options and resources available to deal with the phenomenon [3].

In this context, the Mexican Government through the National Water Commission (CONAGUA), worried for the poor or rather the absence of preventive actions to face droughts in Mexico in the past, developed a comprehensive but practical structure of baseline measures, which included the necessary actions that would really help to minimize drought impacts, better than the costly traditional governments responses.

Due to the severity of last 2011-2012 drought, CONAGUA concluded by the end of 2012 this initiative in the form of Guidelines which would give to the 26 river basin councils, independent from CONAGUA, a direction on what, who, when, where and how, related to measures against possible next droughts. Such guidelines were officially issued on 22 November 2012.

©2016 North Sea

The Mexican Federal authorities decided to give support to this initiative with the development of the National Program Against Drought (PRONACOSE), which ensures the framework for a comprehensive and participative implementation. The preparation of this Program was initiated by December 2012 under CONAGUA's leadership. By the time of the implementation kickoff of the Program, CONAGUA was invited to attend to Geneva, Switzerland, on March 13, 2013 for the High-level Meeting on National Drought Policy (HMNDP) to present how Mexico plans to face the drought phenomena. It is worth noticing that Mexico's National Drought Program meets several of the recommendations referred to during this important event.

Among its goals, the PRONACOSE aims to share the concepts and principles behind it as well as the implementation experiences to keep it on a permanent and dynamic improvement.

II. Background

Mexico has an area of 1,964,375 km² and 66% of its territory is classified as desert or semi-desert. It has a population of 120 million people and a large scattering of populations under 2500 inhabitants, which increases their vulnerability to drought.

The parallels 14°32'27" and 32°43'06" N limit southern and northern extremes of Mexico which also contain the greatest deserts of the world (Fig. 1). Mexico has a high recurrence of droughts and its history reveals some periods of water and food scarcity that have caused migrations like those of the Mayan and Teotihuacan civilizations [4]. In recent times, drought events have caused major impacts in hindering economic activities and sometimes affect the commitments established in the 1944 Water Treaty between Mexico and the United States.

With respect to the attention of drought (and of other natural phenomena) Mexico has "a wide gap between the total disbursement in reconstruction against the investment in prevention; and not investing in prevention lead to excessive economic and social costs which also compromise the sustainable development of the country" [5].

Traditionally, Mexico has acted with emergency assistance programs once the drought occurs to assure water and food supply, to keep proper health conditions, to restore affected economy (through financing and subsidies), and to promote projects or infrastructure for relief.

Recent experience with the 2011-2012 drought, the most severe event of scarcity since 1941 in the North and Central Mexico affected (at different stages and levels) around 70% of the territory and has represented up to payments of almost US $6.5 million out of nearly US $47.5 million authorized from the Natural Disasters Fund (FONDEN) towards the alleviation in ten states.

There is a strong urgency to generate a radical change of strategy in the Mexican Government as well as in the society towards a stronger participation, clear definition of public frameworks for planning and investment, and real operational local drought preventive plans.

III. Discussion

3.1. Towards a comprehensive drought policy in Mexico

In December 2013, CONAGUA began to design and implement the National Program Against Drought, PRONACOSE, to face the drought with a comprehensive and participative approach. The goal is to identify all kind of actions which will allow timely, coordinated and efficient decisions for both drought mitigation and prevention, considering regional features and agreeing such actions with local authorities and water stakeholders.

PRONACOSE, was launched by the Mexican President in January 10, 2013 and within the CONAGUA on February 2013. The highlight of this initiative is that the 32 States and the Local Governments have a key role of the efforts, as well as all the water users through the 26 river basin councils which cover all the Mexican territory (Fig. 2).

PRONACOSE has a comprehensive and participative approach for the period 2013–2018 in several ways:

(a) It includes both: prevention and mitigation through respectively the estimation of needed resources, the definition of actions and the construction of a structure for the organization of stakeholders; and the reduction of impacts on people, goods, infrastructure, activities, as well as on the environment.

(b) It enhances: forecasting, early warning and data dissemination, which includes both: (i) the periodic collection and analysis of hydrometric and climatic data, and information of reservoirs and that of drought location or its levels or degrees of intensity; and (ii) the spreading of drought information so to guide the implementation of actions.

(c) It promotes: coordination of governments from the federal, state and municipal levels (for joint programs and resources) and water users involvement. The later includes training for the understanding the monitoring information and the options for user cooperation in water demand reduction actions and an efficient water use.

(d) It supports: a drought plan for each of the 26 river basin councils and drought plans for major water users. The first implies that authorities and users within their respective river basin council design and later implement their plan based on local features. The plans for major water users look for specific actions for them (major water utilities, irrigation districts or industrial facilities).

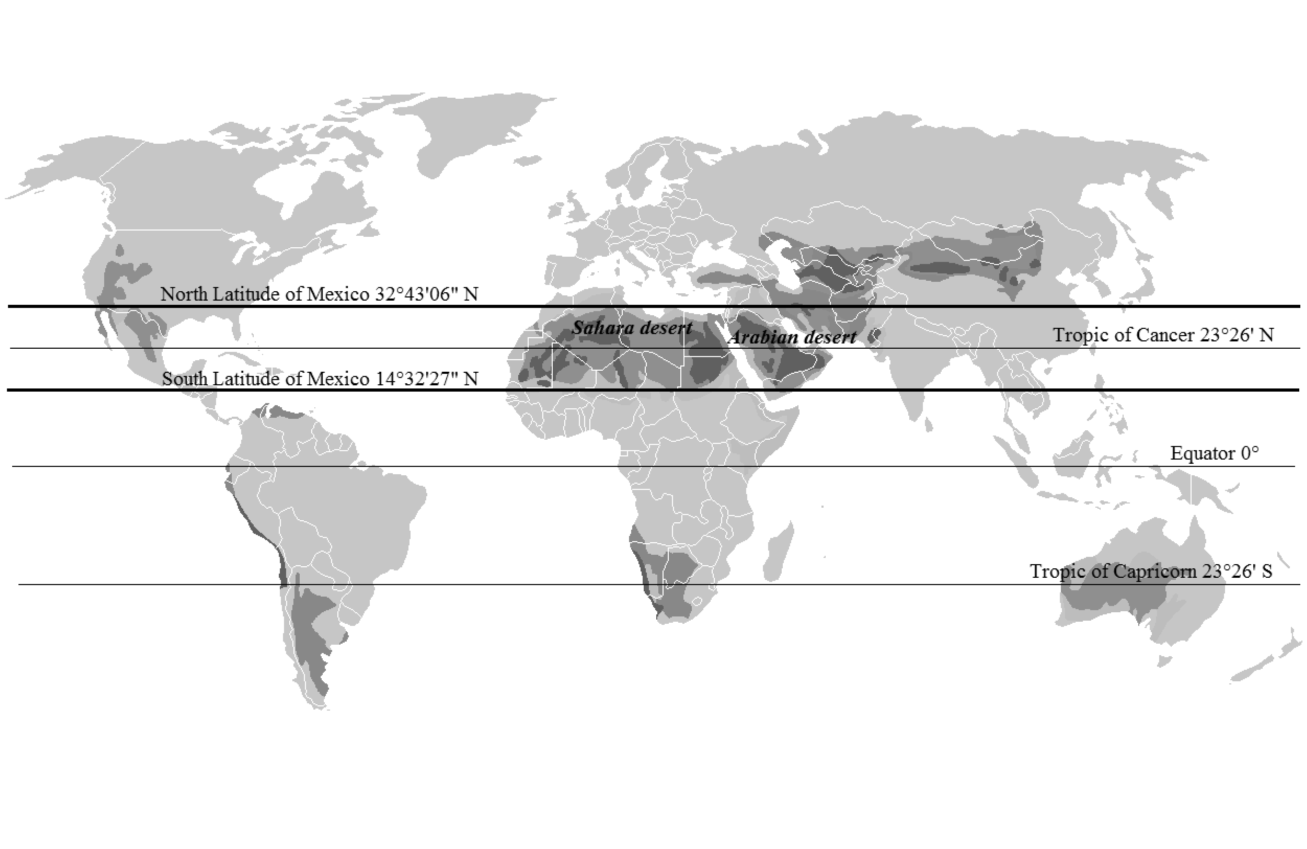

Fig.1, Location of Mexico regarding the greatest deserts of the world.

(e) The local implementation also implies that water users and authorities in the river basin council will define triggers to implement agreed actions based on official drought evolution information. Also they should agree on a range of voluntary. Measures which are expected to bring major water economies as well as mandatory measures.

A key principle is the development of such plans implies increasing complexity and improvement with time (a dynamic planning) but it is expected that an increasing involvement of stakeholders will come with the time of implementation as well as with evaluation and feedback (Fig. 3).

PRONACOSE will need the conjunction of existing federal programs and eventually their alignment with the basin plans. To reach this the Program considers an Interagency Commission and an Expert Committee. Both will review, inform, enrich and support the program, the implementation of the plan and the needed drought research. The Interagency Commission is composed by a total of thirteen Federal Agencies: CONAGUA, Interior, Environment, Agriculture and Rural Development, Economy, Energy, Health, National Defense, Marine, Education, Social Development, Land Use and Tourism. The Expert Committee considers researchers as well as high profile professionals from different parts of the country.

3.2. BASIS

CONAGUA started in 2009 the development of guidelines to deal with drought based on the California State's guidebook for urban zones [6] and other drought plans including a collection of experiences from many cities of the world. CONAGUA issued by 2012 the final document [7] based on Mexico's National Water Law.

The guidelines to deal with drought indicate: (i) how CONAGUA will announce the beginning and the ending of a Drought (at the severe stage), and (ii) recommendations on which are the desired characteristics for the actions that should be developed and adopted by the 26 river basin councils and by the major water users so that their territories could effectively face a drought, as well as evaluate their performance after the end of the event.

The document considers facing all stages or levels of a drought through actions before, during and after the occurrence. Before the drought level refers to the design of actions, quantification of necessary resources, and planning. During the phenomena level is related with the harmonic implementation of early planned actions. And after the occurrence level considers as necessary the evaluation, recovery of resources and improvements derived from learning.

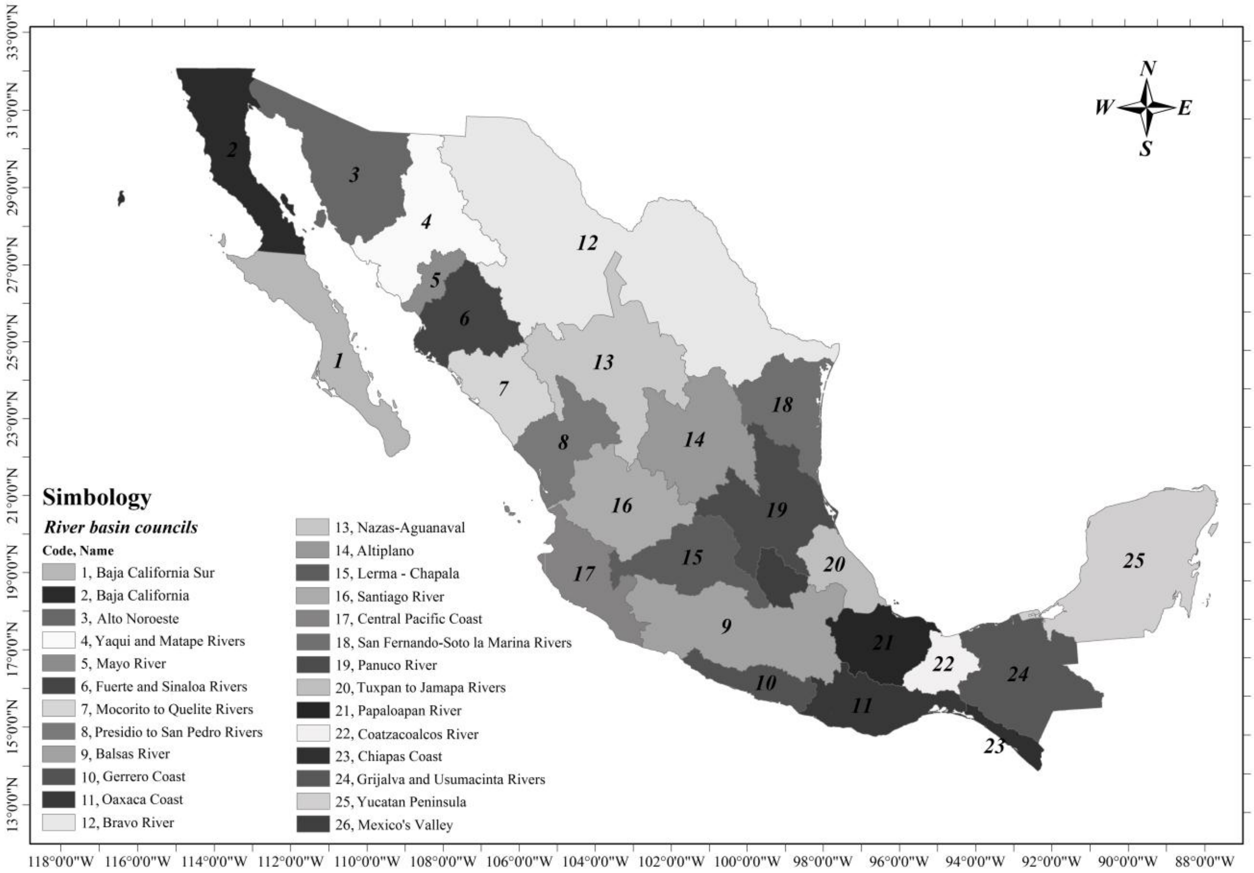

Fig. 2, Map of the 26 river basin councils covering the country in Mexico.

Although CONAGUA is interested in determining and announcing severe droughts to assure water supply to all the population, continuous monitoring and timely communication to society since first stages of droughts is part of the strategy, so that river basin councils could initiate their actions as agreed (Fig. 4). Information of stage and evolution of drought indexes for each river basin council is available at the official website of the National Meteorological Service (SMN) (smn.conagua.gob.mx).

The legal principles underlying the guidelines are derived from the National Water Law [8]. According to this Law, jurisdiction is given to the CONAGUA to regulate the exploitation and use of national water, as well as to control and to preserve water quantity and quality. Related to extreme weather events (such as droughts) that threaten people, productive areas or facilities, CONAGUA is responsible for issuing general regulations and supporting federal plans and programs directed to prevent and attend them as well as to take the necessary measures, usually transitory, to ensure domestic and public-urban supply. Besides, CONAGUA may support the organization and participation of water users, with the collaboration of state and local governments to improve water management to decide and to make commitments.

3.3. Steps and goals

During 2013 efforts were directed essentially for the development of the 26 river basin councils plans for droughts. Such plans define the basin drought features, vulnerability, triggers, actions and how they would be implemented and evaluated with the river basin council's participation and CONAGUA guidance. Later in the period 2014– 2018 the implementation of major actions supported by federal, state or local resources, or by funding from private sector or from international institutions will take place to improve the plans.

3.4. Components

There are two basic elements (Fig. 5) that comprise the National Program Against Drought: Prevention (monitoring-awareness, and basin plans and by major water user, evaluation and research), and Mitigation or Reactive Attention (action during and after the drought event).

The principles under the program have been planned and executed, not necessarily in order of importance, include:

(a) developing local capacity inside and outside CONAGUA to ensure the permanence of PRONACOSE past six years;

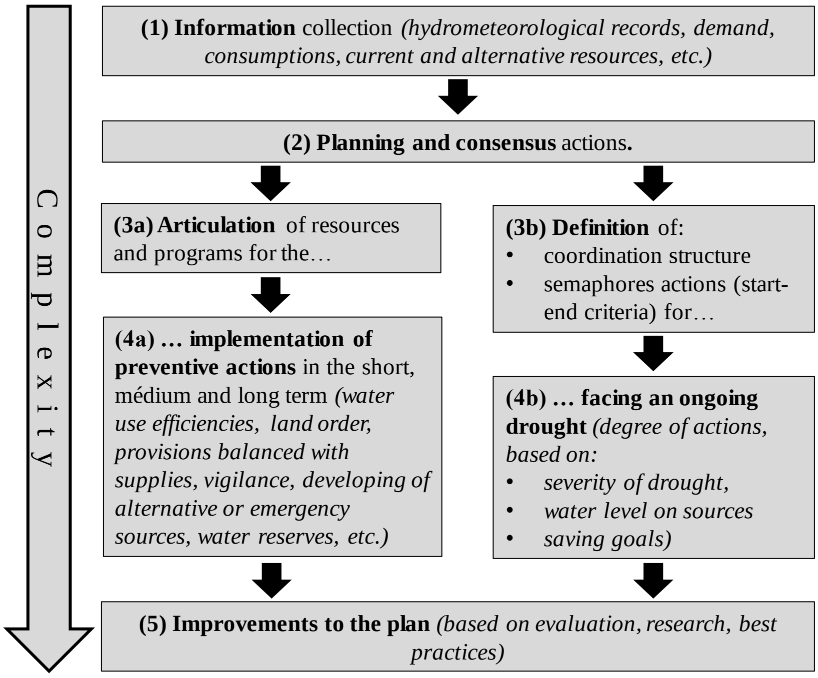

Fig. 3, Increasing complexity and involvement of stakeholders with time during the development of river basin council plans for drought.

(b) initiate an aggressive training program on basic concepts of drought and successful stories seeking to have the largest number of national and international experts on this issue both in the monitoring and evaluation;

(c) raising awareness on local water stakeholders initially through information occurrence and vulnerability to drought at the basin level (later at relevant water users in terms of use of water) and allow a first program of *ad hoc* preventive and mitigation measures at will and implementation possibilities for later evaluation, adjustment and improvement on the basis of the experience;

(d) coordinate and direct the programs of federal institutions supported by an interagency committee and working groups founded in law whose mission will be to guide and assess the PRONACOSE and fund the actions proposed by local stake- holders at the basin level;

(e) include the participation of experts and researchers to strengthen and link the solutions to the needs identified during the development of the programs of measures as well as to the general PRONACOSE implementation;

(f) ongoing communication and outreach program that emphasizes the concepts of occurrence, vulnerability, participation and prevention as well as understanding the evolution of drought; and

(g) an assessment of PRONACOSE indicators based on the implementation and impact of preventive measures reducing vulnerability to drought.

The program considers three main lines of action: (a) the formulation and implementation of preventive and mitigation programs (including monitoring and alerting), (b) acts of authority to ensure drinking water supply and (c) institutional coordinated attention based on prevention and mitigation. For the line of action (a), the PRONACOSE has five components: (1) formulation, implementation and evaluation of Programmes of

Stakeholders will together:

Before drought	During drought	After drought
• Design the actions to reduce vulnerability	• Implement actions	
• Set a coordination structure to address drought		• Evaluate to get a better plan, and restore conditions

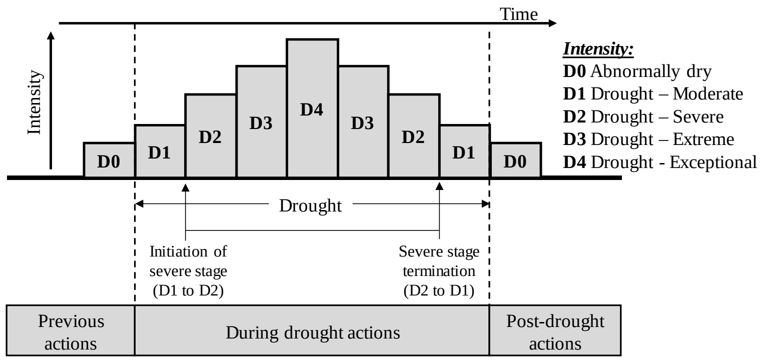

Fig. 4, Left: river basin council's stakeholders actions to face droughts; right: scheme of stakeholders actions according to drought intensity through time, highlighting severe stage initiation and termination which CONAGUA will announce.

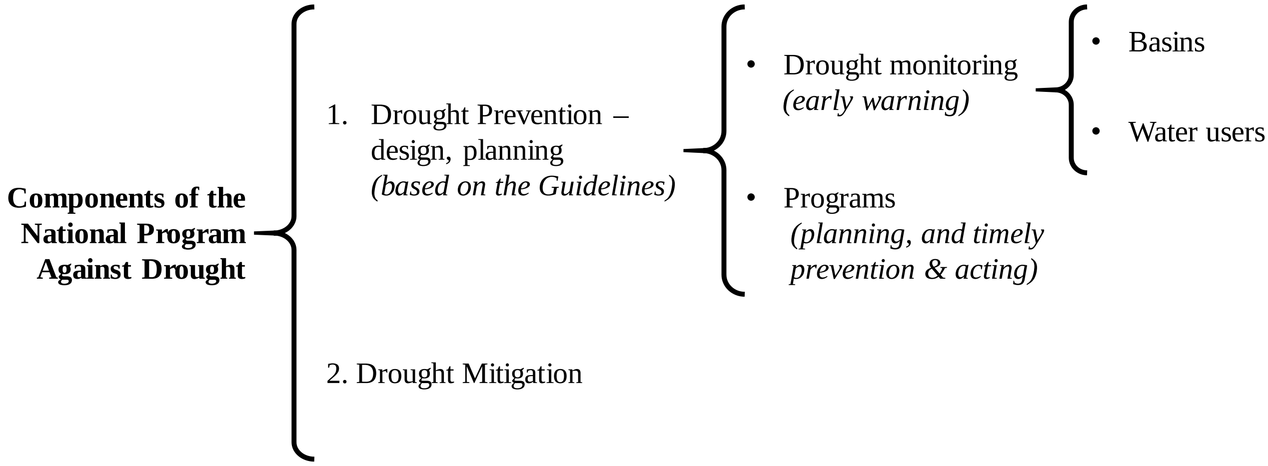

Fig. 5, The elements and components of PRONACOSE.

Preventive and Mitigation Drought Measures; (2) drought alert and monitoring; (3) development and strengthening of the institutional framework for dealing with drought: establishment of the Inter-ministerial Commission for the attention of droughts and floods and committees or working groups to inform, support, guide and evaluate the program; (4) research; and (5) training, communication and dissemination.

For the line of action (b), there are two components: (1) the establishment of administrative legal protocol and (2) the publication and implementation of the overall arrangements to guarantee the supply of water for human consumption as long as the drought reaches the severe degree or higher status and remains in it.

The final line of action (c) has two components: (1) the coordination with the National Natural Disasters Fund and the other federal government agencies programmes, (2) ongoing review of these programs and their operation rules for an effective and efficient way to mitigate the effects of drought.

CONAGUA is also conducting the visit from different world drought experts so that they can review and offer recommendations on plans design, drought analysis, and on the use of information. Efforts are also being carried out to develop a formal coordinated platform in charge of the investigation on defined lines for drought applied studies.

Decentralized attention of drought will nest the development of local capacities. In this sense, local universities are to be the coordinators within each river basin council for the elaboration of drought plans containing prioritized actions based on the guidelines published by CONAGUA some weeks before (22 November 2012) the initiation of the PRONACOSE.

3.5. The Programmes of Preventive and Mitigation Drought Measures (PMPMS)

The PMPMS has the general objective of minimizing social, economic and environmental impacts of possible drought situations and have been conceived as planning instruments that will serve as the basis for the right decision making within the river basin councils about the drought in the different sectors of the water users. The process for the elaboration of each one of the 26 PMPMS was formed of eight steps (Fig. 6): 1) the program objectives and the guiding principles were established within the river basin councils; 2) the characterization of the historical droughts and their impacts is carried out; 3) the evaluation of the current vulnerability to droughts was executed; 4) the

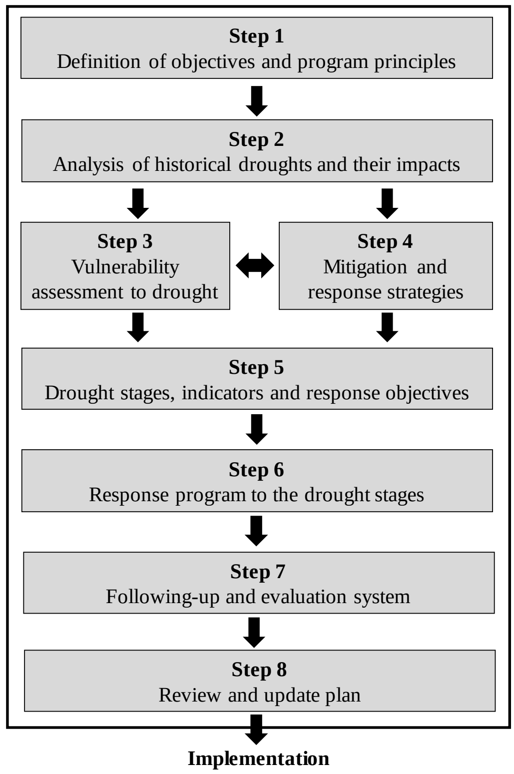

Fig. 6, PMPMS elaboration process development chart.

strategies of mitigation and response to a drought were specified; 5) the identification of the different stages of the drought and the corresponding signs and response objectives was performed; 6) a detailed program on the responses for each stage of the drought was fulfilled; 7) an indicators system for the following-up and evaluation of the program was prepared; 8) a reviewing and updating plan of the document was determined.

In summary, each one of the PMPMS includes the following: the physical and socioeconomical characterization of the basin at issue; the analysis of the historical droughts and their impacts; the evaluation of the current vulnerability to droughts; the stages and signs of the drought and the measures that can be implemented within the river basin councils to face the drought in three ways: before the phenomenon occurs (strategic measures), when it is starting (tactical measures) or when it is already happening (emergency measures), such as it is described below [9]:

a) Strategic measures. These types of measures mean actions taken in a long term (having a duration of more than two years) and they normally have an institutional and infrastructural nature that are part of the hydrological planning. For example: the building of infrastructure to keep water or the agreement and regulations development for its distribution amongst the various catchment users.

b) Tactical measures. They are short-term actions (with a duration going from some months up to two years) that are planned and validated early within the drought program. They shall be activated at yellow and red alerts. For example: when there is an increase in water prices or the reutilization of grey waters for garden irrigation or any other non-priority uses.

c) Emergency measures. They are actions taken in a very short-term (with a duration of weeks or months) and their objective is that of facing the water deficit caused by a drought when it is already there or when it is already at an advanced stage and they will vary according to its seriousness and the level of effects in the catchment. For example: water distribution through tankers amongst the population or its rationing and reduction for certain purposes.

It is important to mention that the distinction between the strategic measures, the tactical measures and the emergency measures depends on the synchronization and the manner that each river basin council implements them. For instance, the wells renovation (that is, the restoration of the water production in the wells to its most efficient manner through various treatments and methods), it can be considered as a strategic measure if it is done on an everyday basis to assure that the wells are in good working conditions when there is a drought or it can be also a tactical measure in case it is done after a drought declaration. Ultimately, it can also be an emergency measure if it is carried out when the drought is in an advanced stage and it is required to extract water from the subsoil urgently.

In addition to the above, in each one of the PMPMS are specified a basis for the implementation of actions, distinguishing between the supply side (offer of water), related to construction and distribution systems; and on the demand side that impact the use and consumption by users. This is known as the management or operation of supply and demand for water in drought conditions. As well, in the following tables are presented some examples of preventive and mitigation drought measures proposed for each of the major sectors of water users: municipal water systems (Table 1); the hydro-agricultural sector (Table 2); and the residential, industrial and commercial uses (Table 3).

TABLE 1, EXAMPLES OF PREVENTIVE AN MITIGATION DROUGHT MEASURES FOR MUNICIPAL WATER SYSTEMS

Objective	Measure	Type*		
		S	T	E
Improve the water distribution service in municipal systems	Increase of water rates depending on the consumption		x	x
	Repair of leaks	x	x	
	Install or replace measurement systems	x		
	Implement distribution water systems		x	x
	Replace obsolete pipelines	x		
	Build wastewater treatement plants	x		
	Distribute water in tank cars			x
	Make agreements with bottlers		x	x
	Make a resource inventory	x	x	
Create new water supplies, preserve or extend existing ones	Find new water sources	x		
	Drill deep wells	x	x	x
	Enable deep wells	x	x	x
	Build rainwater harvest systems	x		
	Recharge aquifers by storm sewers	x		

*Types: S = Strategic measure; T = Tactic measure; E = Emergency measure.

TABLE 2, EXAMPLES OF PREVENTIVE AN MITIGATION DROUGHT MEASURES FOR HYDRO-AGRICULTURAL SECTOR

Objective	Measure	Type*		
		S	T	E
Improve the water use efficiency in irrigation	Coating of main channels	x		
	Coating of secondary channels	x		
	Dam operation policies	x	x	
	Curves of guarantee from users	x	x	
	Water volume measurement	x		
Create new water supplies, preserve or extend existing ones	Drilling deep wells	x	x	x
	Deep wells rehabilitation	x	x	x
	Storage dams	x		
	Water treatment	x		
	Recharge aquifers through drainage	x		
	Runoff management systems	x	x	
	Cleaning sewer lines, canals and dams	x	x	

*Types: S = Strategic measure; T = Tactic measure; E = Emergency measure.

TABLE 3, EXAMPLES OF PREVENTIVE AN MITIGATION DROUGHT MEASURES FOR RESIDENTIAL, INDUSTRIAL AND COMMERCIAL USES

Objective	Measure	Type*		
		S	T	E
Reduce water consumption in household	Installation of water saver devices	x		
	Replacement of traditional systems for efficient technologies	x		
	Reuse of gray water for garden irrigation		x	x
	Leak repair in hydraulic installations		x	x
	Reduction in use of air-conditioning systems		x	x
	Restriction of garden irrigation with drinking water			x
	Restriction of car washing with drinking water			x
	Restriction of sidewalk washing with drinking water			x
	Restriction of swimming pools filling			x
	Restriction of new gardens planting			x

*Types: S = Strategic measure; T = Tactic measure; E = Emergency measure.

In addition to preventive and mitigation measures that are listed in Tables 1, 2 and 3, in the PMPMS are proposed others of general nature, with long-term trend (strategic measures), which can be implemented at national level, for example:

- In terms of governance, promote monitoring of strict observance of the National Water Law (NWL) and the application of sanctions for non-observance.
- Respect and enforce the agreements of the Technical Committee of Hydraulic Works Operation, in regard to the annual volumes assigned to draw from the dams for different water uses.
- Implement a payment program for hydrological services of CONAGUA (soil conservation to maintain its infiltration capacity) similar to the payment for environmental services of the National Forestry Commission (CONAFOR).
- Establish agreements of water distribution inside of each basin, and agreements for water transfers between neighboring basins, when drought conditions so require.
- Promote that CONAGUA assume operational and financial control of the operator agencies of drinking water and sanitation.
- Promote the modification of the Mexican Official Standard NOM-011-CNA-2000 in order to improve the estimation of water availability from aquifers be calculated with real data of extracted volumes, and not based on concession volumes.
- Implement mechanisms in the existing legislation to enable that CONAGUA could count with water volumes reserved for use in times of drought.

Finally, it is noteworthy that in all activities mentioned before, the Mexican Institute of Water Technology (IMTA) has played an important role, as this institute has provided the necessary technical support for the designing and implementation of the PRONACOSE.

3.5. CHALLENGES

Among the main challenges for the National Drought Program development and implementation is the adoption of a new water culture and strategy by water users and government agencies which comprises the prevention, planning and evaluation of the drought plans as the main asset to face a recurrent natural phenomena. Also the alignment of the federal, state and local fund programs to the directives of the drought plans is critical due to a very long history of a reactive approach. It is well known that droughts occur in Mexico but it is not well assimilated that it should be considered as the present and future natural occurring condition in a climate change scenario and that should be the baseline for the National Development Plan and the framework for a new National Civil Protection System. The funds to reduce the present vulnerability are high and the possibilities to get the financing are opposite. Thus another challenge is the funding of Mexico's vulnerability reduction to drought. An option is to access the world Climate Change Adaptation Funds. Finally, a drought communication strategy from the beginning is also critical for the acceptance of the drought measures and for the real evaluation of the success or failure of the Program.

3.6. Main interests in Mexico

There are three main interests in Mexico with regard to its National Program Against Drought:

- To guarantee the permanency of the drought planning and implementation for the future;
- To manage real social involvement in the development and implementation of the drought measures on a permanent basis; and
- To ensure that the reduction of drought vulnerability is one cornerstone of the Mexican strategy for climate change adaptation in compliance with the Climate Change General Law and the National Water Law.

IV. Way forward

The first planning phase of the Program was completed in 2013 but the implementation evaluation during the following four years will lead to another planning exercise and the issuing of new developed and improved basin and major water users plans for 2018 and onwards. The first phase effectively concluded with 26 completed plans for river basin councils which were analyzed by four international experts from USA, Spain and Brazil; they enriched the elaboration of the plans and shared comments for possible collaboration for drought monitoring and analysis.

Points to be properly addressed during the first four years are: the carrying out of the planned prioritized action with convergent resources, the development and testing of protocols for coordinated actions prior to the occurrence of a real drought, and the communication of plans out of the river basin councils looking for public appropriation.

Since the very beginning of the conception of CONAGUA's guidelines in 2009, decentralization of drought attention was considered as a key issue to maintain efforts beyond administrative changes. The complement of this key issue is the effective appropriation of plans by citizens.

Directions for basin councils through local universities were given to ensure, as far as possible, attention to social, financial and environmental aspects (especially water issues). Future versions of plans will improve such considerations.

A natural path to maintain the drought plans in place and keep them ongoing is to support them in a new National Civil Protection System and with the Climate Change and Water Laws mechanisms and instruments. This will give them financial support as well.

V. Conclusion

Mexico is enveloped in a transition process that is going from a reactive approach centered in the management of the crisis caused by droughts to a preventive approach focused on the risk management. The aim of the National Program Against Drought is that of anticipating droughts by foreseeing solutions to satisfy the demand by avoiding situations of water shortage and conflicts between users for its use. The comprehensive vision of this program includes preventive and mitigation measures; improvements in knowledge generation and sharing of usable information for coordinated actions among stakeholders; and local conception and implementation of measures in each of the 26 river basin councils that integrate the Mexican territory. Drought risk can't be completely eliminated but this program is useful to mitigate its effects.

References

[1] World Meteorological Organization (WMO). *Vigilancia y alerta temprana de la sequía: conceptos, progresos y desafíos futuros.* Ginebra: WMO, 2006.

[2] D. Ortega-Gaucin and I. Velasco. "Aspectos socioeconómicos y ambientales de las sequías en México", *Aqua-LAC*, **5**, pp. 78-90, 2013.

[3] D. Ortega-Gaucin. *Sequía en Nuevo León: vulnerabilidad, impactos y estrategias de mitigación.* Apodaca: Instituto del Agua del Estado de Nuevo León, 2012.

[4] E. Florescano. *Breve historia de la sequía en México*. 2nd edition. Mexico: CONACULTA, 2000.

[5] National Center for Disaster Prevention (CENAPRED). "Financing Risk Prevention Activities in Mexico: The Fund for Disaster Prevention (FOPREDEN)." *The United Nations Framework Convention on Climate Change's Regional Meeting on Loss and Damage in Latin America as a Result of Climate Change*, Mexico City, July 23-25, 2012.

[6] Department of Water Resources of the State of California. *Urban Drought Guidebook 2008, Updated Edition*. Available at: http://digitalscholarship.unlv.edu/water_pubs/3

[7] Ministry of the Environment and Natural Resources (SEMARNAT). "Guidelines establishing the criteria and

mechanisms for issuing general agreements in emergencies by the occurrence of drought, as well as preventive and mitigation measures, which may be implemented by the national water users to achieve an efficient use of water during drought", Official Government Gazette, México, D.F., November 22, 2012.
[8] Ministry of the Environment and Natural Resources (SEMARNAT). "National Water Law". Official Government Gazette, Mexico, D.F., April 29, 2004 to the latest amendments or additions on 8 June 2012.
[9] National Water Comission (CONAGUA). *Programa de Medidas Preventivas y de Mitigación de la Sequía del Consejo de Cuenca del Río Balsas*, México: SEMARNAT, 2013.

Journal of Energy Challenges and Mechanics

ISSN 2056-9386

http://www.nscj.co.uk/JECM/

Editor:

Dr. Henry Tan
University of Aberdeen, Scotland, United Kingdom

Scope:

Since James Watt, a Scottish inventor, improved efficiency of the steam engine, human civilization relies more and more on a steady supply of energy. Today we are at a transitional age. On the one hand, we see technology advances in the exploration and development of oil and gas, a depleting resource; we see growth in handling aging and decommissioning. On the other hand, we see ideas and plans for new energy infrastructure. This journal is about energy challenges and the underlying mechanics, involving multiple disciplines in science, technology, management and policy-making. Mechanics, fundamentally, is about force and the related behaviours, where force is about relationships, including those physical, human and social. For mechanics, the journal covers interactive boundaries with many other disciplines. For energy, topics include both fossil fuels and many different forms of renewable energy; also, issues related to energy economy, energy policy, efficiency, safety, environment and ecology will also be covered.

North Sea

Cove Bay, Aberdeen, Scotland, United Kingdom